

THE GROWTH OF SHORT FATIGUE CRACKS  
IN A MEDIUM CARBON STEEL

by

PAUL DAVID HOBSON

Thesis submitted to the University of Sheffield  
for the Degree of Doctor of Philosophy  
in the Faculty of Engineering

University of Sheffield  
Department of Mechanical Engineering

August 1985

**To Nicoleta**

THE GROWTH OF SHORT FATIGUE CRACKS  
IN A MEDIUM CARBON STEEL

CONTENTS

	Page No
Preface	i
Acknowledgements	ii
Summary	iii
Nomenclature	v
Introduction	vi
 <u>CHAPTER ONE GENERAL LITERATURE SURVEY</u>	
1.1 Historical Background	1
1.2 Crack Initiation	2
1.2.1 Demarcation between "Initiation" and "Propagation"	5
1.3 Crack Propagation	6
1.3.1 Linear Elastic Fracture Mechanics	7
1.3.2 Gross Yield Conditions	12
1.4 Short Crack Growth	13
References for Chapter One	17
Figure Headings for Chapter One	21
Figures for Chapter One	22

## CHAPTER TWO   EXPERIMENTAL WORK

2.1	Material	28
2.2	Test Machine	29
2.3	Specimen Design and Preparation	30
2.4	Extensometry	31
2.5	Experimental Techniques	35
2.5.1	Crack Detection	35
2.5.2	Plastic Replication	37
2.6	Failure Criterion	40
2.7	Test Programme	41
	References for Chapter Two	45
	Figure Headings for Chapter Two	46
	Figures for Chapter Two	47

## CHAPTER THREE   RESULTS

3.1	Fatigue Tests	53
3.1.1	Stress-Strain Behaviour	53
3.1.2	Fatigue Behaviour	55
3.2	Crack Growth Results	56
3.3	Threshold Tests on Notched Specimens	62
	References for Chapter Three	66
	Figure Headings for Chapter Three	67
	Figures for Chapter Three	68

## CHAPTER FOUR SHORT CRACK LITERATURE SURVEY

4.1	Introduction	82
4.2	Cumulative Damage Testing	83
4.3	Minimum Crack Lengths suitable to LEFM Analyses	87
4.4	Grain Boundary Effects	88
4.5	Short Crack Growth Models	90
	References for Chapter Four	97
	Figure Headings for Chapter Four	103
	Figures for Chapter Four	104

## CHAPTER FIVE ANALYSIS OF CRACK GROWTH RESULTS

5.1	Derivation of Short Crack Growth Equation	106
5.2	Application of Short Crack Growth Results	109
5.2.1	Short Crack Growth in 7075-T6 Aluminium Alloy	109
5.2.1.1	Crack Growth within the First Grain	109
5.2.1.2	Long Crack Growth	110
5.2.1.3	Lifetime Prediction	111
5.2.2	Short Crack Growth in a medium Carbon Steel	114
5.2.2.1	Crack Growth in the First Grain	114

5.2.2.2	Long Crack Growth	119
5.2.2.3	Lifetime Calculations	121
	References for Chapter Five	123
	Figure Headings for Chapter Five	125
	Figures for Chapter Five	126

## CHAPTER SIX DISCUSSION

6.1	Stress-Strain Behaviour	141
6.2	S-N Curves	143
6.3	Crack Growth Considerations	146
6.3.1	Long Crack Growth	147
6.3.1.1	Fractography	148
6.3.1.2	Crack Sectioning	148
6.3.1.3	Long Crack Growth Equation	150
6.3.2	Short Crack Growth	151
6.3.3	Grain Size Effect	154
6.4	Cumulative Damage Testing	155
6.5	Plastic Replication Technique	158
	References for Chapter Six	160
	Figure Headings for Chapter Six	161
	Figures for Chapter Six	162

APPENDICES

Appendix I          Crack Growth Results

Appendix II         Short Crack Growth in an Engineering  
Component

## PREFACE

This dissertation is based on the findings of research carried out in the Department of Mechanical Engineering at the University of Sheffield.

The content of this dissertation is original except where specific references are made to other work. No part of this dissertation has been submitted to any other university for a degree.

*Paul D. Hobson*

P. D. HOBSON

August 1985

## ACKNOWLEDGEMENTS

I wish to thank the Head of the Department of Mechanical Engineering for the use of the laboratory facilities, and both the Science and Engineering Research Council and the Central Electricity Generating Board for financial support.

I am especially grateful to my supervisors Professor K.J. Miller and Dr. M.W. Brown for their help, guidance, and most of all their encouragement throughout the time of this project. The assistance of Dr. De Los Rios, in particular with the practical problems of the replication studies also deserves a special thanks.

I would also like to acknowledge Mr. D. Puttergill, Mr. J. Smith and Mr. E. Hardwick who manufactured the specimens and extensometer parts, and Mr. J. Goodliffe for help with the electronic control system of the fatigue machine. The photographic skills of Mr. D. Hallford and Mr. C. Jackson were also much appreciated, as was the amazing gift (of being able to read my handwriting) of Monika Akid who typed this thesis and Kirstie Johnson who traced the figures.

## SUMMARY

Short crack growth behaviour was studied using a method of plastic replication on hour-glass shaped specimens of a medium carbon steel which were subjected to push-pull fatigue testing at ambient temperature. Crack lengths were measured from replicas using an optical microscope from which the growth rate could be calculated.

A theory for short crack growth is presented which may be expressed mathematically by the equation:-

$$\frac{da}{dN} = C_1 (d - a)^{1-\alpha} a^\alpha \quad (\text{for } a < d)$$

where (a) is crack length, (d) is a characteristic dimension between adjacent microstructural obstacles to crack propagation,  $C_1$  is a function of stress or strain range and  $\alpha$  is a constant. For the medium carbon steel used in this study (d) was equated to the ferrite band length which contained the growing crack. This theory was used to model short crack growth in an Aluminium alloy T6-7075 Al and for the medium carbon steel used in this project.

By using a second equation to describe "long" crack growth of the form:-

$$\frac{da}{dN} = C_2 a + D$$

where  $C_2$  is a function of the applied strain range and  $D$  is a constant, it was then possible to describe the complete history of crack growth. By obtaining short crack growth data for different stress levels, quantitative expressions of these two equations were calculated from which fatigue lifetime predictions could be made by integration of the equations for any stress level. Using this method an estimate could also be made of the percentage of fatigue lifetime spent in the initiation and growth of short cracks.

## NOMENCLATURE

The symbols most often used in the text are listed below. Those which have been infrequently used are defined in context.

a	Crack length
$a_f$	Crack length at failure
$a_o$	Initial crack length
$a_s$	Surface crack length
$a_{th}$	Crack length at threshold
d	Microstructural dimension
E	Youngs Modulus
K	Stress intensity factor
N	Number of cycles
$N_f$	Number of cycles to failure
R	Stress ratio
$R_a$	Centre line average roughness
$R_e$	Maximum roughness depth
V	Voltage
W	Specimen width
X	Distance from crack tip to nearest grain boundary
Y	Geometry factor
$\Delta K_{th}$	Threshold stress intensity factor
$\epsilon$	Strain
$\sigma$	Sigma
$\nu$	Poissons ratio

### Subscripts for strain:

e	elastic
p	plastic
t	total

### Superscripts for strain:

l	axial
d	diametral

## INTRODUCTION

Chapter one presents a brief history of fatigue studies from the early nineteenth century to the present day, and outlines reasons for increasing interest in the area of short crack growth.

An experimental programme of fatigue testing aimed at studying the growth behaviour of short cracks is described in Chapter two, with results from these tests given in Chapter three.

Existing work concerning short crack growth is reviewed in Chapter four, and a new theory which incorporates microstructural features into a short crack growth equation is presented in Chapter five along with the analysis of crack growth results in the light of this theory.

Chapter six discusses the results and their implications whilst Chapter seven deals with the conclusions derived from this work.

## CHAPTER ONE

### GENERAL LITERATURE SURVEY

#### 1.1 Historical Background

The industrial revolution transformed Britain from a mainly agricultural country into a predominantly industrial one. This change brought about a more extensive use of machinery, for example, in the development of the railway and mining industries. With the advent of the new technologies, mechanical failures became more common with resulting losses, not only in financial terms, but often in terms of human life.

It was noticed that many components and structures which had performed satisfactorily under repeated load applications for several years suddenly failed for no apparent reason. One suggestion was that failure must have been brought about by a change in the material in such a way that it had made the material tired. The word "fatigue" was coined to describe such failures, and engineers began to experiment on its nature and causes.

In 1830, Albert [1] performed repeated loading tests on mining hoists, and later, Wohler [2] carried out the first programme of fatigue tests after it was noticed that railroad axles were failing through fatigue. Although research into fatigue has come a long way since these pioneering days, over

half of all mechanical failures are still caused by fatigue. More recently, fatigue was found to be the cause of failure of the Comet aircraft in the 1950's, and also a DC-10 airliner in 1979.

Nowadays, it is realised that rather than fatigue being a result of the material itself becoming tired, it is a consequence of the initiation and growth of microcracks which then propagate through the material and eventually cause a component or structure to fail.

## 1.2 Crack Initiation

Crack initiation in a polycrystalline metal, generally, takes place at the free surface. Here the surface grains are the only ones which are not fully supported by neighbouring grains, which makes it easier for plastic deformation to take place. Also surface grains are in contact with the atmosphere and are therefore more susceptible to environmental effects.

Having established that cracks tend to initiate at the surface of a metal, the next step was to examine preferred initiation sites. Naturally initiation will take place at areas of weakness which can be either of a mechanical or a metallurgical nature.

On a typical engineering surface, the roughness of the metal varies depending on the type of finish. For a coarse

ground finish a centre line average (CLA) of  $2\mu\text{m}$  may not be unusual, whereas for a fine turned or fine ground finish a CLA value of  $0.125\mu\text{m}$  is typical. However, regardless of whether a surface is turned, ground, milled or highly polished, it can be pictured as a series of hills and valleys which act as tiny notches causing stress concentrations that can assist crack initiation.

Apart from notch-like irregularities on the surface of a metal, defects of a metallurgical nature can also be responsible for crack initiation. During cyclic stressing fatigue crack initiation is generally preceded by the localisation of plastic strain [3]. This gives rise to slip planes which form within surface grains and whose weakest slip planes are favourably orientated with respect to the applied stress system [4]. As cycling continues, these slip lines widen and form slip bands, which were first noticed by Ewing and Humphrey in 1903 [5]. Microscopic discontinuities or slip steps on the surface are created as a result of the presence of these slip bands. In the case of uniaxial loading, if these planes intersect the free surface at 45 degrees, intrusions and extrusions (the latter being flakes of material projecting up to about  $10\mu\text{m}$  from the specimen surface), may be observed [6].

Although there are many individual slip planes at the start of a test, a few slip bands become accentuated at the expense of the rest as a test proceeds, and these are termed persistent slip bands [7]. It is here that fatigue cracks may

eventually form.

However, persistent slip bands are not always the source of crack initiation. It is known that in some two phase metals where grain boundaries may be weaker than the grains themselves (for example, where the weaker phase segregates to the boundary regions), cracks can initiate at a lower cyclic stress than that required to form cracks in slip bands [8].

Guiu et al [9], reported that cracks can also form at grain boundaries as a result of incompatible grain deformation, ie, in cases where the grain boundaries are not intrinsically weak. Grain boundaries may also be more prone to environmental effects, leading to crack initiation.

Non-metallic inclusions can also be the site of crack initiation. There are two ways that the inclusion can lead to cracking. Either debonding of the inclusion from the surrounding matrix takes place or (usually in the case of high cyclic fatigue), the inclusion itself suffers fatigue damage [10]. These inclusions may occur on grain boundaries, again causing crack initiation to occur at grain boundary sites.

It has been stated that cracks can initiate in different ways, the preferred type of initiation being dependent on the microstructure of the metal, and also on the amount of local plastic strain to which the grains or inclusions are subjected. Often there is more than one active mechanism for crack

initiation. Guiu et al [9], performed tests on pure polycrystalline  $\alpha$ -Iron and found that cracks nucleated from an intrusion and extrusion process, and also from grain boundaries due to incompatible deformation in surface grains. However, cracks which initiated from intrusions and extrusions were not associated with the final fracture. Grain boundary crack initiation was also reported by De Los Rios et al [8] who worked on the medium carbon steel which was used for my project. The microstructure for this material consisted of pearlite colonies with a network of ferrite on prior austenite grain boundaries as shown in figure 2.1. Because the ferrite was weaker than the pearlite, the grain boundary ferrite formed the site for crack initiation.

#### 1.2.1 Demarcation between "Initiation" and "Propagation"

Although the terms "initiation" and "propagation" have been used extensively in the literature, the areas to which they refer in the history of a crack vary widely, depending on the definition of the end of the "initiation period". Often a crack is said to be initiating until it has reached some specified length that can be readily detected, eg, one millimetre. Such a demarcation is arbitrary and without any physical basis. In this study the "initiation" period is used to describe the number of cycles where no cracks, however small, have been nucleated, and "propagation" describes the growth of cracks from zero crack length through to the length at failure.

### 1.3 Crack Propagation

Before discussing crack propagation, it is necessary to distinguish between the growth of "short" cracks and that of "long" cracks, as the driving mechanisms are always different for the two cases and therefore cannot be characterised by a single growth law.

Three definitions have been put forward to describe a "short" crack. A crack may be considered small if it is less than some specified length (eg,  $<0.5\text{mm}$ ). Alternatively, if the length of the crack is of the order of less than some controlling microstructural feature, it could be considered short. Finally, when a crack is small compared to its own plastic zone size, it may be described as a short crack.

The first definition bears no direct relation to material properties or the applied stress and strain conditions so it cannot predict any change in crack growth behaviour which is likely to occur.

The second definition is related to material structure; and the third to a limitation of the applicability of Linear Elastic Fracture Mechanics. So both of these last two definitions may be able to explain differences between "short" and "long" crack behaviour.

Before discussing short cracks in more detail, attention will be given in the next section to the propagation of long cracks which are defined to be those cracks which can be uniquely described by Linear Elastic Fracture Mechanics. The bulk of published crack growth studies are concerned with this area.

Recently more emphasis has been focussed on the growth of short fatigue cracks. Attempts have been made to apply long crack growth theories in the short crack regime, and problems that arise in applying these methods will be discussed later.

### 1.3.1 Linear Elastic Fracture Mechanics

When considering a cracked body under loading there are three basic modes of relative displacement of the crack surfaces which can occur, these are shown in figure 1.1. The preferred mode of crack growth depends on the type of loading.

In Mode I, the crack surfaces move directly apart, whereas for Modes II & III (shear modes), Mode II is characterised by the displacement in which the crack surfaces slide over one another normal to the crack fronts and in Mode III the shear is parallel to the crack front.

For each crack surface displacement mode there is a particular elastic stress field associated with the crack in

the vicinity of its tip. In Linear Elastic Fracture Mechanics (LEFM), these stress fields are quantified by their respective stress intensity factors. For example, for Mode I crack extension, the stress intensity factor  $K$  is given by

$$\left. \begin{aligned} K_I &= Y\sigma \sqrt{\pi a} \\ \sigma_{ij} &= \frac{K}{\sqrt{2\pi r}} f_{ij}(\theta) \end{aligned} \right\} \quad (1.1)$$

which is derived from Westergaard's solution [11]. Here  $\sigma_{ij}$  is the stress tensor,  $f_{ij}$  is a function of  $\theta$ , and  $r$  and  $\theta$  are polar coordinates taking the crack tip as the origin (see reference [12]),  $a$  is the crack length and  $Y$  is a geometry factor.

Paris suggested that because the stress intensity provides a complete description of the stress field around a crack tip, it should also control the rate of fatigue crack propagation [13]. This is expressed in the equation known as the Paris Law.

$$\frac{da}{dN} = A (\Delta K)^m \quad (1.2)$$

where  $\Delta K$  is simply defined as the difference between the maximum and minimum stress intensities encountered during each cycle.

In order to use this equation to describe crack growth,

it is first necessary to examine the limits of its applicability, which are discussed in the rest of this chapter.

It is assumed in the derivation of equation 1.1 that all the fine detail of microstructure may be replaced by a homogeneous hypothetical continuum such that every portion is assumed to exhibit identical microstructural physical properties which are essentially properties of the bulk material. In situations where crack growth is influenced by microstructural variations the Paris Law could not necessarily be expected to be a good model to describe crack growth.

Figure 1.2 shows a plot of crack growth rates obtained for long cracks for different values of  $\Delta K$ . For convenience the plot has been split up into three regions. For the linear part of the growth curve in region B, crack growth can adequately be described by the Paris Law.

In region C, there is a large effect of microstructure which explains the curves deviation from linearity. However, this region is of limited interest as by the time a crack has entered this phase of growth, the greatest proportion of the lifetime of the component or structure will have expired.

Of more interest is the crack growth in region A. In this region the applied stress levels are invariably very low and crack extension is of the order of one atomic distance per

cycle (ie,  $10^{-7}$  mm per cycle). Crack growth in this region has been observed to be intermittent, [14], which gives support to the theory that the cracks are subject to microstructural variations [15].

In figure 1.2, point X is the threshold stress intensity factor  $\Delta K_{th}$ . This can be defined as the highest stress intensity factor for which no crack growth can be detected. It is not possible to say whether there exists a genuine threshold value since for very low growth rates ( $< 10^{-4} \mu\text{m}$  per cycle), practical tests are difficult due to the length of time required to detect any crack growth. Because of this it is normal to take the threshold stress intensity factor as that which produces a pre-defined growth rate (eg,  $10^{-4} \mu\text{m}$  per cycle).

Further evidence of microstructural influence on crack growth has been provided in experiments to discover the effect of grain size on  $\Delta K_{th}$ . However, it is well known that refining the grain size changes the yield strength of a material, which will alter the plastic deformation behaviour of the material. Benson [16], using a method whereby the yield strength could be controlled independently by changing the precipitation hardening contribution, was able to study the effect of changing grain size while keeping the yield strength constant. For the ferritic steel used in his study when grain size increased  $\Delta K_{th}$  also increased.

Another limitation of LEFM is that it cannot model situations where plasticity is appreciable. Figure 1.3 shows the stress intensity field at a crack tip. Individual stress components near the crack tip are proportional to  $K/r^{1/2}$  (refer to equation 1.1), where  $r$  is the distance from the crack tip. This predicts infinite stresses at the crack tip itself ( $r=0$ ), which cannot occur in practice and so the elasticity theory breaks down with the formation of a small region of plastic flow. However, as long as the elastic strains are only slightly affected, the behaviour of the bulk crack tip stress field is still adequately described by the stress intensity factor. For this situation to occur the plastic zone size should be a lot smaller than the crack length. Plastic zone size,  $r_p$ , is given by the equation:-

$$r_p = A(\Delta K/\sigma_{cy})^2 \quad (1.3)$$

where  $A$  is approximately  $\frac{1}{2}\pi$  for plane stress, and  $\sigma_{cy}$  is the cyclic yield stress. Used in conjunction with equation 1.1, values for  $r_p$  can be calculated. In general the applied stress range should be well below yield for an LEFM analysis to be justified, ie, less than one third of yield from experimental observations.

### 1.3.2 Gross Yield Conditions

For situations where the plastic zone ahead of the crack tip is extensive attempts have been made to use an effective crack length rather than actual crack length to try to take into account the effect of the plastic zone size and to incorporate this effective crack length into an LEFM type equation [17]. However, such an approach has no physical justification and is unlikely to be applicable in the general case, so great care must be taken in using this type of approach.

For gross yielding conditions crack growth laws have been derived using parameters applicable to the bulk material. One of the simplest models is suggested by Tomkins [18], which can be written:-

$$\frac{da}{dN} = A(\Delta\sigma)^m \cdot a \quad (1.4)$$

for a power-law hardening material.

Because plastic strain rather than stress is probably more important in controlling crack growth in large scale yielding conditions Solomon [19], and Ibrahim [20], preferred to use an equation of the type:-

$$\frac{da}{dN} = A \Delta \epsilon_p^n \cdot a \quad (1.5)$$

where  $\Delta \epsilon_p$  is the plastic strain range.

Both these equations have the advantage that they are very simple to use, but it should be noted that for a constant stress range they predict a linearly increasing crack growth rate and therefore cannot describe any microstructural influence which may be present.

#### 1.4 Short Crack Growth

Short crack growth, for long a neglected area of research, is now becoming increasingly important to design engineers. Recent interest in short cracks derives from the need for higher levels of service stress particularly in the aircraft and power generation industries. Design philosophies based on either S-N curves or the defect tolerant approach ignored the region of short crack growth. In the latter approach, provided the largest defect could be accurately detected in a particular structure, then the design stress could be kept low enough to ensure the integrity of the structure.

In a case such as the manufacture of turbine blades, where great care is taken to ensure that the material contains only very small defects, and that surfaces are well finished, a large percentage of the lifetime can be spent in the

propagation of short cracks (see figure 1.4). In order to make accurate lifetime predictions, this area of crack growth needs be well understood. An example of failure in components made of titanium alloy in which the defect size was  $10\mu\text{m}$  or less was reported by Hicks et al [22]. Failure occurred at stress levels below those predicted for smooth specimen fatigue data and at shorter lives than those predicted from long crack propagation data, suggesting that rapid propagation of short cracks had occurred below the long crack threshold.

This process of short crack propagation at stress intensities below the long crack threshold can be better understood by referring to figure 1.5 which comes from work done by Kitagawa et al [23], on threshold values for specimens with known initial crack lengths. Three distinct regions can be seen on the plot:-

(1) For  $a < a_0$ , the standard fatigue limit applies. It is important to note that cracks may initiate below the fatigue limit in this region but they are unable to propagate past a certain point and therefore become "non-propagating" cracks.

(2) For  $a_0 < a < a_1$ , cracks can grow below the fatigue limit stress level and these cracks can subsequently continue growing to failure.

(3) For  $a > a_1$ , cracks grow according to LEFM which is shown by the fact the experimental results lie on the line described by

the equation:-

$$\Delta K_{th} = Y \Delta \sigma \sqrt{\pi a} \quad (1.6)$$

The experimental points only coincide with the LEFM line for values of stress less than about one third of the yield stress, indicating that LEFM should not be applied to situations of general yield [21].

Transforming figure 1.2, by simply replacing the abscissa with (a) instead of  $\Delta K$ , figure 1.6 is obtained which is a plot of crack growth versus crack length for a given stress range. As well as the characteristic LEFM type equation, these plots also show the more rapid growth of short cracks.

Three distinct cases are observed. For stresses below the fatigue limit, cracks can propagate but are unable to reach the length  $a_{th}$ , where  $a_{th}$  is the corresponding crack length at  $\Delta K_{th}$  for a given stress level. Thus, these cracks become non-propagating.

At the fatigue limit  $a_{th}$  coincides with the short crack growth minimum, for stresses greater than the fatigue limit the short crack growth curve crosses the long crack threshold and so a fatigue crack can subsequently propagate to failure.

Short crack growth is reviewed in more detail in Chapter

Four which considers reasons for the anomalous growth of short cracks as put forward in this literature survey.

CHAPTER ONE - REFERENCES

- [1] ALBERT, W.A.J. (1838)  
Arch. Miner. Geognosie Berg. Huttenkunde 10 p.215
- [2] WOHLER, A. (1871)  
"Tests to determine the forces acting on Railway Carriage  
axles and the capacity of resistance of the axles"  
Engineering 11 p.199
- [3] BROWN, M.W. & MILLER, K.J. (1973)  
"A theory for fatigue failure under multi-axial stress-  
strain conditions"  
Proc. Instn. Mech. Engrs. 187 p.745-755
- [4] FROST, N.E. MARSH, K.J. & POOK, L.P. (1974)  
"Metal Fatigue"  
Clarendon Press, Oxford, p.12-14
- [5] EWING, J.A. & HUMPHREY, J.L.W. (1903)  
Phil. Trans. A200 241
- [6] LYNCH, S.P. (1978)  
"Mechanisms of fatigue and environmentally assisted  
fatigue"  
ASTM STP 675 p.174-203

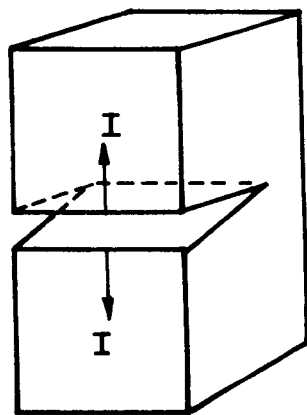
- [7] THOMPSON, N. (1956)  
"Experiments relating to the basic mechanisms of fatigue"  
International Conference on Fatigue, Institution of  
Mechanical Engineers  
Technology Press, Wiley, New York p.527
- [8] DE LOS RIOS, E.R. TANG, Z. & MILLER K.J. (1984)  
"Short crack fatigue behaviour in a medium carbon steel"  
Fatigue Engng. Mater. Struct. 7 p.97-108
- [9] GUIU, F. DULNIAK, R. & EDWARDS, B.C. (1982)  
"On the nucleation of fatigue cracks in pure  
polycrystalline  $\alpha$ -iron"  
Fatigue Engng. Mater. Struct. 5 p.311-321
- [10] EID, N.M.A. & THOMASON, P.F. (1979)  
"The nucleation of fatigue cracks in a low alloy steel  
under high-cycle fatigue conditions and uniaxial loading"  
Acta. Met. 27 p.1239-1249
- [11] WESTERGAARD, H.M. (1939)  
J. Appl. Mech. A49
- [12] KNOTT, J.F. (1973)  
"Fundamentals of fracture mechanics"  
Butterworths, London, p.61

- [13] PARIS, P.C. & ERDONGAN, F. (1963)  
"A critical analysis of crack propagation laws"  
J. Basic Eng. D85 p.528-534
- [14] STANZL, S. & TSCHEGG, E. (1980)  
"Fatigue crack growth and threshold measured at very high frequencies (20kHz)"  
Met. Sci. 14 p.137-140
- [15] HORNBOGEN, E. & GATZ, K.Z. (1976)  
"Microstructure and fatigue crack growth in a  $\gamma$ -Fe-Ni-Al alloy"  
Acta. Met. 24 p.581-592
- [16] BENSON, J.P. (1979)  
"Influence of grain size and yield strength on threshold fatigue behaviour of low-alloy steel"  
Met. Sci. 13 p.535-539
- [17] McCLINTOCK, F.A. & IRWIN, G.R. (1964)  
"Plasticity aspects of fracture mechanics"  
ASTM STP 381 p.84
- [18] TOMKINS, B. (1975)  
"Fatigue Failure"  
International conference on mechanics and physics of fracture, Cambridge

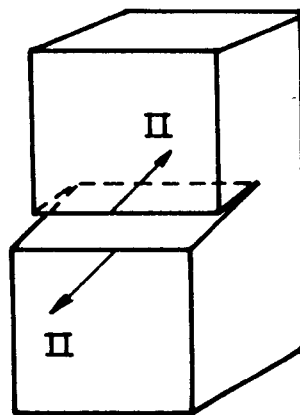
- [19] SOLOMON, H.D. (1972)  
"Low cycle fatigue crack propagation in 1018 steel"  
J. Mater. 7 p.299-306
- [20] IBRAHIM, M.F.E. & MILLER, K.J. (1980)  
"Determination of fatigue crack initiation life"  
Fatigue Engng. Mater. Struct. 2 p.351-360
- [21] MILLER, K.J. (1982)  
"The short fatigue crack problem"  
Fatigue Engng. Mater. Struct. 5 p.223-232
- [22] HICKS, M.A. HOWLERD, C. & BROWN, C.W. (1983)  
"The metallurgy of light alloys"  
The Chamelon Press, London
- [23] KITAGAWA, H. & TAKAHASHI, S. (1976)  
"Applicability of fracture mechanics to very small cracks  
or the cracks in the early stage"  
2nd International Conference on the Mechanical Behaviour  
of Materials, Boston, U.S.A.  
American Society for Metals, Metals Park, Ohio p.627-631

## CHAPTER ONE - FIGURES

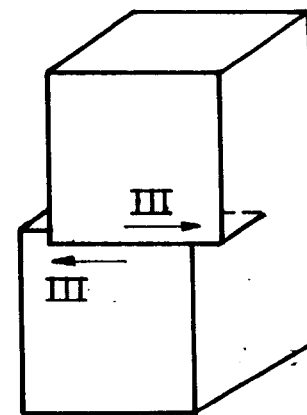
- 1.1 Crack opening modes
- 1.2 Crack growth rates for long cracks under linear elastic conditions
- 1.3 The stress intensity field at a crack tip
- 1.4 The growth of cracks during fatigue of a) pre-cracked and b) plain specimens (from Miller [21])
- 1.5 Crack growth thresholds for short and long cracks
- 1.6 Short crack growth behaviour



MODE I



MODE II



MODE III

FIGURE 1.1 - Crack opening modes

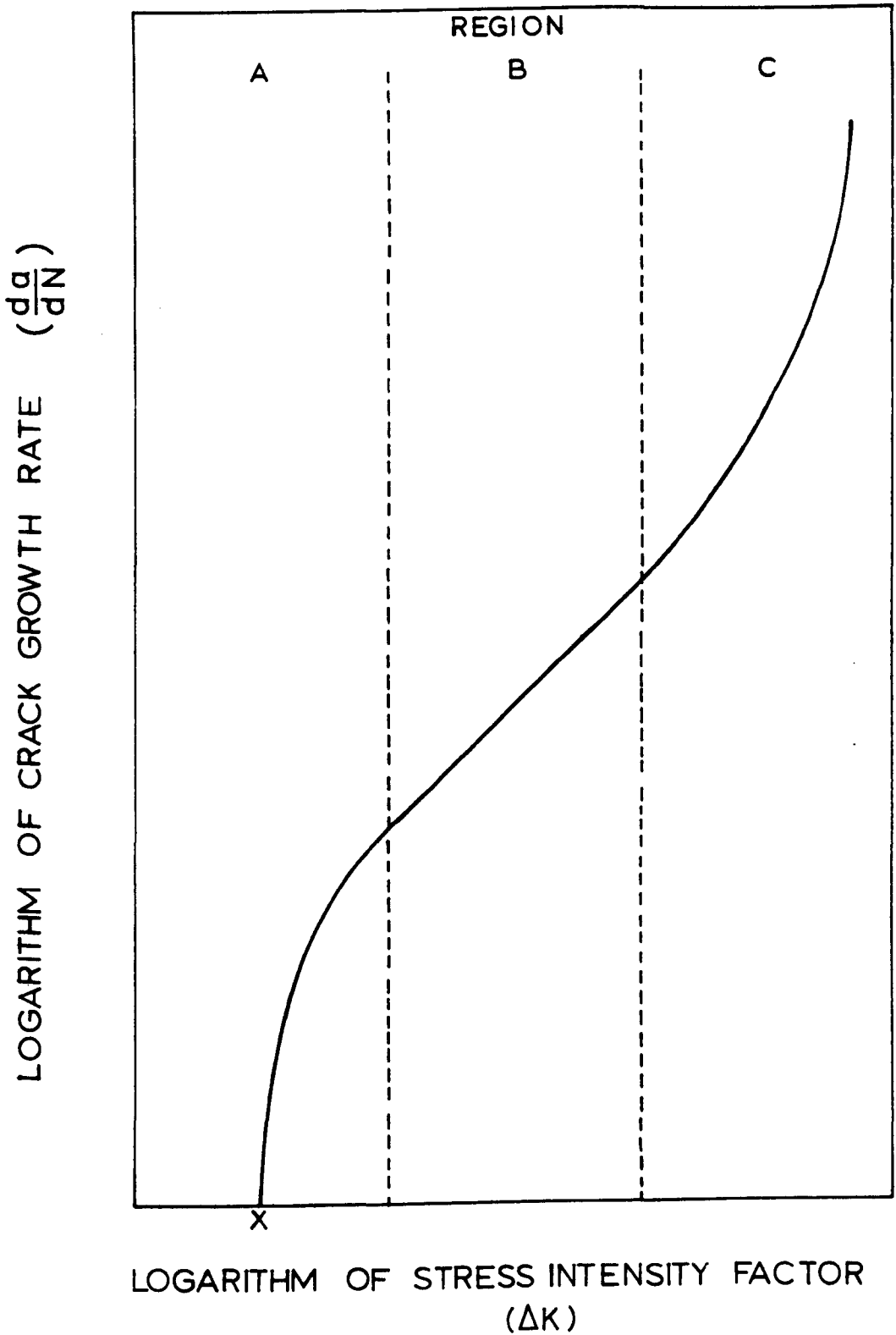


FIGURE 1.2 - Crack growth rates for long cracks under linear elastic conditions

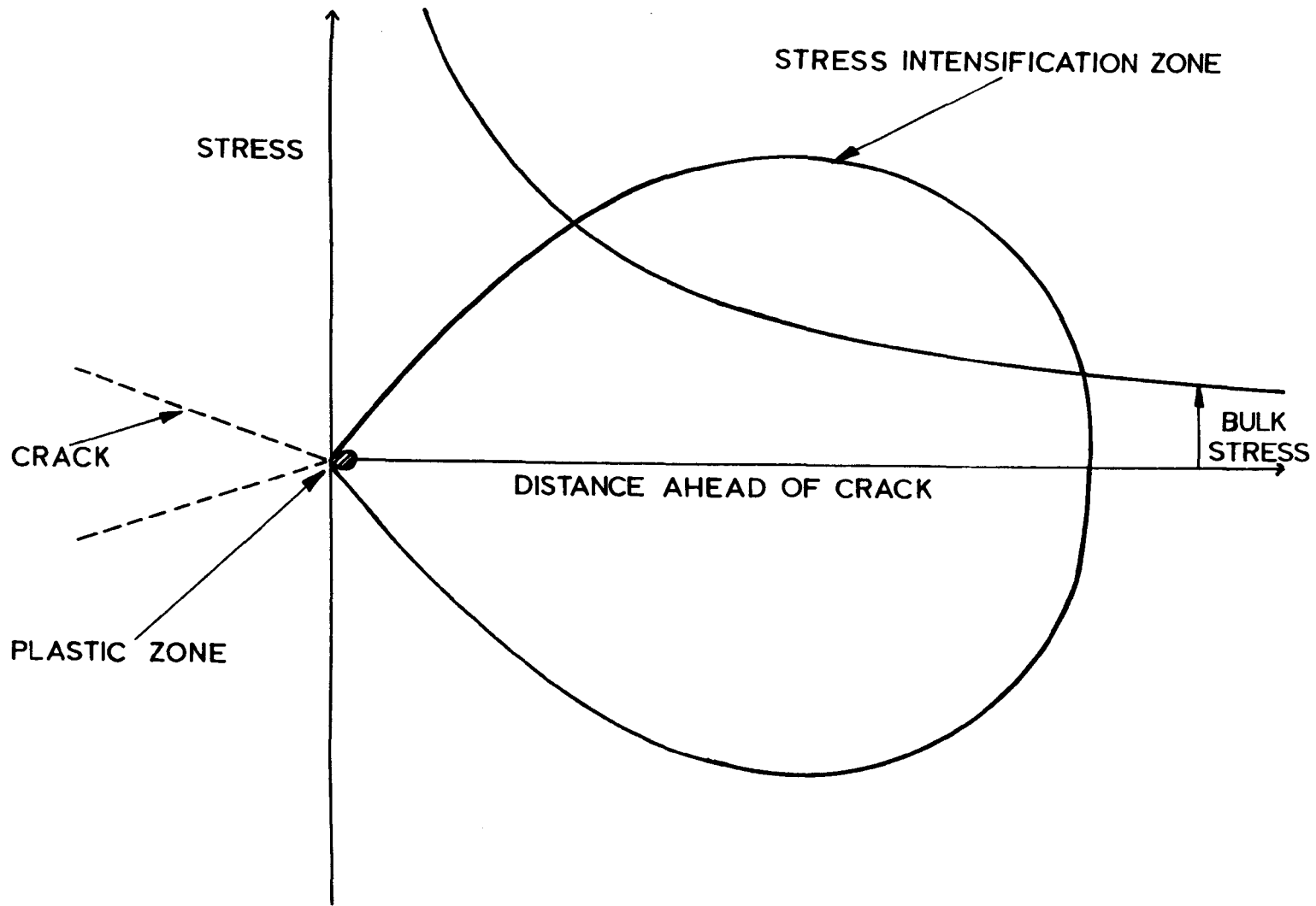
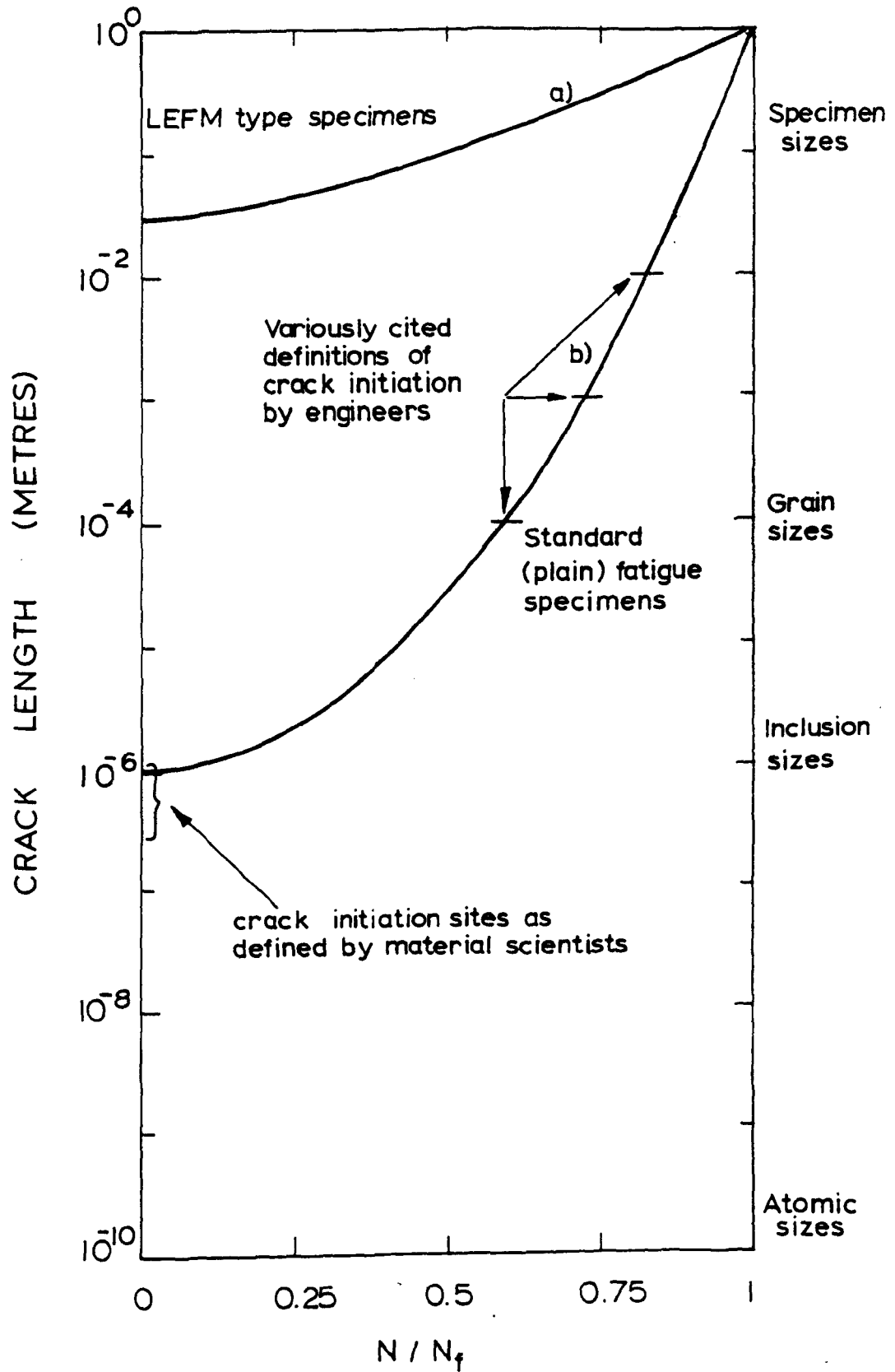


FIGURE 1.3 - The stress intensity field at a crack tip



Reproduced from reference [21]

FIGURE 1.4 - The growth of cracks during fatigue of a) pre-cracked and b) plain specimens

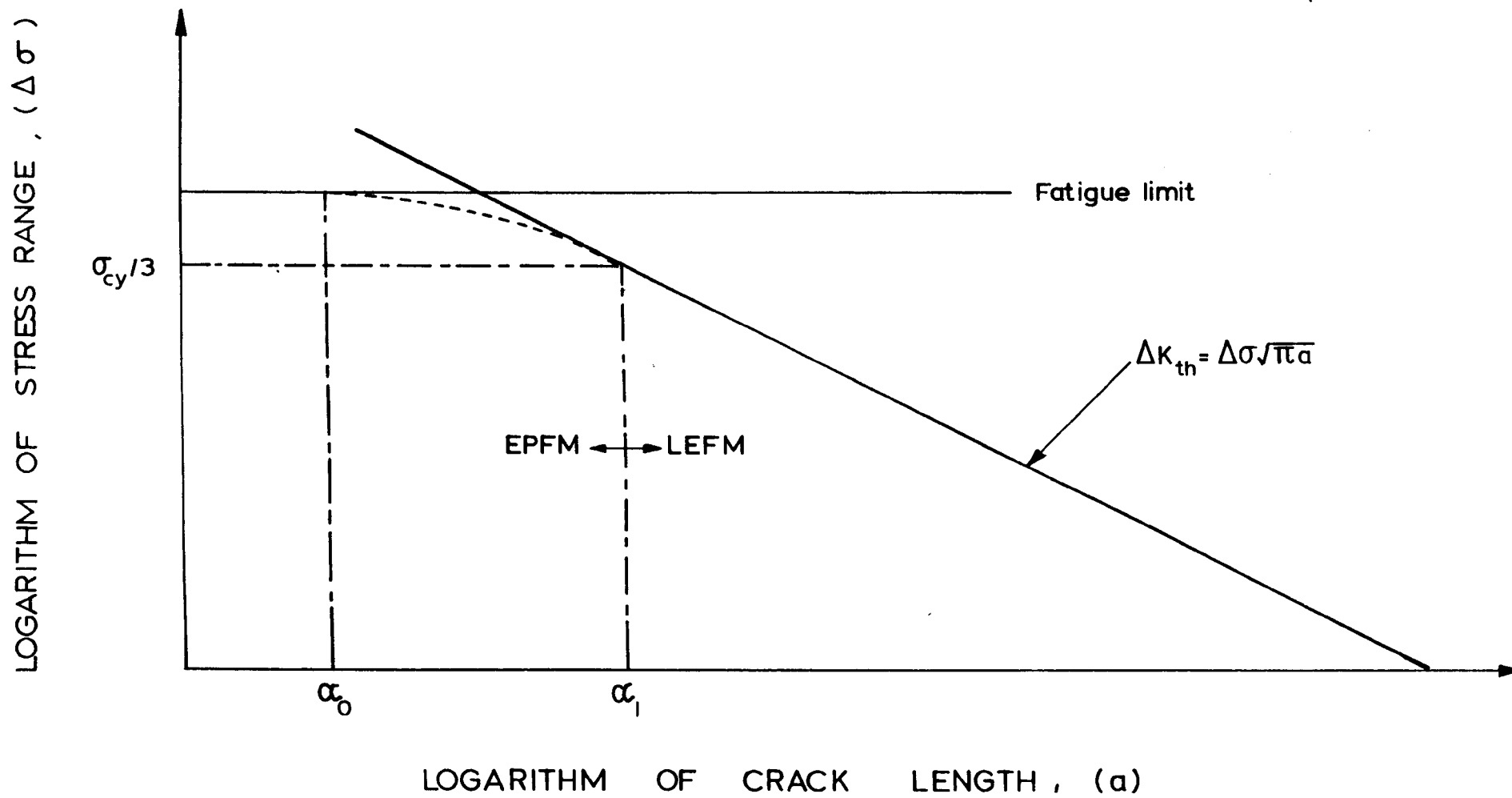


FIGURE 1.5 - Crack growth thresholds for short and long cracks

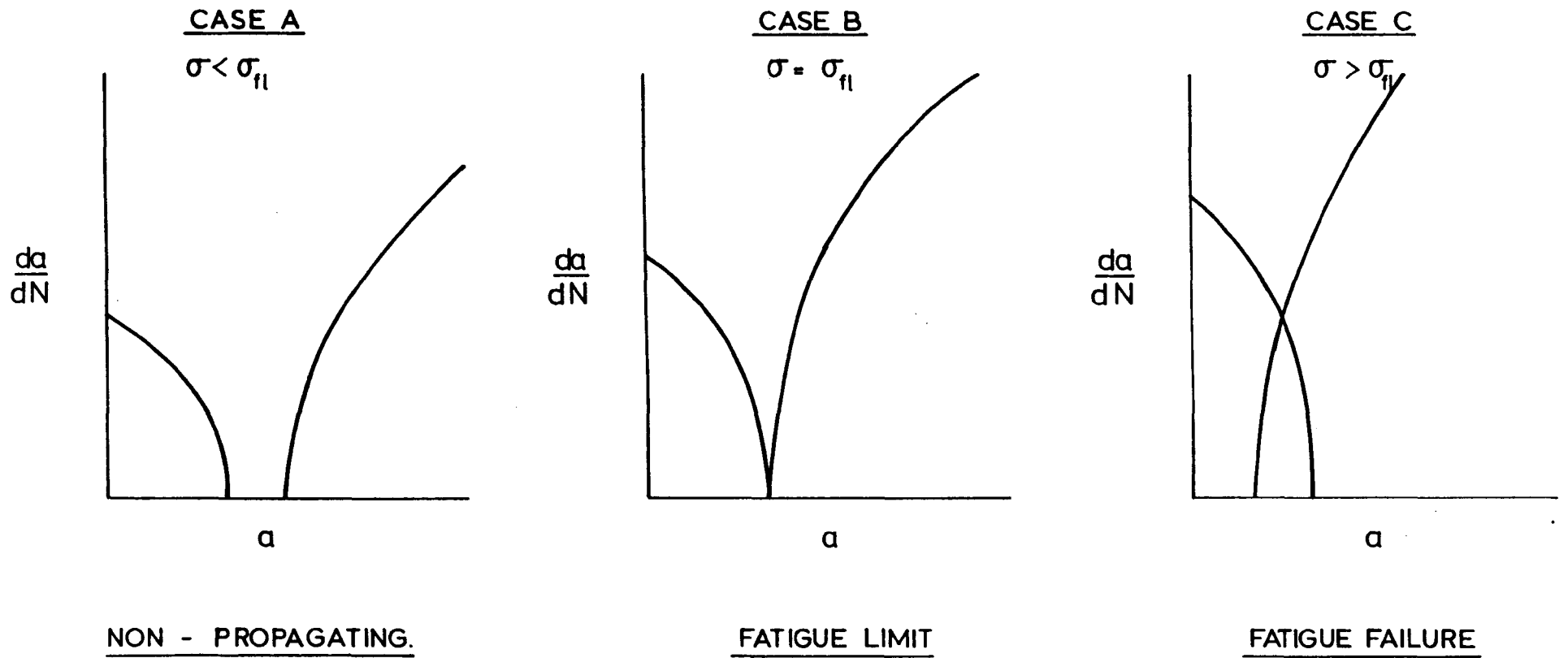


FIGURE 1.6 - Short crack growth behaviour

## CHAPTER TWO

### EXPERIMENTAL WORK

#### 2.1 Material

A medium carbon steel was used for all the tests in this study. The chemical composition of the steel is shown in table 2.1 and corresponds to the specification for EN8. The mechanical properties are shown in table 2.2. This material is widely used in applications where better properties than those for mild steel are required, but the expense of an alloy steel is not justified. Some typical examples are in the manufacture of dynamos, shafts and railway couplings.

Ingots measuring 73mm in diameter by 500mm in length were cast and subsequently hot extruded to form 21mm diameter bars, from which the specimens were made. During the manufacture of the specimens, the feed rate and depth of the final cuts on the lathe were carefully controlled to produce a good surface finish, and to minimize residual stresses due to machining.

Each individual bar was cut into two pieces (for ease of manufacture of specimens). The specimen identification was of the form nXY, where n is either 1 or 2 depending on which half of the bar was used, X denotes the position of the specimen in relation to the bar, and Y designates the particular bar used. In this study only three bars were used so Y was either A, B or

C. This method of identification can be seen in table 3.1, column 1.

After testing, some specimens were cut into sections, mounted, and then etched to reveal the microstructure (shown in figure 2.1). For this material measurements of the prior austenite grain size were made using the method of linear intercepts, from which the average grain size was calculated to be 71 $\mu$ m and the average ferrite band was 97 $\mu$ m in length.

## 2.2 Test Machine

A Mayes machine of the electro-hydraulic servo-controlled type with a static load capacity  $\pm$  250 KN was used for the push-pull fatigue tests. (see figure 2.2).

Three modes of control are available for testing, namely load, position or strain control. A signal generator is able to provide three different waveforms, square, sinusoidal or triangular, at frequencies of 0.02Hz - 180Hz.

A drawing of the grips is shown in figure 2.3, which were designed with the aim of avoiding backlash when going from tension to compression loading and ensuring good alignment of the specimen with the loading system.

### 2.3 Specimen Design and Preparation

A specimen having a mild hour glass profile, as shown in figure 2.4, was chosen for the test programme. It was decided to use this profile partly to enable the strain to be measured and controlled at the minimum section, but mainly because the use of hour glass shaped test pieces limits the area of crack growth to the central region of the specimen, thus restricting the area needed to be replicated for determining crack lengths.

After manufacture of the specimens a Morrison specimen polishing machine (which enables longitudinal polishing), was used to remove the machining marks with 400 grit rough polishing paper. Next, the specimens were heat treated to remove any residual stresses which may have resulted from manufacture or from the rough polishing stage. During this process, the specimens were placed in a furnace (pre-heated to a temperature of 575°C) for one hour. The furnace was then switched off and the specimens were left inside to cool slowly over the next twenty four hours. Care was taken to prevent decarburization by coating the specimens with "Berkatekt 29" prior to heat treatment.

Finally, the specimens were repolished along the gauge length. This involved using progressively finer grit paper, alternately in longitudinal and circumferential directions, ending with circumferential polishing from a 1200 grit paper.

By altering the polishing direction at each stage it was possible to polish out scratches from the previous stage.

Surface roughness measurements were determined using a perthometer. Average readings for  $R_a$ , the centre line average, and  $R_t$ , the roughness depth, were 0.028 and 0.4 $\mu$ m respectively.

Some specimens were then polished with 1 micron diamond polishing liquid to obtain a "mirror finish", thus permitting an examination of the microstructure after etching. A 4% Picral solution was used for initial etching followed by 0.5% Nital solution, both etchants being applied for one minute at ambient temperature.

#### 2.4 Extensometry

To provide the facility for performing tests in strain control in addition to load control, it was necessary to design an extensometer. Because of the hourglass shaped specimens used in this work, only a small region of the working section at the minimum diameter is subjected to maximum stress during testing, so the only possible way of making accurate strain readings is to measure diametral strain rather than axial strain. Therefore any extensometer used in the tests must be of the diametral type, which has a disadvantage that axial strain must be calculated as it cannot be measured directly.

In deriving the formula connecting diametral and axial

strain, first consider the two constituents of diametral and axial strain:-

for axial strain:-

$$\begin{aligned}\epsilon_t^l &= \epsilon_e^l + \epsilon_p^l \\ &= \sigma/E + \epsilon_p^l\end{aligned}\quad (2.1)$$

for diametral strain:-

$$\begin{aligned}\epsilon_t^d &= \epsilon_e^d + \epsilon_p^d \\ &= \nu_e \sigma /E - \nu_p \epsilon_p^l\end{aligned}\quad (2.2)$$

where subscripts t, e & p refer to total, elastic and plastic respectively and superscripts l and d refer to longitudinal and diametral strain.

Here E is Youngs Modulus,  $\nu$  is Poissons ratio, and  $\sigma$  is the longitudinal applied stress, calculated as load divided by minimum cross sectional area. For this specimen the stress concentration caused by the hourglass shape is very small, having an elastic stress concentration of 1.02.

Combining equations 2.1 and 2.2 and using stress and strain ranges together with the plastic Poissons ratio of 0.5 for constant volume plastic deformation,

$$\Delta \epsilon_t^l = 2 \Delta \epsilon_t^d + \left( \frac{\Delta \sigma}{E} \right) (1 - 2\nu_e) \quad (2.3)$$

It can be seen from the above equation that even where the diametral strain range is kept constant, the axial strain will vary as the material either cyclically softens or cyclically hardens. For one which hardens the load range increases as the test progresses which will cause the axial strain range to increase. For the material used in this study which cyclically hardened, stabilization of the load took place early on in the test so it was decided to use diametral strain control directly, without the requirement of a separate strain computer to keep the axial strain range constant throughout the test.

The design of the extensometer employed in the test is shown in figure 2.5 and a photograph showing the extensometer set up is shown in figure 2.6. Expansion or contraction at the minimum diameter causes the two support arms to rotate about the hinge resulting in relative motion of the L.V.D.T. (linear variable differential transformer transducer body and core).

For a diametral extensometer it is necessary to have a method of keeping the sensor at the minimum diameter, since the centre of the specimen is constantly changing position due to

movement of the actuator ram. To solve this problem the extensometer was supported by a system of eight identical axial springs. For ease of movement avoiding inertial effects the extensometer should be light, so the support arms were made out of aluminium. To eliminate the possible problem of transducer wear on an aluminium support arm, a steel screw was introduced at a position directly opposite the transducer. This also made it easier to zero the strain reading prior to starting the test by adjusting the screw, after the transducer had been locked into position.

The hinge was a piece of shim steel held between aluminium blocks in a rigid sandwich formation, so that the arms could only rotate about the middle of the hinge. To oppose the internal spring in the core of the transducer, a diametral spring was added. The tension in this spring should be just enough to ensure that the knife edges remain on the specimen during the tension part of the cycle. Excessive pressure on the specimen can lead to serious indentation from the knife edges which would cause specimens to fail prematurely.

Diametral strains as opposed to axial strains are much smaller, but the design alleviates the problem to some extent since displacements measured by the transducer are a magnification of those experienced at the knife edges because of the lever ratio.

Although tests were performed in a temperature controlled laboratory the extensometer was found to be sensitive to very small variations of temperature due to the cycling of the air conditioning unit. Therefore to compensate for the thermal expansion of the specimen and other parts of the extensometer one knife edge was made from steel and the other from perspex, being materials chosen to provide the required thermal expansion coefficients. To ensure a constant temperature at all parts of the extensometer, a perspex box was built to enclose the extensometer during testing.

Calibration of the extensometer was performed on the test machine using a range of slip gauges in place of the specimen.

## 2.5 Experimental Techniques

### 2.5.1 Crack Detection

Several methods of crack detection have been cited in the literature. Widely used are the methods of potential drop (using either A.C. or D.C. currents), ultrasonics, microscopical observation, and compliance measurements.

In the D.C. potential drop method, a constant current is passed through a specimen by means of leads attached at points remote to the area of cracking. The potential drop across the crack is monitored continuously by leads spot welded close to the crack [1]. As a crack grows the specimen's resistance

increases thereby increasing the potential drop.

The ultrasonic technique uses the fact that high frequency waves transmitted from a transducer into a test specimen are partially reflected from discontinuities such as a crack surface, which enables crack detection [2].

All of these methods except direct observation are more suited to measuring long crack growth in a notched specimen than to short crack growth measurements because short cracks ( $<200\mu\text{m}$ ) either cannot be detected at all, or are not able to be measured accurately.

Furthermore, these methods cannot distinguish between a number of different cracks growing in one area. For example, voltage readings cannot correlate the amount of damage since for tests on a plain specimen several cracks of comparable length may be present very early in the fatigue life and consequently electrical methods are no use in determining individual crack lengths.

A method of crack detection using an optical microscope could be used which has the advantage of direct observation. Disadvantages in this method are the inability to measure crack depths and the requirement of making frequent observations, a most time consuming operation. Also for the round specimens used in this project, there is the need to use low magnifications to obtain sufficient depth of focus.

### 2.5.2 Plastic Replication

Because of the afore-mentioned problems with several crack measurement techniques, a method of plastic replication of the specimen surface was adopted. This method has been widely used in crack growth studies, for example in references [3] and [4].

Several types of replicating material with suitable solvents are available, the most common type being acetate sheet with acetone used as a solvent. The acetate sheets are manufactured in various thicknesses, the selection of which depends on the application required. For situations where access to the area of interest is restricted a thick sheet should be chosen as it can be manipulated more easily than thin sheet which tends to break up when slight pressure is applied to them. However, for this test programme access to the specimen surface was relatively unrestricted and so a thin sheet was used as it was found to give the most faithful reproduction of the specimen surface. Also the thin material, because of its greater flexibility, lay rather flatter when attached, by adhesive tape, to a microscope slide when making observations, thus enabling higher magnifications.

A sheet of replicating material was cut into strips of about 10mm in width, and 25mm in length. The top of a strip was then held by tweezers while acetone was sprayed onto one side of the strip for a couple of seconds. (Care was taken not

to moisten the part which was held by tweezers, otherwise the strip became attached to them). The strip was then quickly held against the specimen and surface tension drew the replica onto the surface as the sheet was wrapped round the gauge length. With practice the replica will adhere to the specimen without any problem of air bubbles or buckling. After five minutes the replica was dry and could be removed with tweezers. Finally the replica was attached to a microscope slide by adhesive tape for observation at magnifications of x100 and x400. A moving microscope stage was used to measure the crack lengths.

For each test replicas were taken for at least seven stages of life but as interest was in the growth of short cracks, replicas were taken more frequently in the early stages. This required the fatigue test to be stopped, and a tensile load (equivalent to the maximum tension during cycling) applied so that the cracks were open during replication. Two replica strips were then applied to the surface, one at the front side and one at the back side of the specimen. This was repeated four times giving eight replicas for each stage.

This procedure required the test to be stopped for about forty minutes per stage, or about five to six hours per test. The effect of these rest periods on the fatigue life was examined by keeping one test running continuously (test 2CB). The resulting lifetime was found to lie between the minimum and maximum lifetimes for specimens tested at the same stress but

subject to rest periods. This suggests little effect of the forty minute rest periods on fatigue life although rest periods are known to effect the fatigue endurance [5].

Replicas from surfaces of etched specimens required special treatment to be able to see metallurgical features. This involved shadowing the replica with gold palladium at an angle from the vertical to show up the slight irregularities on the replica surface, and then coating the replica with carbon. A vacuum chamber was used for the shadowing and coating procedures. Some replicas were then observed in the Scanning Electron Microscope at 6Kv with a spot size of 0.25 m, but features were not always easily seen at low voltages, and increasing the voltage tended to damage the replica.

To help with the location of replicate cracks each specimen was marked with a scalpel at positions one centimetre from the specimen's minimum cross section. These marks were reproduced on the replicas, and helped greatly in finding a particular crack over a range of replicas. As these scratches were not made at the minimum cross section, cracks did not often grow in close proximity to them. Even when cracks were observed to grow across the scratch marks, they did not seem to be influenced, and failure cracks were never observed to initiate from the scratch marks. Another technique used to find the cracks on the replicas, was to first examine replicas taken in the later stages of a test. Cracks are easier to locate on these replicas due to their longer length, then the

cracks are followed through their lifetime looking at these precise locations on the replicas from previous stages.

Disadvantages of using the replica technique are:-

- 1) Rest periods must be introduced, due to the requirement of having to stop tests to take replicas.
- 2) Replicas cannot give a continuous record of crack growth.
- 3) This method cannot be automated unlike the electrical methods.
- 4) Crack depth cannot be measured.
- 5) Debris is removed from the crack during the replication process.
- 6) Acetone or other solvents may affect crack growth.

However, after taking into account the deficiencies in the other methods mentioned in section 2.5.1, replication provides the only realistic way of studying short crack growth, and it produces a library of information available for future study.

## 2.6 Failure Criteria

For load controlled tests failure was defined to be the instant when the specimen broke into two pieces. When a crack is propagating across a specimen, the stress increases due to reduced cross-sectional area, and in the latter stages of a test this propagation will be very rapid close to rupture. However, in the case of strain controlled testing, as a crack

grows the load reduces which extends the time necessary for complete separation to take place. This means that a large crack may be present for quite some time due to the decreasing load. When the load does noticeably decrease it may be argued that since the specimen's load carrying capacity has been greatly reduced the specimen should be deemed to have "failed".

Because of this situation in strain controlled tests it is usual to define failure at that instant of a given percentage of load drop, rather than the breaking into two parts of a specimen.

This is usually chosen as a 1 or 5% load decay, although ideally the moment the load decay begins to take place is a more realistic than an arbitrarily chosen percentage. However, the exact location of the beginning of the load drop off was too difficult to locate accurately, and therefore, a 5% drop off in load was chosen as the failure criterion in strain controlled tests.

## 2.7 Test Programme

The test programme was divided into the following three stages:-

### Stage 1

Fifteen tests were performed in strain control using the extensometer to obtain fatigue lifetime data, over a

range of lifetimes from a few hundred cycles to several thousand cycles. Testing was conducted in fully reversed loading ( $R = -1$ ) at frequencies between 0.06Hz-1Hz with a triangular loading waveform. For each test the load and transducer readings were monitored continuously by means of a chart recorder, and periodically monitored using a data-logger. Hysteresis loops were also recorded at frequent intervals during testing.

### Stage 2

Three load ranges were chosen to give lifetimes of approximately 1,000, 6,000 & 30,000 cycles. Tests were then performed in load control, and interrupted periodically to enable plastic replication of the specimen surface.

Several tests per load range were carried out to enable a number of cracks to be studied for each range. Tests were again conducted in fully reversed loading ( $R = -1$ ) for a triangular waveform, at frequencies between 0.016Hz-0.3Hz. The load signal was monitored continuously using a chart recorder, and periodically by means of the data-logger.

### Stage 3

In order to determine a value for  $\Delta K_{th}$ , a crack was grown from a notched specimen, with crack growth rates being determined using a direct current potential drop system.

Two specimens of the same design as those used in the fatigue

test programs had notches inserted by spark erosion using a 0.1mm diameter wire which produced a notch with a depth of 1mm.

In these tests a potential drop system with a constant current of 20 amps was passed through the specimen from a position remote to the notch, and potential drop leads were attached to measure the voltage across the notch, which was monitored periodically by the data-logger.

Testing was done in fully reversed tension - compression loading at a frequency of 1,000 cycles per minute (16 $\frac{2}{3}$ Hz) with a triangular waveform. The load range was gradually increased until crack growth could be detected, and then reduced until no further crack growth was observed over a period representing a crack growth rate of less than  $5 \times 10^{-6}$   $\mu\text{m}/\text{cycle}$ . At this stage a value for  $\Delta K_{th}$  was calculated. All increases or decreases in the load range were incremental, and before a reduction in load took place the crack was allowed to grow of its induced plastic zones created by previous loadings.

After determining a value for  $\Delta K_{th}$ , the load range was increased to allow the crack to start growing again. When the crack had grown to a length of approximately 3mm the test was stopped and the specimen removed from the machine and broken open in liquid nitrogen. The length of the crack was then measured using a travelling microscope.

A second notched specimen was used to obtain further crack

growth data, from which values of stress intensity  $\Delta K$  versus crack growth rate were obtained.

Results of the test programme are presented in Chapter Three.

CHAPTER TWO - REFERENCES

- [1] HAY, E. & BROWN, M.W. (1981)  
"A D.C. potential drop method to monitor crack growth  
in notches subjected to torsion"  
Fatigue Engng. Mater. Struct. 4 p.287-290
- [2] KILMA, S.J. FISHER, D.M. & BUZZARD, R.J. (1976)  
"Monitoring crack extension in fracture toughness tests  
by ultrasonics"  
J. Test. Eval. 4 p.397-404
- [3] HUNTER, M.S. & FRICKE, W.M.G. Jr. (1956)  
"Fatigue crack propagation in aluminium alloys"  
proc. ASTM 56 p.1038-1046
- [4] LANKFORD, J. & BARBEE, J.G. (1974)  
"SEM characterization of fatigue crack tip deformation in  
stainless steel using a positive replica technique"  
J. Mater. Sci. 9 p.1906-1908
- [5] MILLER, K.J. & HATTER, D.J. (1972)  
J. Strain Anal. 7 p.69-73

## CHAPTER TWO - TABLES

- 2.1 Chemical composition
- 2.2 Mechanical properties

## CHAPTER TWO - FIGURES

- 2.1 Microstructure
- 2.2 Fatigue testing machine
- 2.3 Grip design
- 2.4 Specimen design
- 2.5 Extensometer design
- 2.6 Extensometer set-up

TABLE 2.1

Chemical Composition (% WT)

C	Si	S	P	Mn	Fe
0.4	0.10	0.001	0.005	1.00	Bal

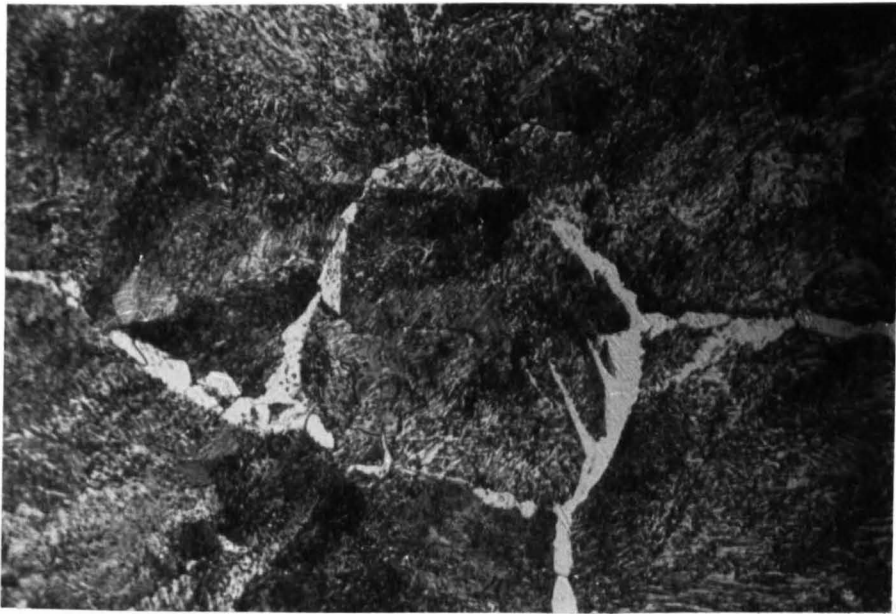
TABLE 2.2

Mechanical Properties

Yield Strength $\sigma_y$ (MPa)	Upper Tensile Strength $\sigma_u$ (MPa)	Reduction in Area $U$ (%)	Elongation to Fracture $e_f$ (%)
392	683	35.86	44.41



x 100



x 500

FIGURE 2.1 - MICROSTRUCTURE

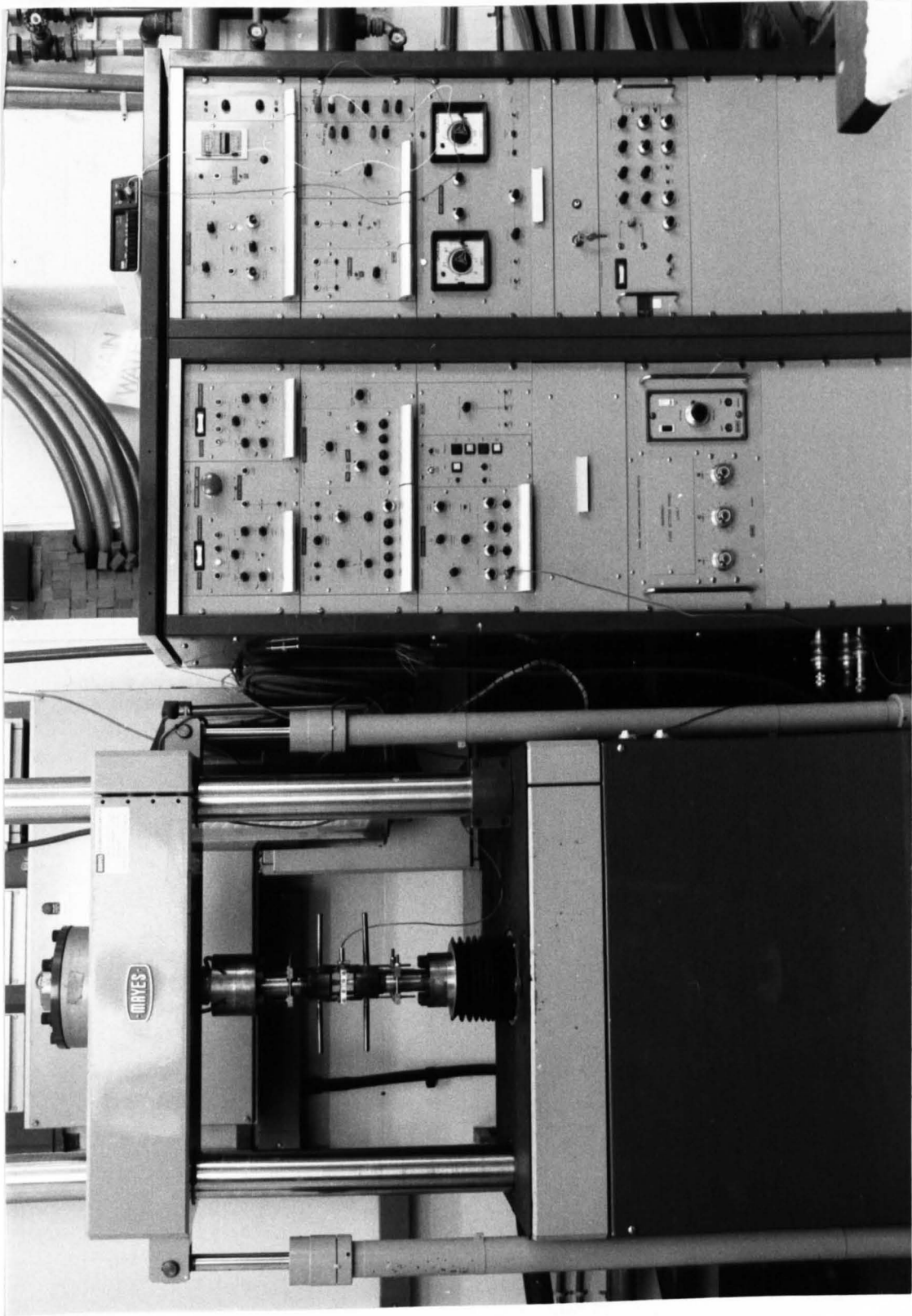


FIGURE 2.2 - FATIGUE TESTING MACHINE

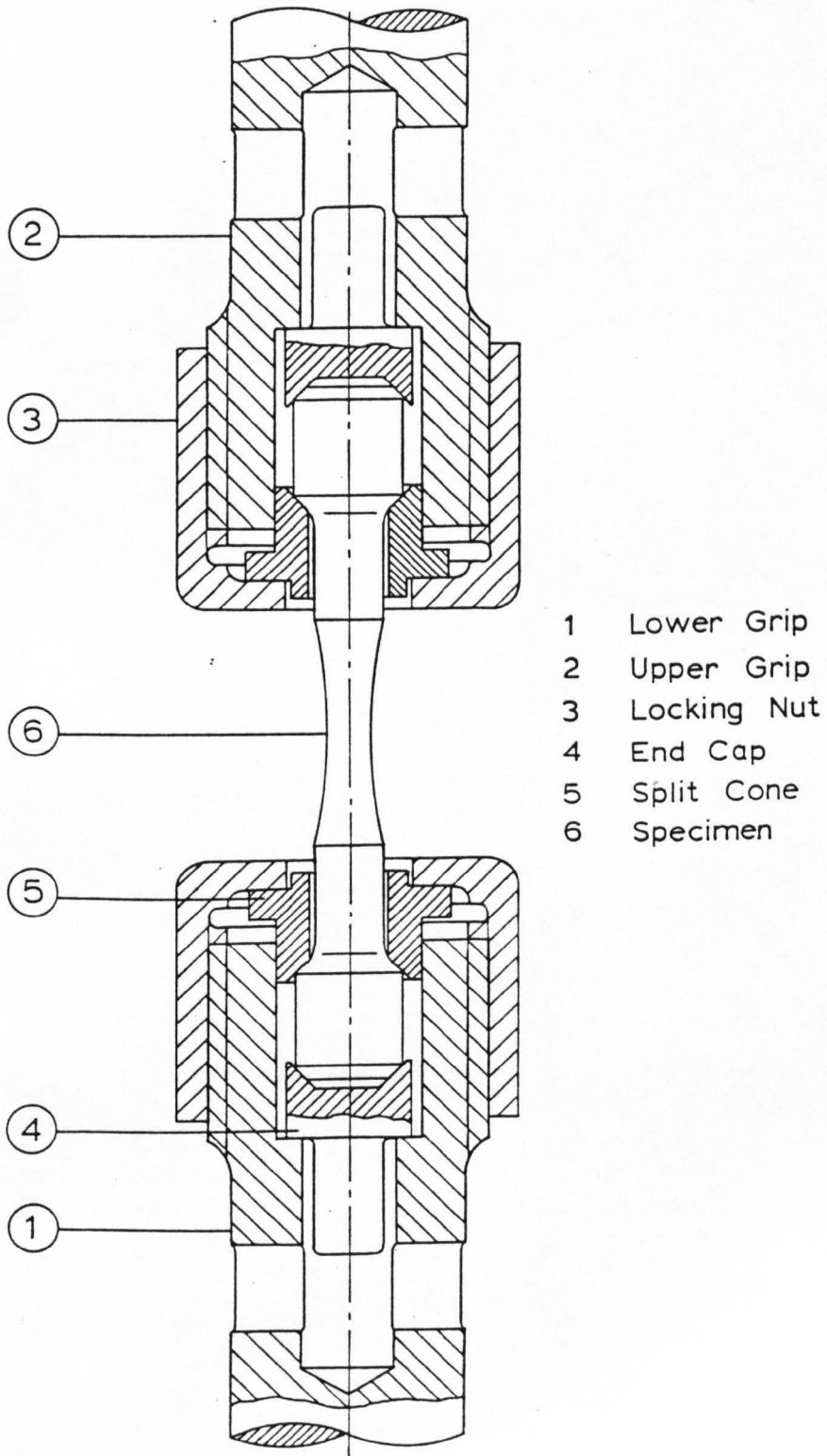


FIGURE 2.3 - Grip design

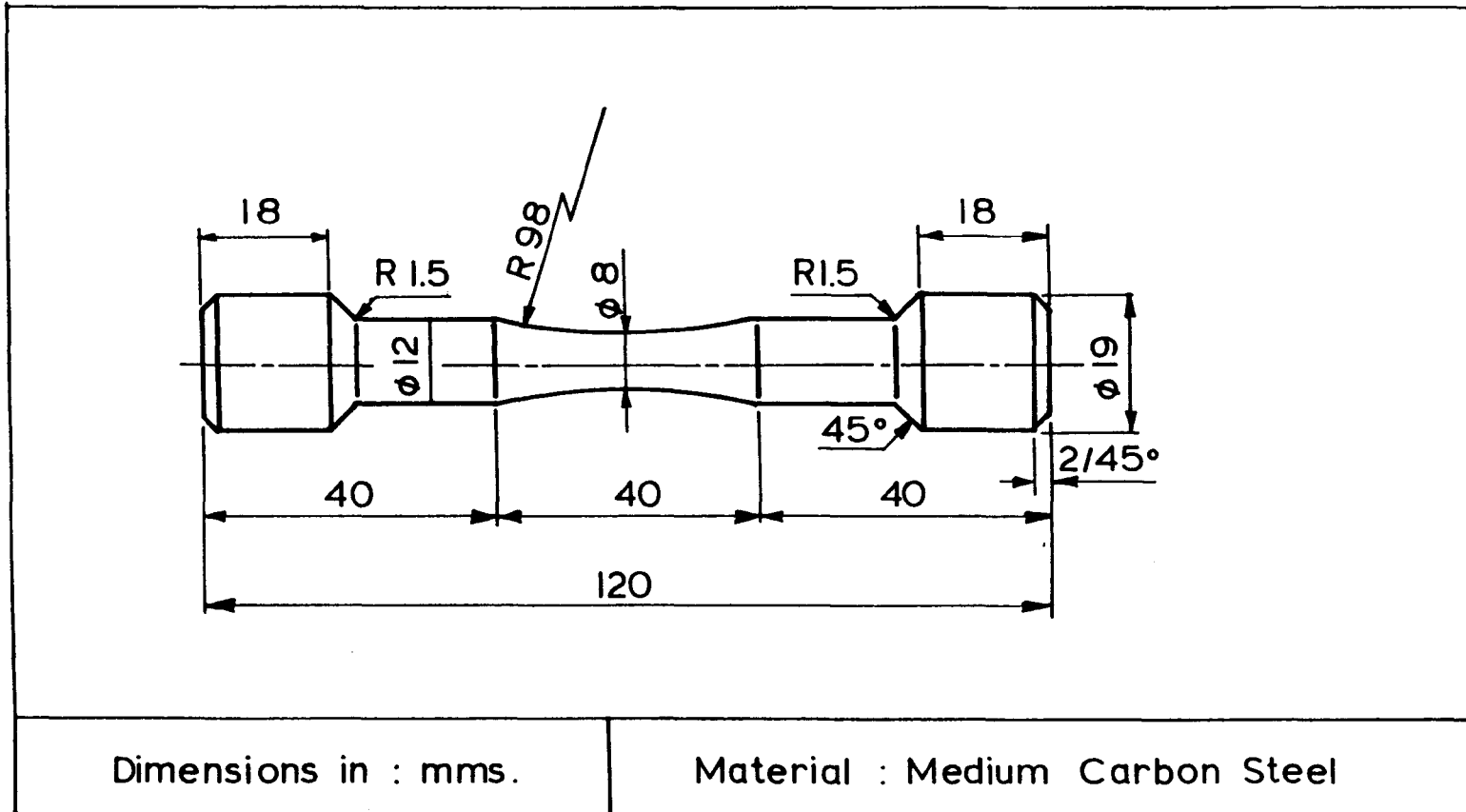


FIGURE 2.4 - Specimen design

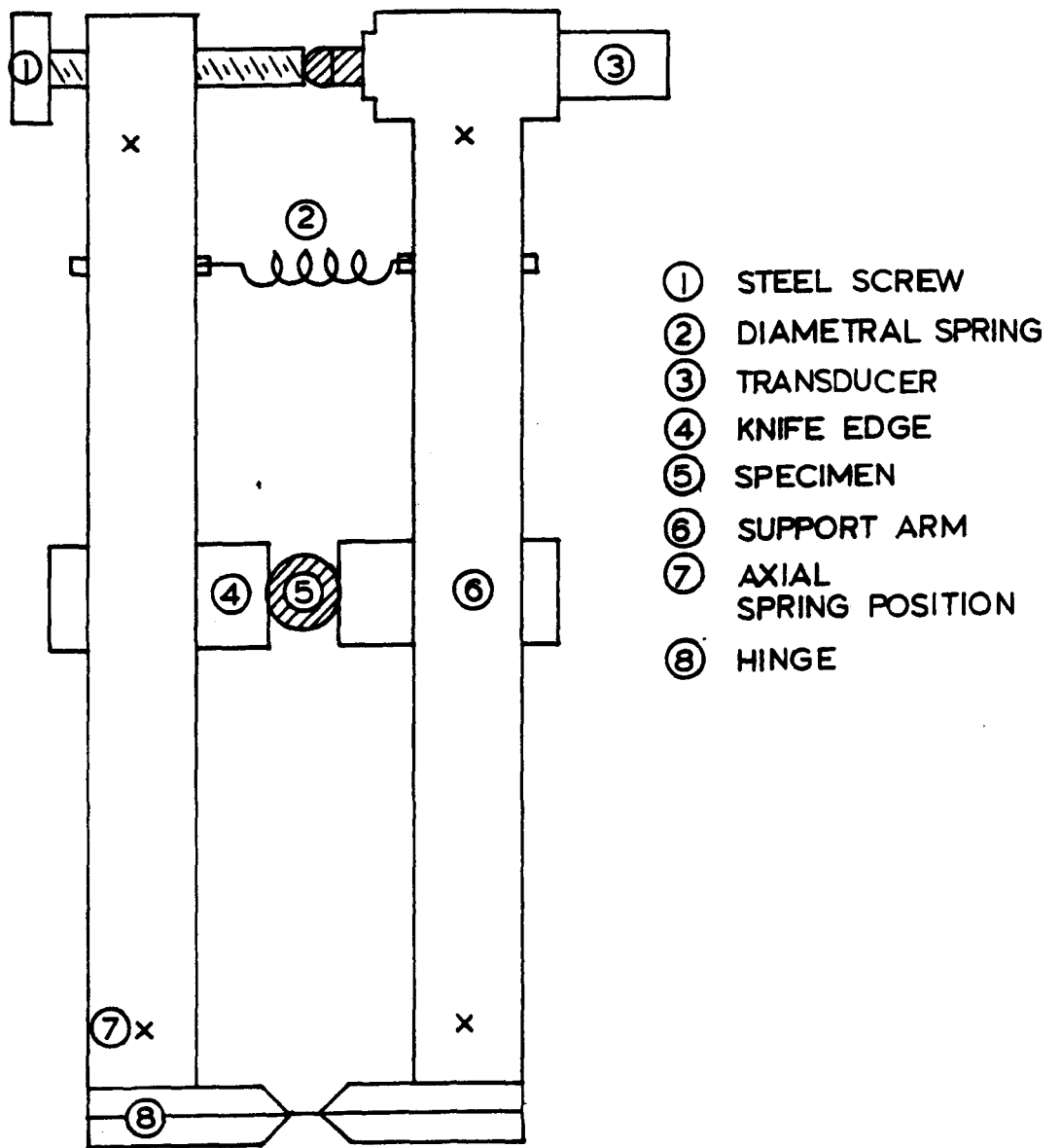


FIGURE 2.5 - Extensometer design

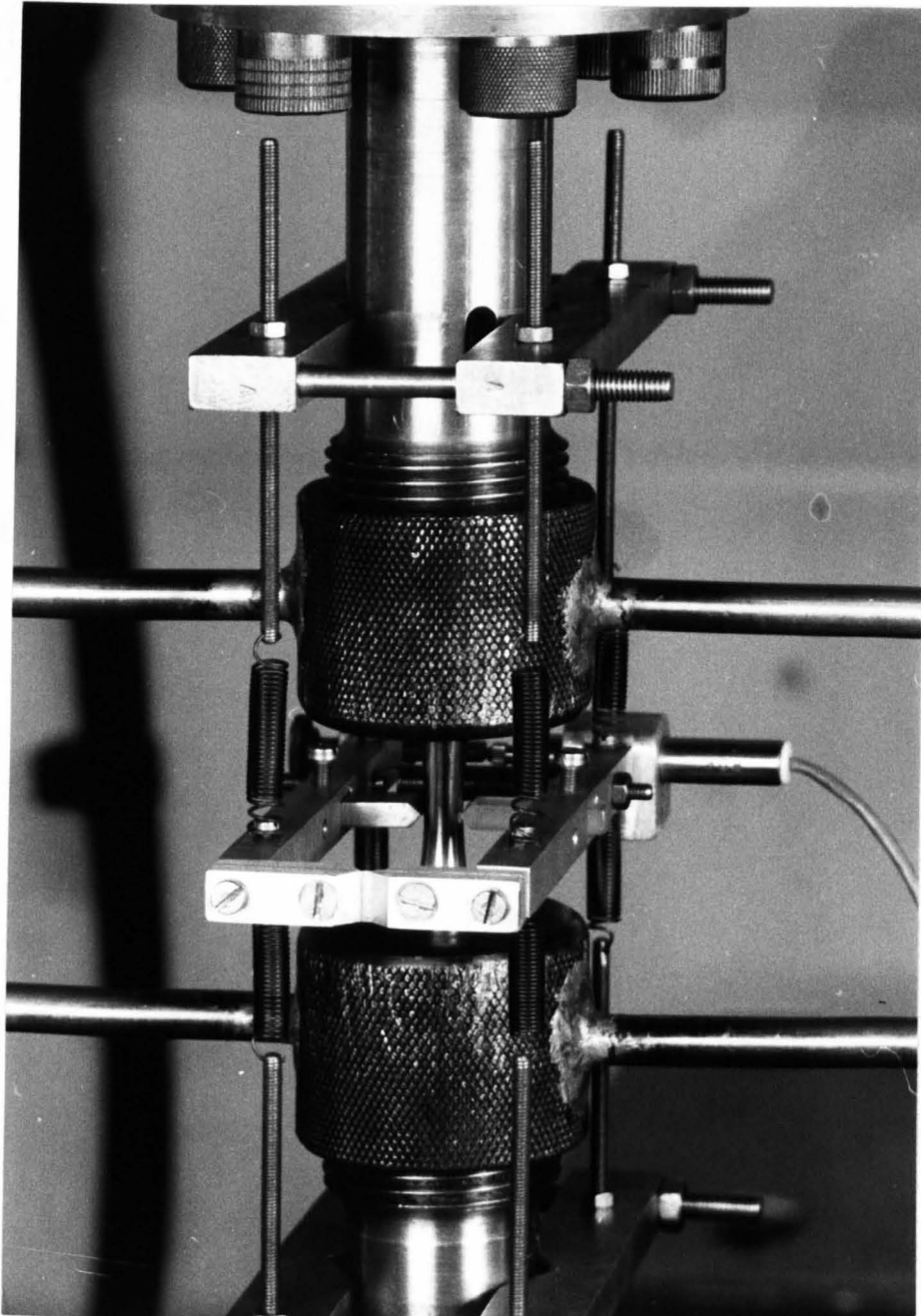


FIGURE 2.6 - EXTENSOMETER SET-UP

52B

## CHAPTER THREE

### RESULTS

#### 3.1 Fatigue Tests

##### 3.1.1 Stress-Strain Behaviour

The results of Stages 1 and 2 of the fatigue test programme described in section 2.7 are given in table 3.1. For strain controlled tests the load was taken to be the maximum load recorded in a test after the initial shake down period was completed involving cyclic softening at low strains and hardening at high strains.

For most of the load controlled tests intermittent plastic replication of the surface was performed. This would have necessitated the removal of the extensometer every time a replica was required, but because of the difficulty in dismantling and assembling the extensometer, maybe six or seven times during a test the extensometer was not always used. In these cases strain ranges were not measured.

The total longitudinal strain range was calculated from the total diametral strain range using equation 2.3 with  $E = 203$  GPa and  $\nu_e = 0.30$ . This can then be used to find the longitudinal plastic strain using equation 2.1.

One specimen was used in a multiple step test, for which

results are shown along with the fatigue test data in Figs 3.1 and 3.2. Figure 3.1(a) shows the resulting stress-strain response plotted on a linear scale, while figure 3.1(b) replots the data on a logarithmic scale from which a least squares best fit gave an equation connecting the stress range (in MPa) and the total longitudinal strain range of the form

$$\Delta\sigma = 3148 \Delta\epsilon_t^{0.315} \quad (3.1)$$

For the best fit line only data for  $\Delta\sigma > 450$  MPa was taken into consideration, due to the significant deviation from linearity at low stresses, around and below yield. Also shown in this figure is the line representing the linear elastic response.

Figure 3.2 shows the relationship between plastic strain range and stress range plotted on a logarithmic scale. A best fit to the data is given by the equation

$$\Delta\sigma = 2013 \Delta\epsilon_p^{0.190} \quad (3.2)$$

where stress is in MPa.

### 3.1.2 Fatigue Behaviour

Figure 3.3 is a plot of strain range versus the number of cycles to failure for both plastic and total strain ranges. As mentioned in section 2.6, for the strain controlled tests a 5% load drop off was defined as failure whereas complete separation was the definition of failure for load controlled tests. The best fit line to the results for plastic strains shown in figure 3.3 is given by the Coffin-Manson relationship:-

$$\Delta \epsilon_p N_f^{0.673} = 2.23 \quad (3.3)$$

where  $N_f$  is the number of cycles to failure.

A similar equation can be derived for total strains.

$$\Delta \epsilon_t N_f^{0.384} = 0.320 \quad (3.4)$$

although this cannot be extrapolated to high cycle fatigue where the elastic strain term is dominant. However, by using stress range rather than strain range the Basquin relationship can be derived given by the equation:-

$$\Delta\sigma N_f^{0.137} = 2553 \quad (3.5)$$

A plot of stress range versus cycles to failure is shown in figure 3.4. Equations 3.3 and 3.5 may be combined to obtain a more useful endurance equation than equation 3.4 for total strain range,

$$\Delta\varepsilon_t = \frac{2553}{E} N_f^{-0.137} + 2.23 N_f^{-0.673} \quad (3.6)$$

which is shown in figure 3.3.

But even this relationship which is widely used, cannot be extrapolated beyond  $10^6$  cycles to failure because of the characteristic knee observed in S-N curves for carbon steels.

### 3.2 Crack Growth Results

The crack growth results from the three sets of tests carried out at stress ranges of 638.5 MPa, 815.9 PMa and 998.4 MPa are shown in tables in Appendix 1.

For each table, column 4 represents the number of cycles completed in a test when it was temporarily stopped to enable replication of the surface. The measured surface crack length ( $a_s$ ) at each stage of this replication is shown in column 5, which was taken to be the linear distance between the two crack tips.

Columns 8 and 9 refer to the change in crack length  $\Delta a_s$  and number of cycles  $N$  respectively between two successive replica stages. For this interval, the mean rate of crack growth can be calculated as a simple fraction, which is shown in column 10. Because this crack growth rate is more representative of the speed of the crack at a crack length halfway between the two stages, a mean value of crack length,  $a_{s,mean}$ , is also calculated as shown below:

$$\begin{aligned}
 a_{s,mean} &= \frac{a_{s,i} + a_{s,i-1}}{2} \\
 &= a_{s,i} - \frac{\Delta a_s}{2}
 \end{aligned}$$

where  $a_{s,i}$  is crack length at the current stage  
 $a_{s,i-1}$  is crack length at the previous stage.

Values of  $a_{s,mean}$  are shown in column 11, which are used in conjunction with crack growth rates in the analysis presented in the next chapter.

Cracks less than about 30 microns in size were difficult to measure and the results shown in Appendix I only record cracks when they could be found and measured with reasonable accuracy. At very short lengths where the crack is both short and narrow it is difficult to distinguish the crack from other microstructural features. The first recorded length for each crack was not always derived from the first replica because of

this problem. Other readings of crack length which could not be recorded included cases where the crack ends were difficult to locate, or where occasionally a gap seemed to exist in the middle of a crack which may have been due to a poor impression of the surface.

Figure 3.5 shows the growth pattern for a particular crack (test 18 crack No. 1), which is illustrated by a series of photographs in figures 3.6a - 3.6f. For this crack, figure 3.6a shows the crack beginning to grow at an angle of about 45 to the specimen axis. When it had reached a length of 86 microns both ends of the crack changed their direction, (figure 3.6d), and by the time the crack was 294 microns long the growth was perpendicular to the stress axis. At a crack length corresponding to the time when both ends of the crack changed direction the crack growth rate slowed down considerably, as observed in figure 3.5. This behaviour was typical of most cracks which showed rapid initial growth followed by a period of retardation and subsequent accelerating growth.

For those cracks which did not show the initial rapid growth before a period of slowing down, in all but one case (test 28 crack No. 5) over a quarter of the fatigue life of the specimen was completed before the crack was detected. This suggests that the crack may have already completed the first stage of the typical growth pattern before it was detected.

In order to try to determine whether or not the slowing down

of cracks was due to microstructural features some specimens were etched to reveal the microstructure. It was then noticed from replicas which had been coated (as described in section 2.5.2) that small cracks propagated in the ferrite plates which surrounded the prior austenite grain boundaries, see figure 2.1. After initiation in the ferrite, the crack continued its growth along the ferrite plate until the end of the plate was reached. At this point the crack propagated through the adjoining ferrite plate situated along the next austenite grain boundary, which usually involved a change in direction. To reach the next ferrite plate it was often necessary to propagate into the pearlite. After traversing the next ferrite plate the crack growth then continued along the ferrite plate to fracture. The point at which a crack slowed down corresponded to the crack reaching the end of the ferrite plate in which it was initiated.

In order to show these details clearly in a photograph, a specimen was etched and then fatigued for about one third of its lifetime. The test was then stopped and the specimen removed. Before photographing, the specimen surface was lightly polished with diamond grit and re-etched to show the cracks more clearly.

Four cracks produced in this test are shown in figures 3.7a - 3.7d. In figure 3.7a a crack is beginning to grow within one ferrite plate. Figure 3.7b and 3.7c show cracks which have grown a distance of one whole plate, and figure 3.7d shows a

crack changing direction to grow along the next plate of ferrite.

Figures 3.8a and 3.8b show photographs of a ferrite plate on the surface of an etched specimen at a magnification of x 8800- taken in a scanning electron microscope. The ridges in the photograph reveal the lamellar pearlite structure with the smooth area being the ferrite.

Some more observations can be made about the pattern of crack growth. Those cracks which did experience a slowing down of the crack growth rate did not all slow down to the same rate, which could be a result of the relative ease of initiation compared to how favourable the orientation of the next ferrite plate is for continuing crack growth.

Certain cracks showed a second period of retardation in crack growth rate, although this was not usually as pronounced as the first; this effect was probably related to the crack having traversed two ferrite plates prior to moving on to the next one.

At the end of life some cracks seemed to have arrested, becoming non-propagating (eg, test 19 crack No 1), but it may be that the fatigue life of the specimen was exhausted (due to another crack causing failure), before these cracks had time to propagate to the next ferrite plate.

From surface observations, those ferrite plates which initiated cracks intersected the surface at an angle between  $45^\circ$  and the normal to the stress axis. This range of angles for surface crack growth is to be expected for a stage I crack in tension loading growing at an angle of  $45^\circ$  into the specimen (see figure 1 of reference [1]).

More cracks were initiated in the shorter life tests, and in these tests there was evidence of cracks joining together. Re-orientation of crack growth rarely occurred since for those cracks with branches, the branch didn't grow beyond a few microns and where large branches were found on later replicas, it was always traced back to the merging of two cracks.

For all the cracks recorded, after the period of slowing down the cracks entered a second rapid growth period which implies that a single crack did not dominate life until the very final stage when the "failure" crack propagated to fracture very quickly.

An increase in growth was noticed when cracks joined together, which naturally occurred more frequently as cracks increased in length towards the end of a test. At the very end of life fracture often was the result of two or more cracks joining together.

### 3.3 Threshold Tests on Notched Specimens

Fatigue crack growth and threshold data were determined in Stage 3 of the test programme described previously in section 2.7. Results obtained from the threshold test were derived from potential drop readings which needed to be converted into crack lengths.

In reference [2] a relationship is given between voltage  $V$ , and crack length of a central through crack in a wide plate namely:-

$$\cosh (AV) = \sec \left( \frac{\pi a}{2W} \right) \cosh \left( \frac{\pi y}{2W} \right) \quad (3.7)$$

where  $2y$  represents the p.d. lead spacing,  $2W$  is the specimen width and  $A$  is a constant for a fixed current passing through the specimen. This equation assumed that a crack is growing straight; which was shown to be true for these tests after examination of the fracture surfaces. Although specimens used in this study had a circular cross-section, a reasonable approximation should be provided by equation 3.7 if initial and final crack lengths are measured and subsequent crack lengths then calculated by interpolation.

Expanding both sides of equation 3.7 and ignoring fourth and higher order terms:-

$$1 + \frac{A^2 V^2}{2} = 1 + \frac{1}{2} \left( \frac{\pi a}{2W} \right)^2 + \frac{1}{2} \left( \frac{\pi y}{2W} \right)^2$$

which simplifies to:-

$$A^2 V^2 = \left( \frac{\pi a}{2W} \right)^2 + \left( \frac{\pi y}{2W} \right)^2 \quad (3.8)$$

By using two pairs of p.d loads, see figure 3.9, at positions (a) and (b) (corresponding to lead spacing for  $y_a$  and  $y_b$  approximately 1mm and 15mm respectively), with a corresponding pair of voltage readings  $V_a$  and  $V_b$ , substitution into equation 3.8 gives:-

$$\left( \frac{V_a}{V_b} \right)^2 = \frac{a^2 + y_a^2}{a^2 + y_b^2} \quad (3.9)$$

Measured values of  $y_a$  and  $y_b$  may then be used directly in equation 3.9 to derive the crack length. Due to the curvature of the actual specimens, measured values for  $y_a$  and  $y_b$  would not be expected to yield accurate values of crack length.

To overcome this problem the real values of  $y_a$  and  $y_b$  were not used. However, values for  $V_a$  and  $V_b$  were obtained at the beginning and end of the test together with the corresponding initial and final crack lengths of the test resulting in two simultaneous equations (from equation 3.9)

which could then be solved for  $y_a$  and  $y_b$ .

These calculated values for  $y_a$  and  $y_b$  were then substituted back into equation 3.9 which was rearranged to give an interpolation formula for crack lengths throughout the test. Then by using a second order polynomial fit to sets of seven successive data points of crack lengths, (a) versus cycles, (N), the value of crack growth rate  $da/dN$  was determined, following ASTM standard E647.

In order to calculate the stress intensity factor, the standard equation is:

$$\Delta K = Y \Delta \sigma \sqrt{\pi a} \quad (3.10)$$

where Y is a geometry factor. An equation of the form:

$$Y = 16.89 \left( \frac{a}{w} - 0.164 \right) + 0.97 \quad (3.11)$$

provides a good fit to data given in [3] for  $0 \leq \frac{a}{w} \leq 0.56$ , in

which a similar specimen to the one used in my tests was subjected to axial loading (the geometry of the specimen is shown in figure 3.9).

Using equations 3.9, 3.10 and 3.11, a stress intensity factor,  $\Delta K_{th}$ , of  $6.0 \text{ MPa}\sqrt{\text{m}}$  was calculated from the experimental data in figure 3.10. Here threshold was defined as the point

where the crack growth rate was  $10^{-7}$  mm/cycle.

As mentioned in section 2.6, by raising the load after determining the threshold value, low crack growth rate data were obtained for this specimen, and another notched specimen was used to supplement the data. This is also shown in figure 3.10. The spurious points where crack growth rate decreases with increasing  $\Delta K$  are always at the start of a test which is a result of aforementioned anomalies in the growth of short cracks.

Three different symbols are plotted for results from the first notched specimen, which correspond to changes in load range.

CHAPTER THREE - REFERENCES

- [1] BROWN, M.W. & MILLER, K.J. (1979)  
"Initiation and growth of cracks in biaxial fatigue"  
Fatigue Engng. Mater. Struct. 1 p.231-246
- [2] GILBEY, D.M. & PEARSON, S. (1966)  
"Measurement of the length of a central edge  
crack in a sheet of metal by an electrical  
resistance method"  
R.A.E. Tech. Report 66402
- [3] DAOUD, O.E.K. CARTWRIGHT, D.J. & CARNEY, M. (1978)  
"Strain energy release rate for a single edge cracked  
circular bar in tension"  
J. Strain Anal. 13 p.83-89

### CHAPTER THREE - TABLES

#### 3.1 Fatigue tests results

### CHAPTER THREE - FIGURES

- 3.1 a) & b) Stress range versus strain range
- 3.2 Stress range versus plastic strain range
- 3.3 Strain range versus cycles to failure
- 3.4 Stress range versus cycles to failure
- 3.5 Crack growth results (test 2GA, crack no. 1)  
obtained from plastic replicas
- 3.6 a) - f) Photographs of plastic replicas taken at  
different stages of life for one particular  
crack (test 2GA, crack no. 1)
- 3.7 a) - d) Photographs showing microstructural effects  
of short crack growth
- 3.8 a) & b) Photographs of a ferrite plate obtained on a  
scanning electron microscope
- 3.9 Experimental set-up for a D.C. potential drop  
system
- 3.10 Crack growth rate versus stress intensity factor  
for notched specimens

**TEXT  
BOUND INTO THE  
SPINE**

TABLE 3.1

Fatigue Test Results

Specimen Number	Load Range $\Delta P$ (KN)	Stress Range $\Delta \sigma$ (MPa)	Total Strain Range $\epsilon_t$	Plastic Strain Range $\epsilon_p$	Cycles to Failure $N_f$	Type of Control
2BA	57.5	1,128.3	0.03042	0.02487	589	Strain
2CA	50.3	1,101.9	0.02485	0.01942	890	Strain
2FC	43.0	900.4	0.01913	0.01469	1,621	Strain
2DC	41.9	866.0	0.01895	0.01469	2,201	Strain
1CC	38.5	795.8	0.01306	0.00915	2,878	Strain
2HC	37.4	783.1	0.01312	0.00926	4,913	Strain
1BC	36.6	737.3	0.00911	0.00548	8,802	Strain
2AA	33.7	714.3	0.00647	0.00295	18,277	Strain
1EC	25.7	553.5	0.00455	0.00185	51,313	Strain
1DC	24.0	477.3	0.00327	0.00092	90,983	Strain
2CC	24.1	501.4	0.00355	0.00109	120,531	Strain
2DA	26.8	527.1	0.00299	0.00039	151,608	Strain
2GC	23.4	486.8	0.00324	0.00084	159,138	Strain
2AC	22.0	459.6	0.00274	0.00048	352,754	Strain
1AC	22.2	450.3	0.00245	0.00023	583,000	Strain
1CB	50.2	998.4	-	-	1,186	Load
1BB	50.2	998.4	-	-	1,192	Load
1FB	50.2	998.4	-	-	1,385	Load
1AB	40.6	815.9	-	-	5,246	Load
1EB	40.5	815.9	-	-	5,889	Load
2CB	40.6	815.9	-	-	6,694	Load
2DB	40.5	815.9	-	-	7,028	Load
1FC	32.2	657.9	0.00811	0.00487	16,085	Load
2EA	31.9	638.5	-	-	26,467	Load
2GA	32.3	638.5	-	-	29,324	Load
1EA	31.9	638.5	-	-	30,767	Load
1DA	31.1	638.5	-	-	31,911	Load
1AA	32.1	638.5	-	-	34,301	Load
2EB	32.2	638.5	-	-	39,391	Load
1FA	32.3	643.2	-	-	46,107	Load
2FA	31.7	638.5	-	-	47,959	Load

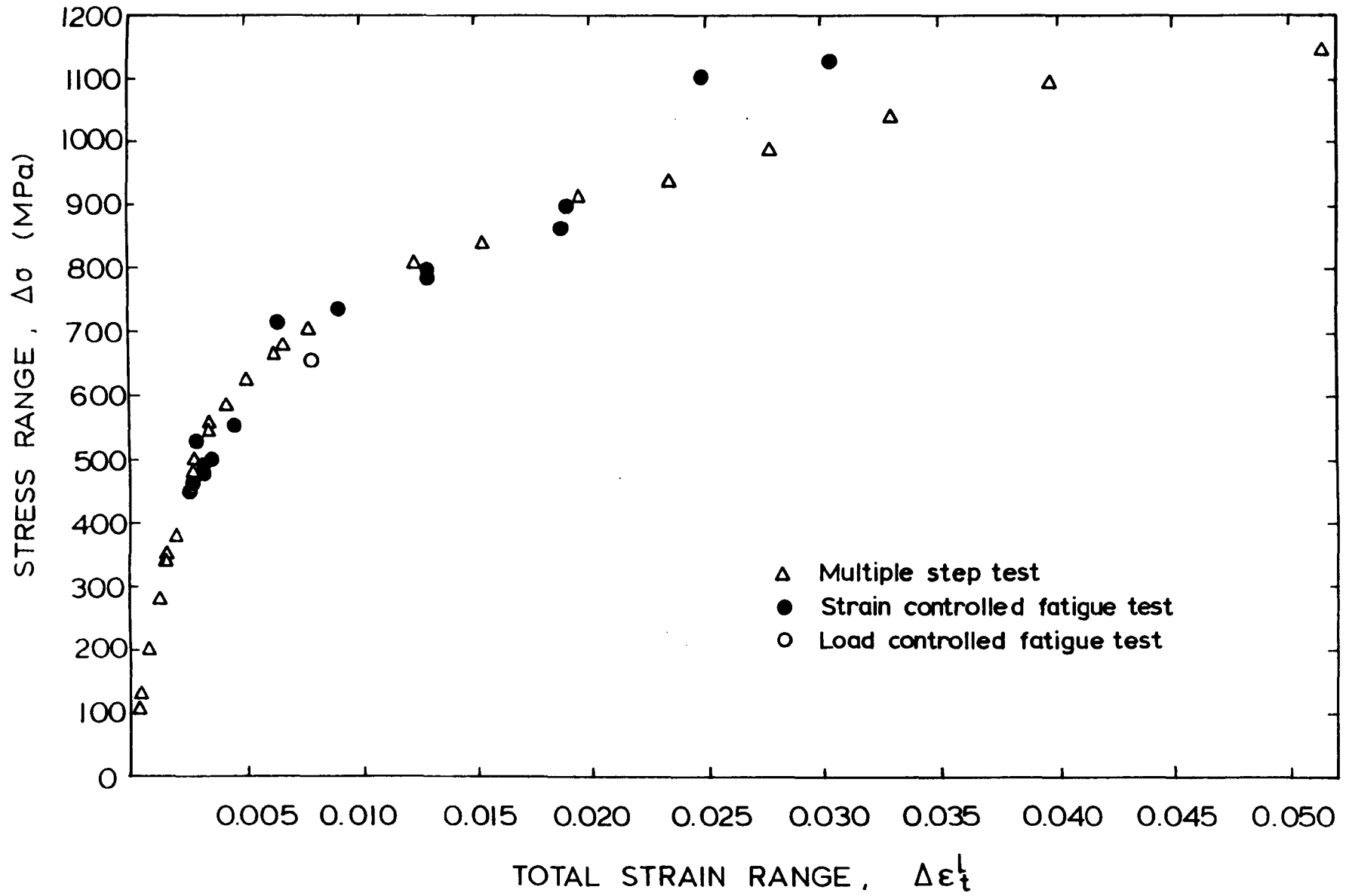


FIGURE 3.1a - Stress range versus strain range

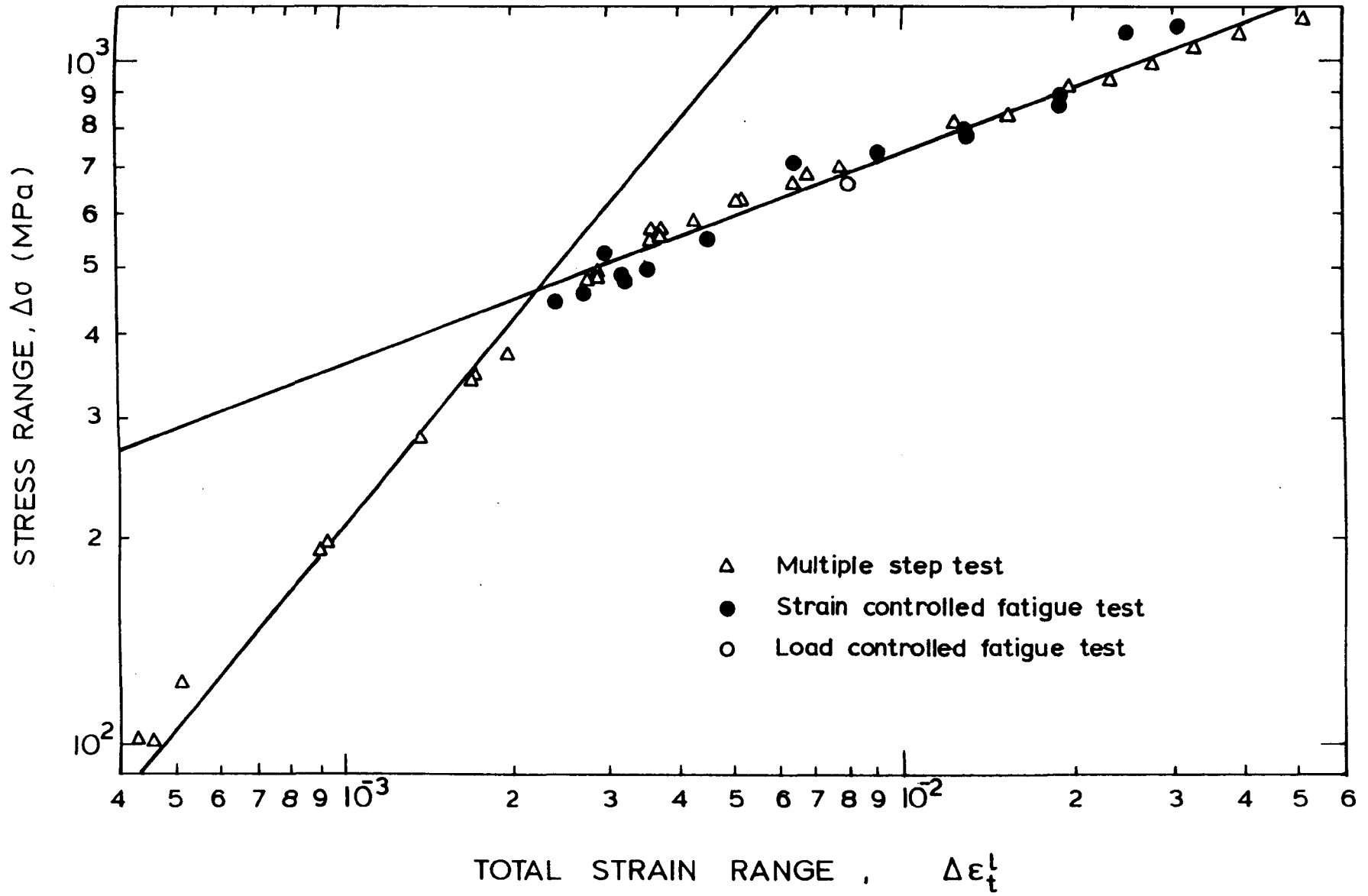


FIGURE 3.1b - Stress range versus strain range

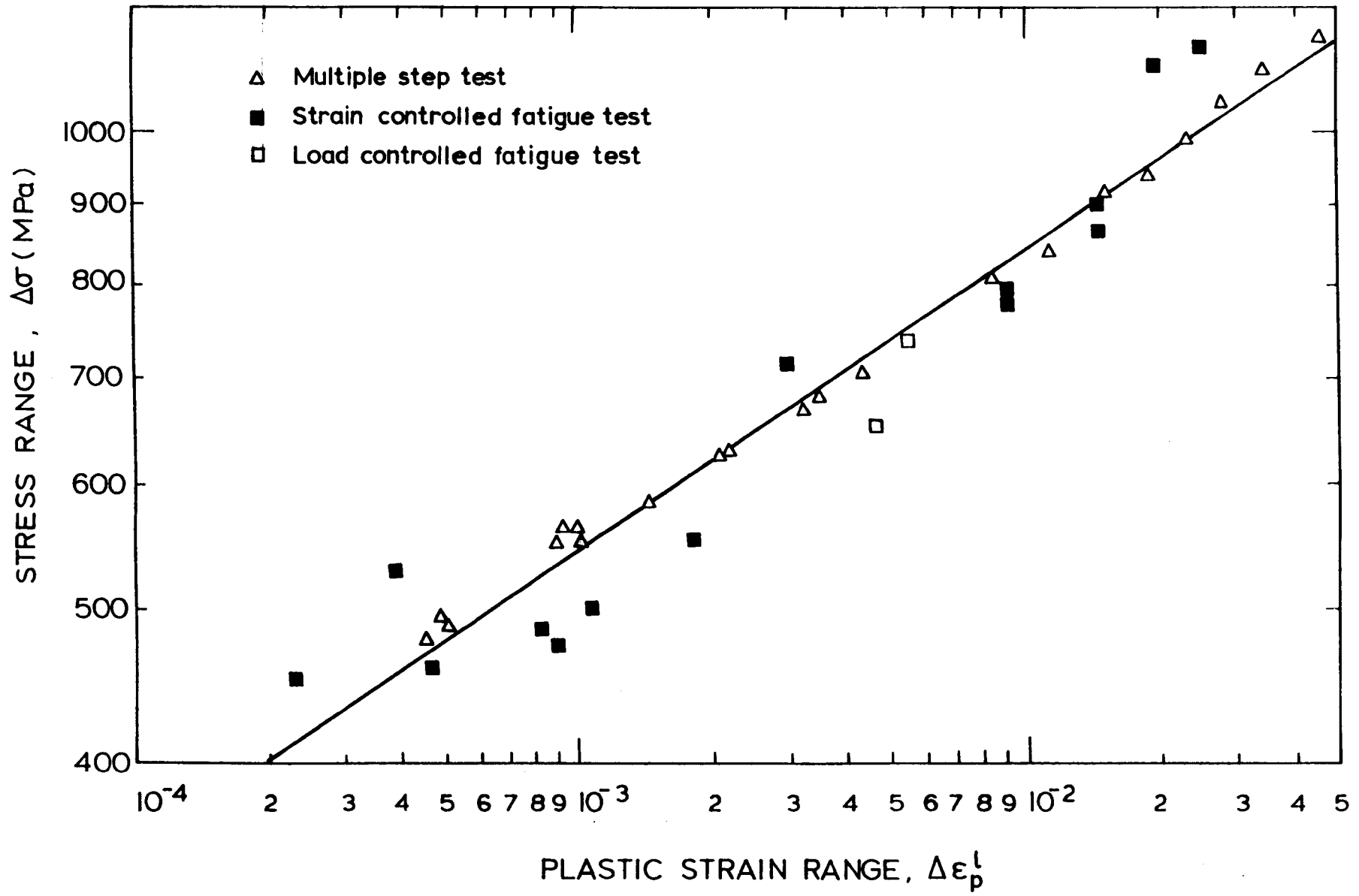


FIGURE 3.2 - Stress range versus plastic strain range

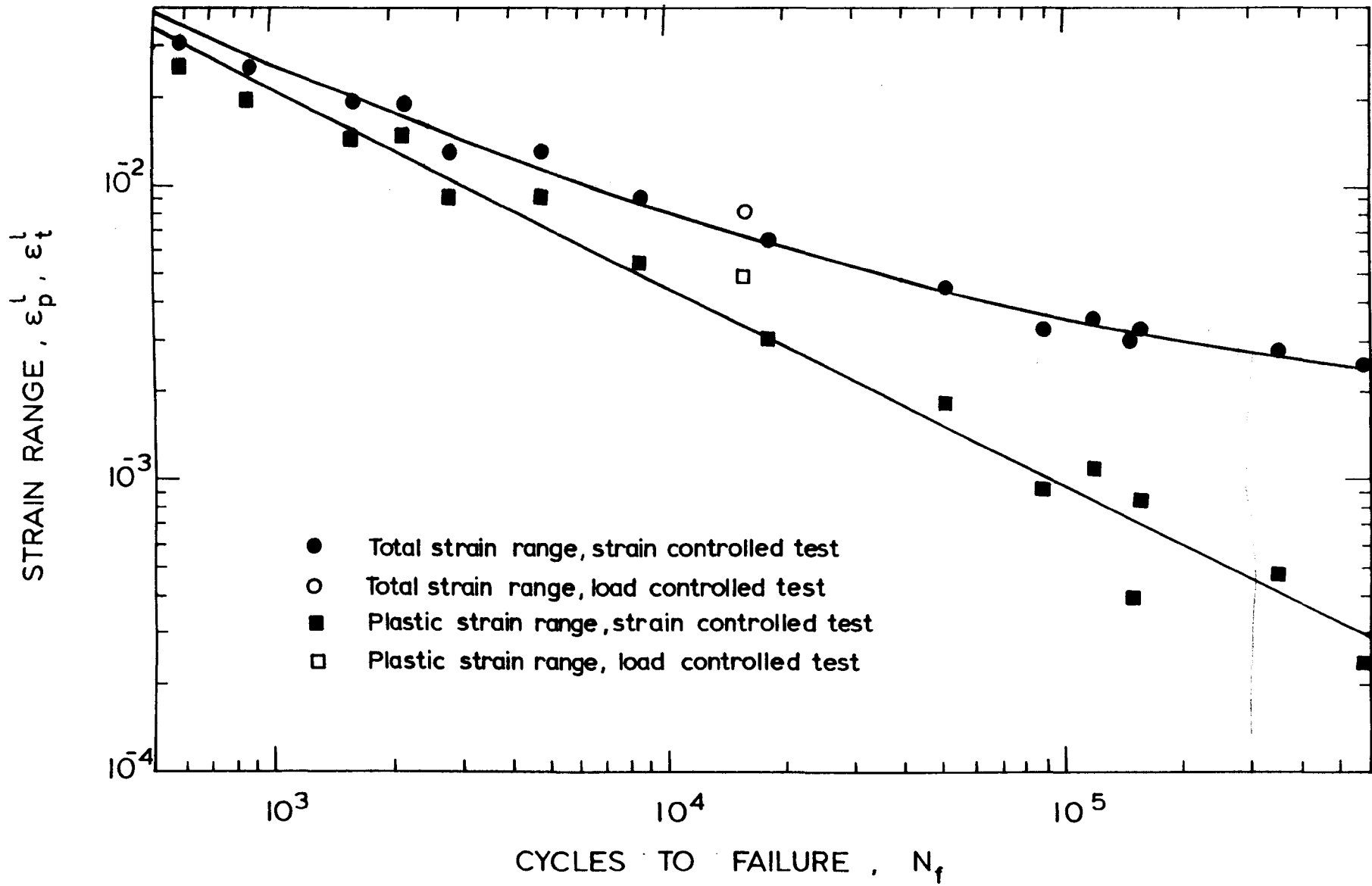


FIGURE 3.3 - Strain range versus cycles to failure

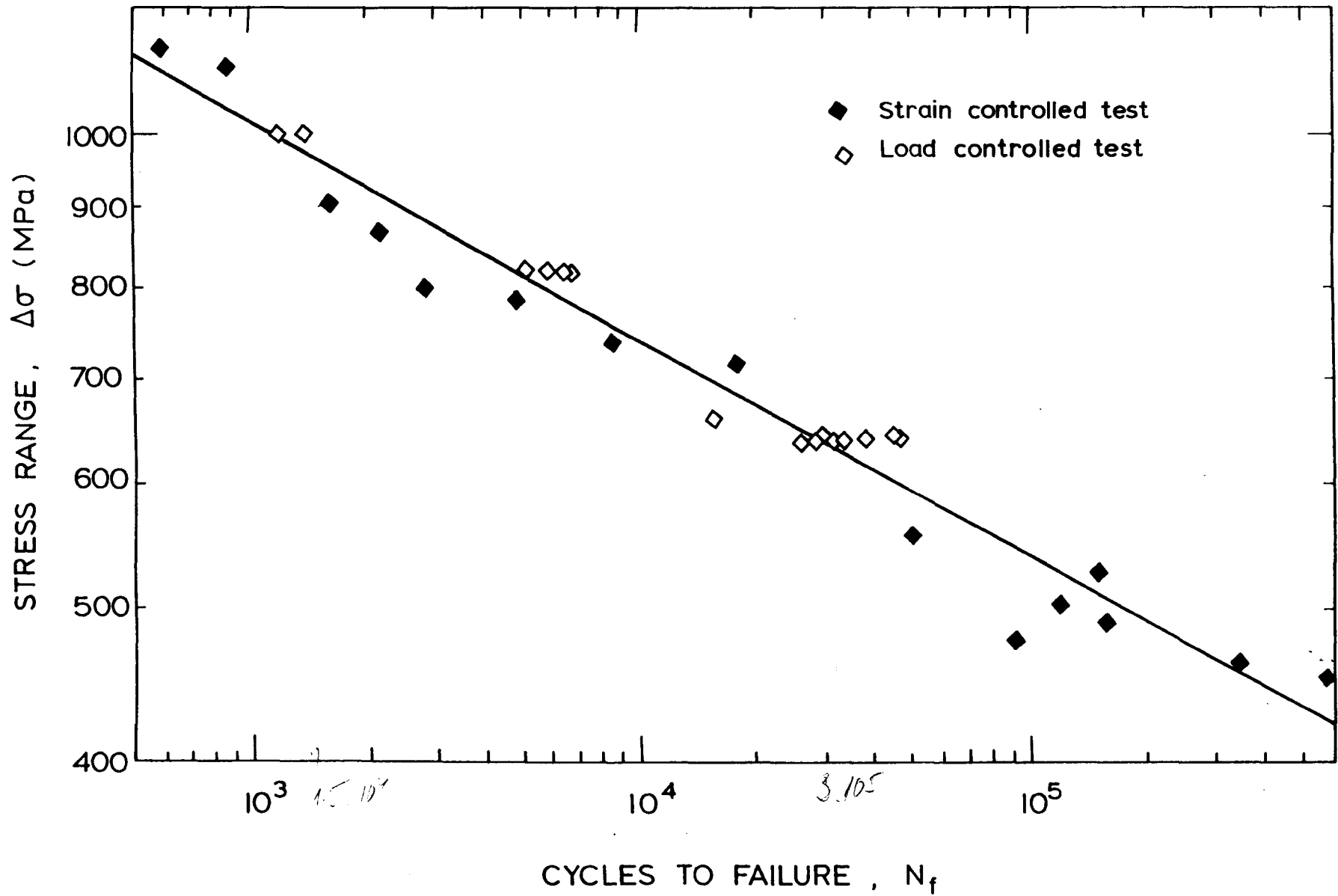


FIGURE 3.4 - Stress range versus cycles to failure

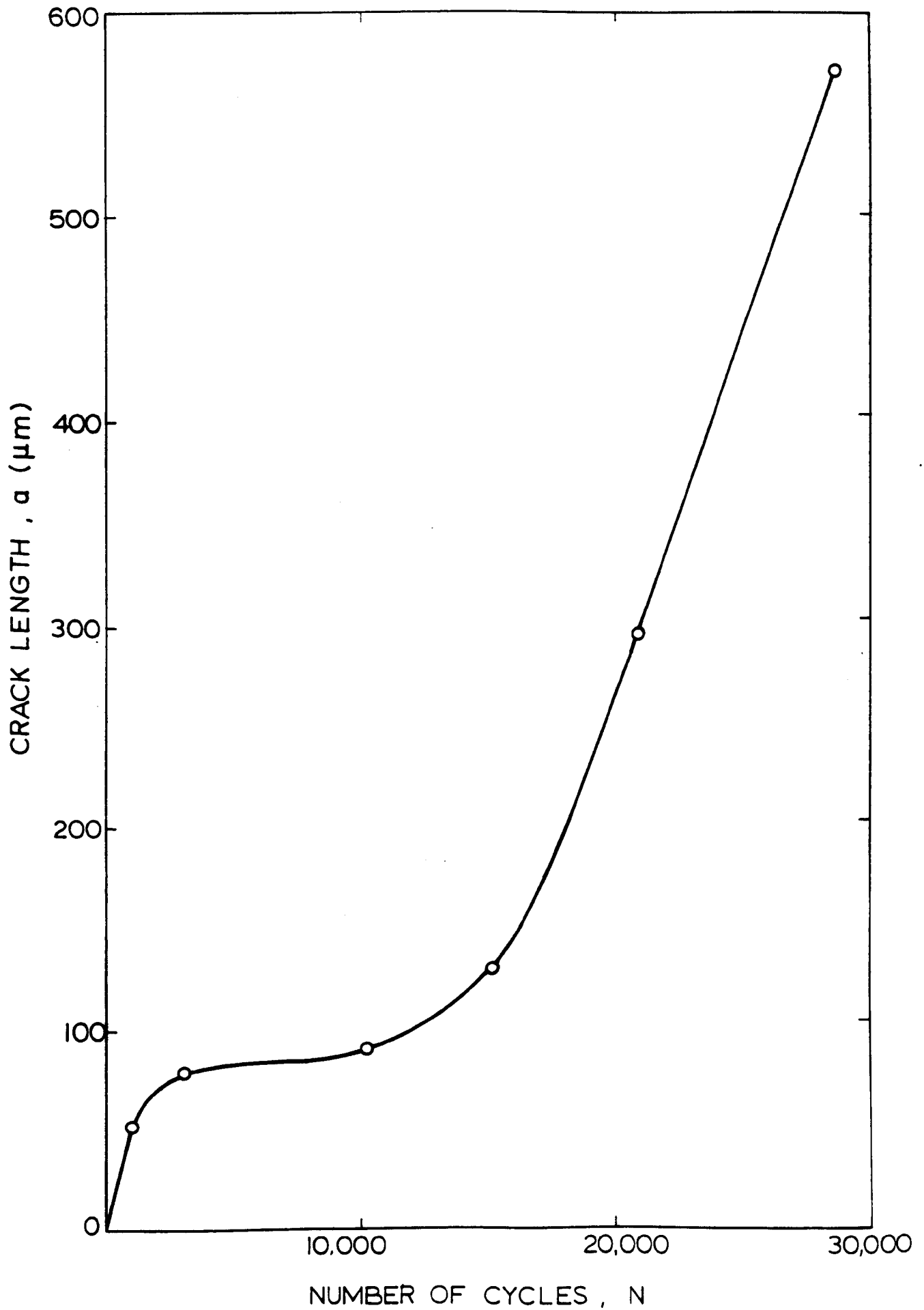


FIGURE 3.5 - Crack growth results (test 2GA, crack no.1) obtained from plastic replicas

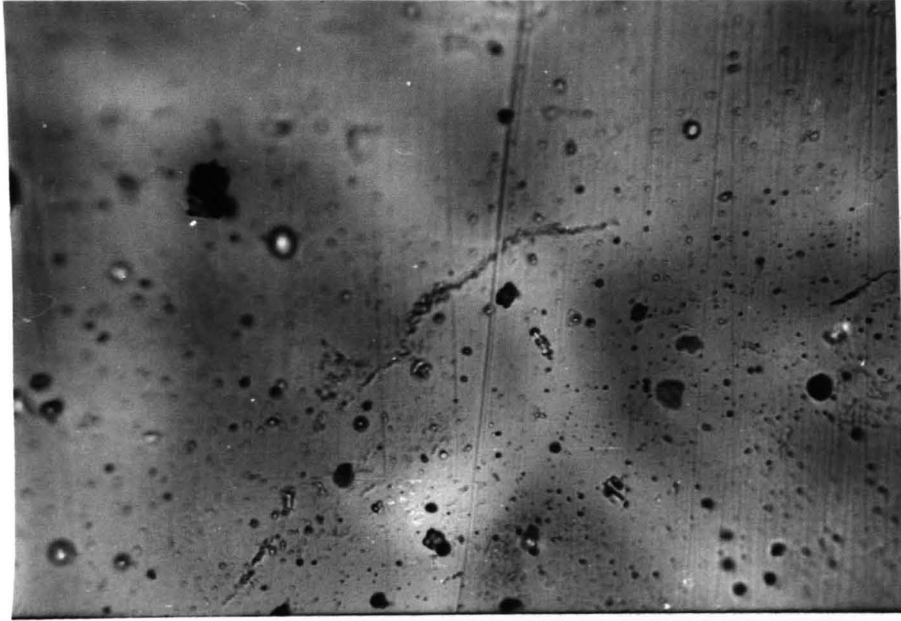


(a) x 550  
at 1000 cycles

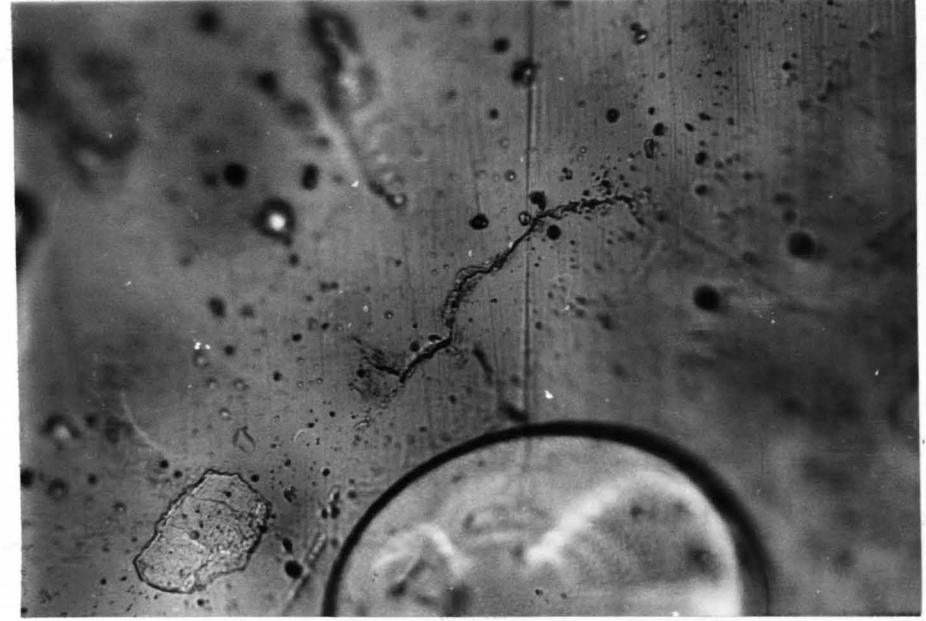


(b) x 550  
at 3000 cycles

FIGURE 3.6 - PHOTOGRAPHS OF PLASTIC REPLICAS TAKEN AT DIFFERENT STAGES OF LIFE FOR ONE PARTICULAR CRACK (TEST 2GA)

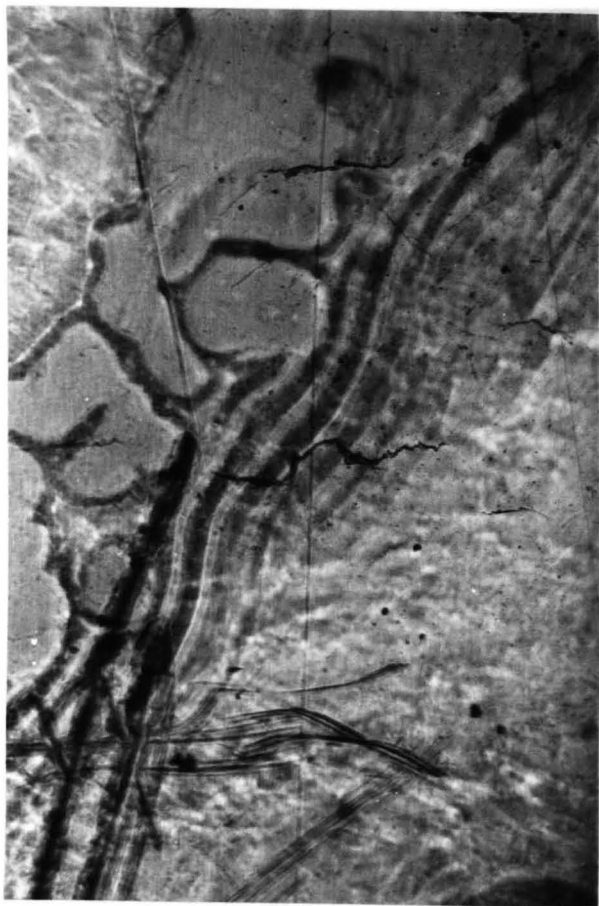


(c) x 550  
at 6166 cycles

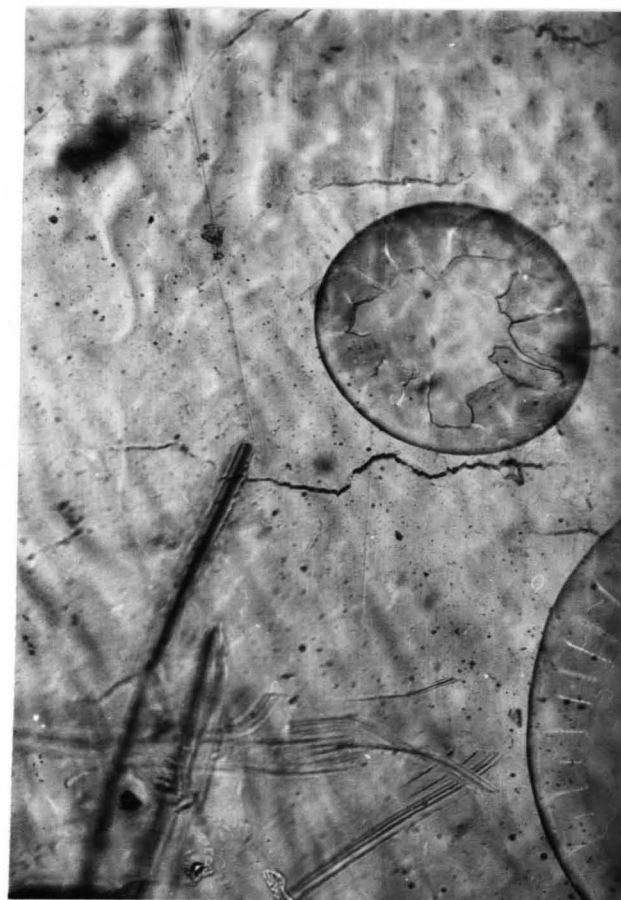


(d) x 550  
at 10140 cycles

FIGURE 3.6 - (CONTINUED)



(e) x 110  
at 20873 cycles



(f) x 110  
at 28640 cycles

FIGURE 3.6 - (CONTINUED)

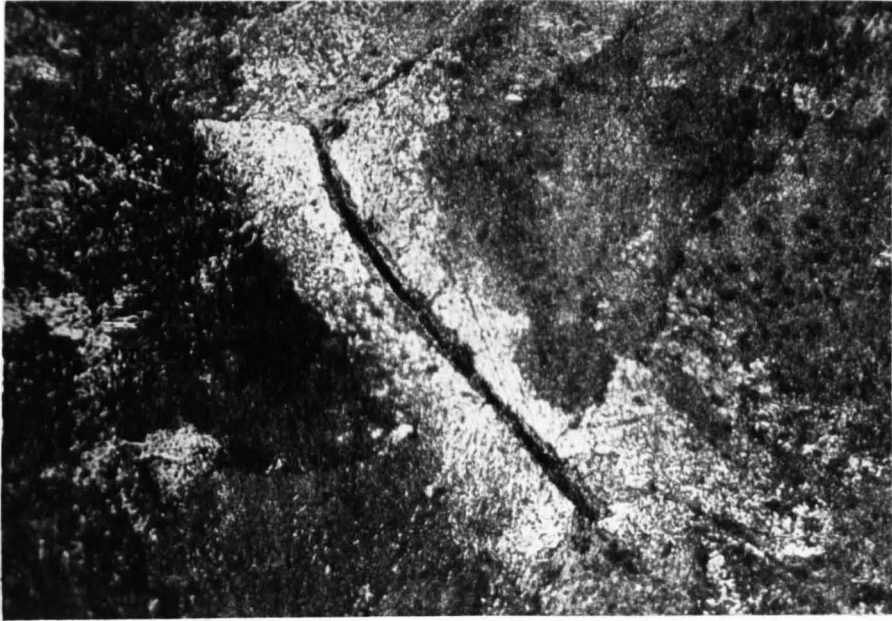


(a) x 550

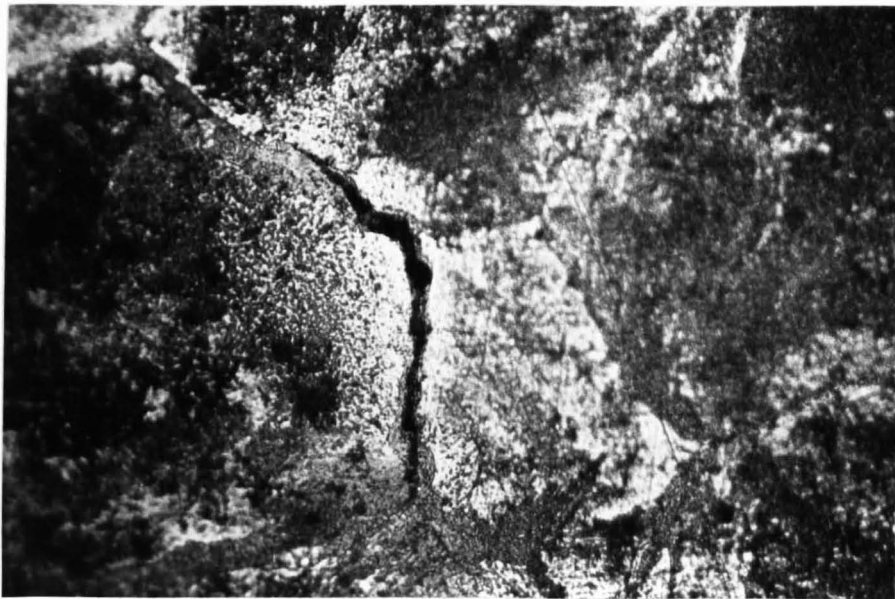


(b) x 550

FIGURE 3.7 - PHOTOGRAPHS SHOWING MICROSTRUCTURAL EFFECTS ON SHORT CRACK GROWTH

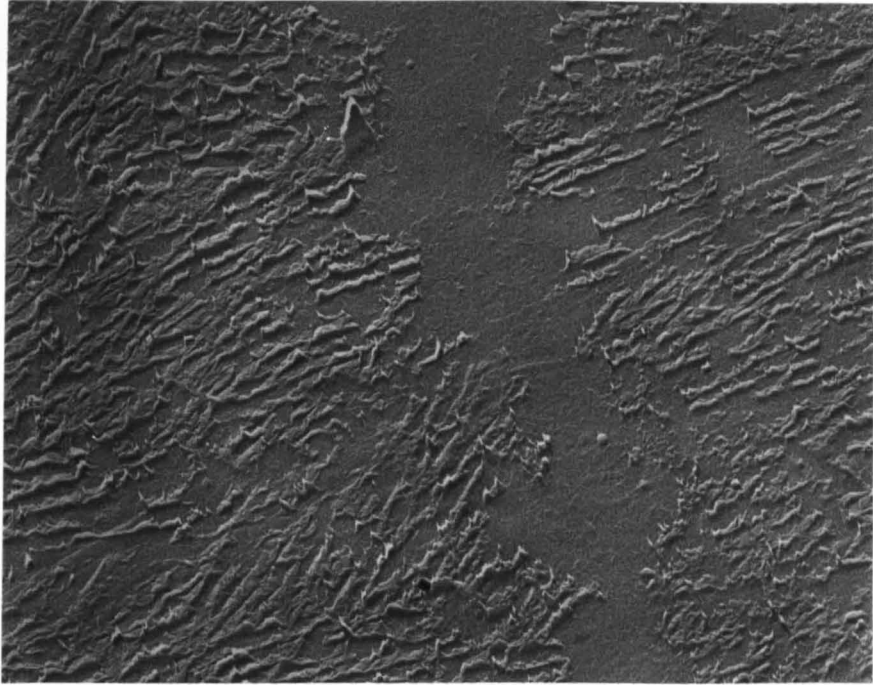


(c) x 550

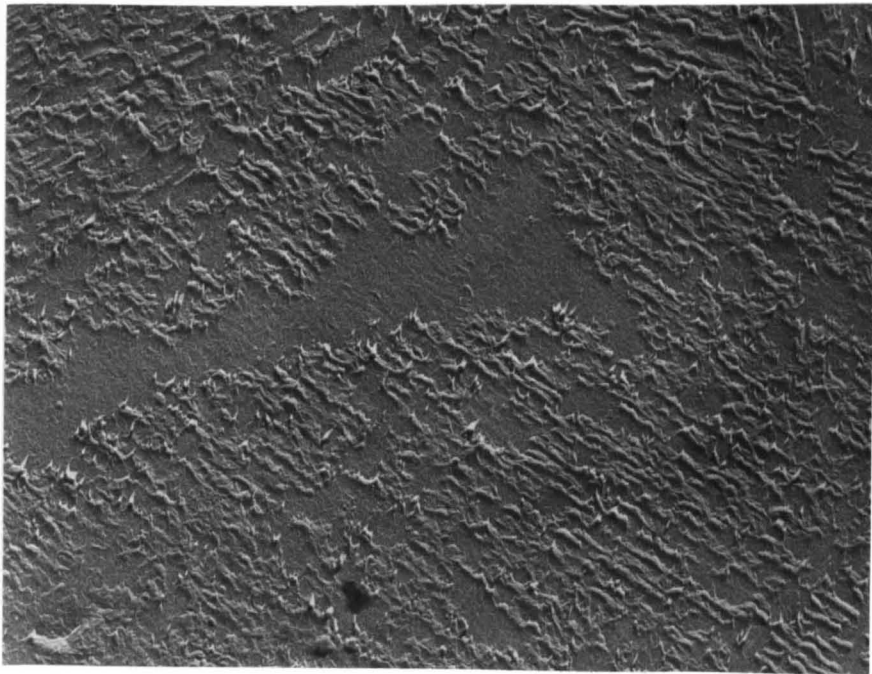


(d) x 550

FIGURE 3.7 - (CONTINUED)



(a) x 8800



(b) x 8800

FIGURE 3.8 - PHOTOGRAPHS OF A FERRITE PLATE OBTAINED ON A SCANNING ELECTRON MICROSCOPE

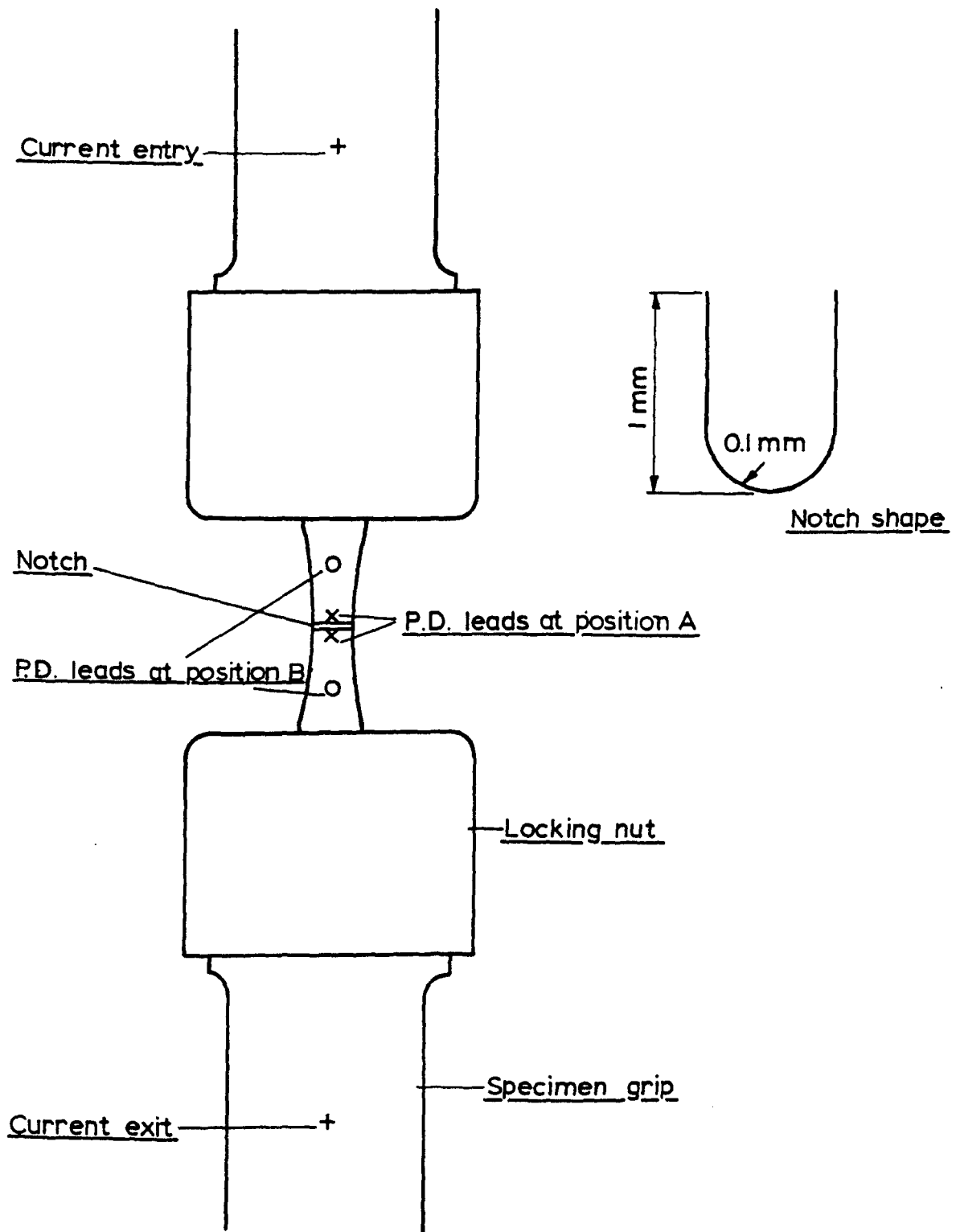


FIGURE 3.9 - Experimental set-up for a D.C. potential drop system

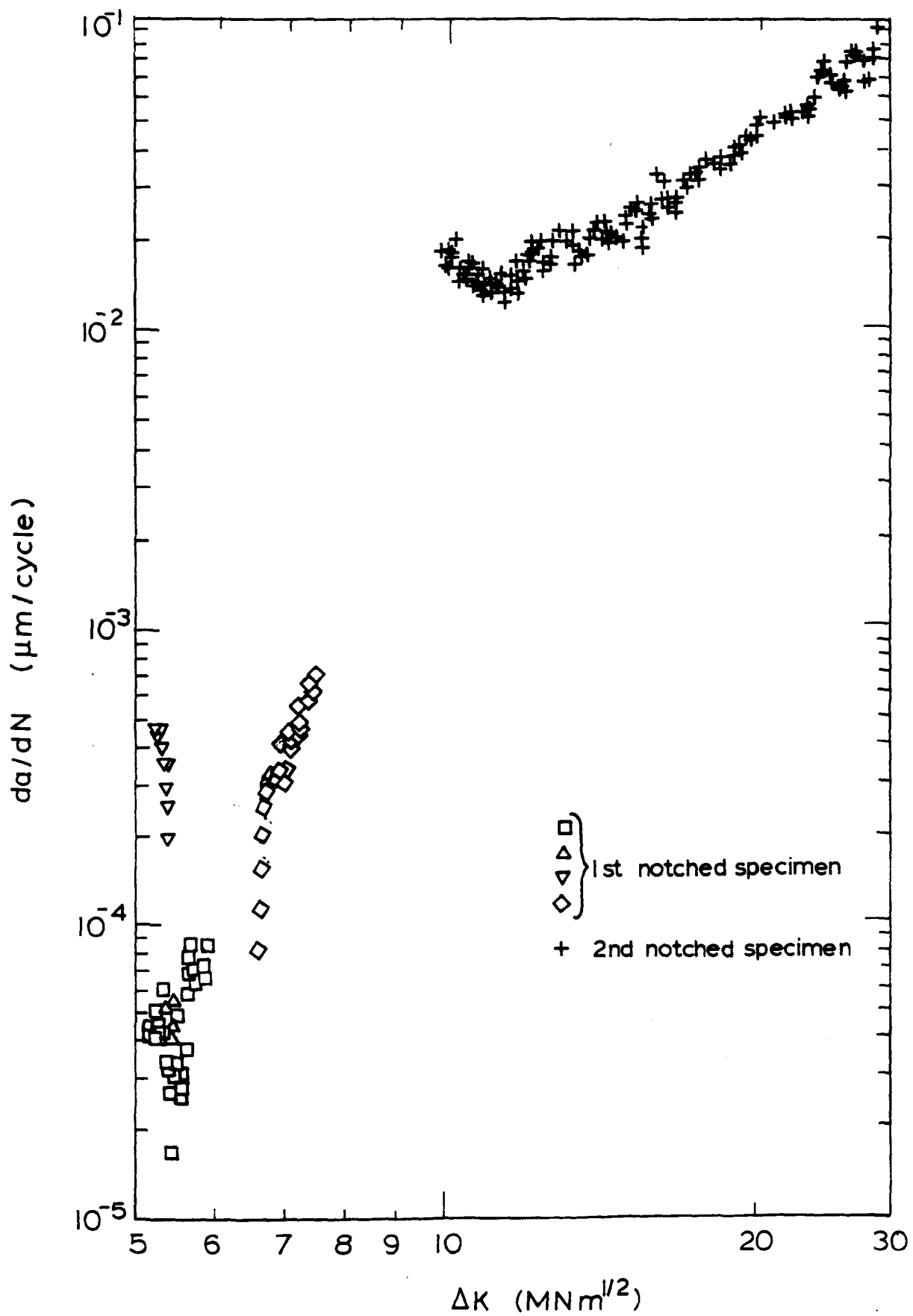


FIGURE 3.10 - Crack growth rate versus stress intensity factor for notched specimens

CHAPTER FOUR  
SHORT CRACK LITERATURE SURVEY

4.1 Introduction

The current trend of increasing attention being focussed on the growth of short cracks comes not only from the practical need for higher levels of service stress, as mentioned in chapter one, but also from the inability of traditional methods of fatigue analysis, such as fracture mechanics, to provide adequate mathematical models.

Although anomalies in growth rates for short cracks have been noted for several years, serious attempts to model this behaviour have only been carried out in the last few years. In their work in 1956, Hunter and Fricke [1], using rotating beam specimens in high cycle fatigue of 6061-T6 Aluminium alloy noticed cracks inexplicably slowing down at about 300  $\mu$ m in length. Several cracks were observed by using the plastic replication method for each specimen which ruled out the possibility of this phenomenon being an isolated occurrence for one particular crack, or one test result.

Later, De Lange [2] presented results on short crack growth in 26 St Aluminium alloy and also for Steel 35 CD 4. For both these materials a decrease in crack growth rate was observed after the crack had traversed a distance of four or five grains.

## 4.2 Cumulative Damage Testing

Before proceeding to more contemporary work in which crack growth was monitored and attempts were made to model this anomalous growth of short cracks, one area of research relevant to short crack growth which has been of much interest for many years is that of Cumulative Damage testing. In this approach microscopic crack lengths are inferred rather than measured directly. For a specimen cycled at several different load ranges, Palmgren [3] and Miner [4], proposed that the sum of the proportions of lifetime accumulated at each load level was unity. This may be written algebraically as:

$$\sum_{i=1}^p \frac{n_i}{N_i} = 1 \quad (4.1)$$

where  $n_i$  is number of cycles applied for a particular load level,  $N_i$  is the expected lifetime of a constant load amplitude test at that load level, and  $p$  is the number of different load levels used in a test.

Frost et al [5] demonstrated that the Palmgren-Miner law is in fact a result of the integration of a simple crack growth law such as the standard L.E.F.M. expression given in equation 1.2. Therefore, any significant deviation from the result of equation 4.1 can be interpreted as the inability of a particular crack growth law to model the history of the complete growth of

a crack. Since such models are derived for long crack data, any such discrepancy must arise from the number of cycles required for the birth of a crack and its growth to a length beyond which the model can be applied accurately. (This argument assumes that the number of cycles in unstable Stage III crack growth is negligible).

Attempts to modify equation 4.1 have been made in order to model situations where the Palmgren-Miner Law has been found to be inappropriate. Manson et al [6] in their Double Linear Damage Rule split up the fatigue life into an "initiation" and a "propagation" period. Both areas were then expressed as a function of the number of cycles to failure using a best-fit to experimental results. Such methods can only give a best-fit solution to their tests and cannot give any direct information regarding the mechanisms of crack growth or indeed the rate of crack growth.

Instead of modifying the original Palmgren-Miner Law, Ibrahim [7] assumed that crack growth could be adequately described by a simple equation which, from dimensional analysis, was argued to take the following form:

$$\frac{da}{dN} = C_1 a \quad (4.2)$$

where  $C_1$  is some function of the applied strain range and material properties.

The initiation zone was then defined to cover the initial period of crack growth where equation 4.2 was not applicable, and would cause error if used with equation 4.1.

Two stage cumulative damage tests were then performed for specimens fatigued in torsional loading. The sequence of loading was from a low to a high strain range, the second strain level being sufficiently high that the assumption of there being no significant initiation period at this strain level could be made. Figure 4.1 is a plot of the fraction of life spent at the lower strain level (x) against the fraction of life spent at the high strain level (y) for a series of tests. The dotted line (x+y=1) represents the Palmgren-Miner Law.

By integration of equation 4.2, equation 4.3 is obtained for the two level test, if  $xN_{f1}$ , the period spent at the low strain range, exceeds  $N_{i,1}$ , the number of cycles to initiation.

$$1 - \frac{x(N_{f1}) - N_{i1}}{N_{f1} - N_{i1}} \log_e \left( \frac{a_f}{a_i} \right) = y \text{Log}_e \left( \frac{a_f}{a_o} \right) \quad (4.3)$$

where  $N_{f1}$  is the number of cycles to failure at the initial strain level, and  $N_{i,1}$  is the number of cycles to initiation at this strain level. Note that  $a_f$  is the final crack length at failure,  $a_i$  is the crack length at the end of the initiation period, and  $a_o$  is the initial crack length, taken to be the

maximum peak to trough distance from surface roughness measurements.

Line OP in figure 4.1 represents the linear equation 4.3, in which a value for  $N_{i,1}$  may be derived from point P, representing the instants at which the experimental points start to deviate from that straight line. Once  $N_{i,1}$  has been estimated using a best-fit procedure,  $a_i$  can be found by substituting the value of  $N_i$  back into equation 4.3.

One of the problems associated with this method lies in the accurate location of point P. As can be seen from figure 4.1, it is not at all obvious from the experimental results where exactly linearity ends. Hence it is necessary to perform a large number of cumulative damage tests which even then can only define  $a_i$  for the particular strain level tested. Secondly, no model was proposed to describe crack growth for the region represented by the arc PQ. It is apparent that if cracks in that study did in fact slow down at a short length, as observed in references [1] and [2], the curve PQ may be concave rather than convex.

The values of  $a_i$  determined by Ibrahim, were very small indeed, less than three microns for the largest value of  $a_i$ , which corresponded to a lifetime of 700,000 cycles. Any error in the value of  $a_i$  is caused either by the problem of locating point P, or by the possibility that equation 4.2 was not a good model to describe crack growth from  $a_i$  to  $a_f$ , or by the assumed

value for  $a_0$ .

#### 4.3 Minimum Crack Lengths Suitable to LEFM Analyses

Another approach used to predict the extent of the anomalous behaviour of short cracks was presented by Taylor and Knott [8], [9], who used the Kitagawa plot [10] to define crack lengths  $l_0$ ,  $l_1$ ,  $l_2$  shown in figure 4.2. Here  $l_1$  represents the length of a pre-existing crack which may be present in a specimen without reducing its fatigue limit. For cracks of length less than  $l_2$  the stress intensity approach cannot be used to estimate the crack growth threshold, and  $l_0$  is the intersection of the two asymptotes representing the endurance limit and the constant threshold stress intensity factor range.

For a number of short crack studies in the literature, Taylor made a note of the average grain size ( $d$ ). A correlation of  $l_2 = 10d$ , and  $l_0 = d$  was found to fit well with all the studies, although a shortage of data prevented a relationship between  $l_1$  and  $d$  being formulated. This work gives support to the reasoning that a crack must be much larger than microstructural features before L.E.F.M. parameters can be used accurately.

Smith [11] quotes a value of 0.025 mm as a minimum crack length suitable to a stress intensity approach. However, as Lankford [12] pointed out, this value relates only to the application of fracture mechanics to the prediction of the

threshold of incremental crack advance, as finite rates of crack growth give a more complicated relationship possibly involving microstructural effects. But this anomalous value seems too low even for threshold predictions in the light of Taylors work [8], and appears to provide a lower bound crack size below which L.E.F.M. can never be used for short crack growth.

#### 4.4 Grain Boundary Effects

Experimental observations have now been carried out on several materials and different reasons have been cited in the literature to explain odd growth patterns. Lankford has worked on AISI 4340 steel [13], a nickel base superalloy [14], and 7075-T6 Aluminium alloy [15] [16]. In the work on the high strength steel, retardations in crack growth were observed at crack lengths between 4 and 20 $\mu$ m, which correspond to the minimum and maximum prior austenite grain size respectively. Similar behaviour was observed by Stalen [17], with retardation periods when the crack length was of the order of the grain size. The calculated plastic zone size corresponded to at least one third of the crack length, so use of an L.E.F.M. parameter as in this study will not be accurate. Also, as L.E.F.M. predicts crack growth rate increasing with increasing crack length, it is unable to model the situation where crack growth rate actually decreases with increasing crack length.

Lankford's work on Aluminium alloy [15] also noted a

retardation in crack growth at a value of the grain size dimension ( $16\mu\text{m}$ ). Later work [16] demonstrated that in an atmosphere of dry nitrogen, short crack growth measurements followed the same general pattern suggesting that the short crack growth anomalies were not a result of environmental effects.

Other workers have noticed grain boundary effects. Brown and Hicks [18] working on Titanium alloy IMI 685 suggested that the amount of crack retardation was a function of the difference in orientation between grains as a crack passed from one grain to another. If the orientation was favourable the crack would not be slowed down as much as in badly orientated grains where crack arrest might result. De Los Rios et al [19], who used the same material studied in this thesis, but performed tests in torsion rather than tension, noted cracks initially growing quickly but slowing down as they approached microstructural obstructions. In this material this occurred when the crack reached the end of a ferrite plate and had to cross pearlite in order to continue propagation along the next ferrite plate.

Rather than quote more examples from the literature, it is perhaps more instructive to consider some of the models which have been used to describe short crack growth. These models have usually tried to incorporate either grain boundary blockage or crack closure, or alternatively a combination of both effects.

#### 4.5 Short Crack Growth Models

In the concept of crack closure, a crack is described as closed if the crack faces touch at points near to the crack tip. Originally it was thought that this only occurred in situations where compressive stresses were present, but Elber's work in 1970 [20] demonstrated that this was not always the case. Now if the amount of closure was observed to be different for long cracks and for short cracks, it might be possible to incorporate this effect into a short crack growth model.

A grain boundary "blockage" model was presented by Chang et al [21] who used the concept that crack propagation cannot occur until a critical strain energy is exceeded at the crack tip, and thus an incubation period results for cracks when they meet grain boundaries. To calculate this incubation period the applied stress amplitude, crack length and the distance of the surface crack tip to the next grain boundary ( $X$ ) is used.

This model was later extended to remove the original constraint that crack length had to be constant throughout the incubation period [22]. The new model was formulated in terms of the following integral:

$$\int_{N_s}^{N_s + N_d} \sqrt{2aN} (\tau_{\text{eff}} - \tau_0)^2 dN = \beta_2 \quad (4.4)$$

where  $2a$  is the crack length at  $N$  cycles, and  $\beta_2$  a material parameter, proportional to the energy required to propagate a crack through a grain boundary.  $\tau_{\text{eff}}$  is the effective surface shear stress, which in turn is a function of the applied stress amplitude and grain orientation.  $N_s$  is the number of completed cycles when the crack tip reaches the grain boundary,  $N_d$  the number of cycles comprising the incubation period, and  $\tau_0$  is the minimum effective shear stress necessary for dislocation motion. Note that as crack length increases, equation 4.4 will predict less incubation,  $N_d$ , at subsequent grains which agrees with experimental observation. This model can explain the retardation of cracks at grain boundaries but does not explain the very fast growth rates observed by cracks before they reach the grain boundaries. Therefore, crack closure was incorporated into the model, and a combination of both incubation and closure was found to give closer agreement with their experimental results.

Zurek et al [23] presented two models, one for crack closure and the other for grain boundary effects incorporated into a standard L.E.F.M. type equation. They used a relationship stated elsewhere [24], that crack closure was directly proportional to the distance from the crack tip to the nearest grain boundary ( $X$ ), giving the stress  $\sigma_{\text{cc}}$ , at crack closure as:

$$\sigma_{cc} = \frac{\alpha X \sigma_{\max}}{2a} \quad (4.5)$$

where  $\alpha$  is a material parameter from which they derived a crack growth equation of the form:

$$\frac{da}{dN} = C \Delta K^n \left[ 1 - \alpha X \left( \frac{1.12 \sigma_{\max}}{\Delta K} \right)^2 \right]^n \quad (4.6)$$

where  $C$  is a constant. In conjunction with this another model to describe the incubation period at a grain boundary was formulated given by:

$$\left( \frac{da}{dN} \right)_m = \frac{da}{dN} \left[ 1 - \frac{\Delta N_i}{\Delta N_p + \Delta N_i} \right] \quad (4.7)$$

where  $(da/dN)_m$  the measured crack growth, is assumed to be a function of the unhindered growth rate  $da/dN$ ,  $\Delta N_p$  is the number of cycles spent in propagation as a crack moves across a grain and  $\Delta N_i$  the number of cycles during which the crack is arrested at the grain boundary. The fraction  $\Delta N_i / (\Delta N_p + \Delta N_i)$  is determined experimentally by counting the proportion of cracks arrested at the grain boundary.

At this point it is worthwhile to discuss problems

associated with the measurement of crack closure. These techniques employ either a compliance method using for example strain gauges or transducers, or use non-compliance methods such as potential drop or acoustic emission. However agreement between methods has not always been observed. Frandson et al [25] noticed differences in closure measurements when comparing the reading using a compliance method to that of an acoustic method. These problems are heightened when trying to measure closure for short cracks.

James [26] states that none of the above methods are suitable for measuring closure in microcracks and so he used direct measurement of the surface crack opening displacement by deflecting cracked specimens in a jig mounted on a Scanning Electron Microscope. Morris also reports using a similar technique in his work [27].

Different mechanisms can be responsible for closure, such as plasticity induced closure, surface roughness induced closure and oxide induced closure [28]. Until more work has been done on crack closure, it is hard to separate the mechanisms or to obtain reliable measurements. It is difficult to apply analytical methods based on closure arguments to long crack growth, let alone short crack growth models.

Returning to microstructural effects Lankford and Chan [29] recently presented a model for short crack growth which used a modified L.E.F.M. equation, with misorientation between

grains as well as grain boundary effects taken into account. The crack growth for short cracks was expressed as

$$\frac{da}{dN} = C_1 K^n \left[ 1 - \left( 1 - \frac{\tau_B}{\tau_A} \right) \left( \frac{D - 2X}{D} \right)^m \right] \quad (4.8)$$

where  $X$  is the distance from the crack tip to the nearest grain boundary,  $\tau_A$  and  $\tau_B$  represent the resolved shear strains in adjoining grains A and B respectively, and  $D$  is the grain diameter, with  $m$  and  $n$  being constants. For a crack growing from grain A to grain B with a ratio of  $\tau_B/\tau_A$  greater than 1 it would be relatively easy to initiate slip in the next grain B. However, for  $\tau_B = 0$ , equation 4.8 predicts arrest at the grain boundary.

Both Zurek's [23] and Lankford's approach [29] have had some success when applied to their own experimental data, but it is questionable whether the equations are physically valid when it is admitted that L.E.F.M. is unsuitable for application to short crack growth because of the breakdown of one of its fundamental assumptions, namely that the material is an isotropic continuum. So whether the stress intensity factor should be used at all, even with a "fudge" factor, is extremely doubtful.

De Los Rios et al [19] used a model to describe short crack growth in high cycle torsional fatigue. The crack growth rate was given by

$$\frac{da}{dN} = \frac{f \tau (D - a)}{\mu} \quad (4.9)$$

where D was slip band length, f the fraction of dislocations occurring in the slip band,  $\tau$  the shear stress acting on the slip band and  $\mu$  the shear modulus. This model was successful in predicting growth rates for individual cracks compared to data taken from replicas. However, to reproduce the critical crack growth in a fatigue specimen where there are a number of cracks growing at several different speeds, it is necessary to try to model the crack which eventually grows into the failure crack in order to make lifetime predictions. For this to be achieved a statistical approach to the crack growth results for several cracks needs to be applied.

A review paper is presented in [30], with particular reference to the influence of microstructure on short crack growth. In this paper the effects of crack size relative to microstructural dimensions, and plastic zone size are considered. Several pieces of work are reviewed for a wide range of materials including steel, Nickel base superalloy, Titanium alloy and also Aluminium alloy. Where crack lengths were larger than the average grain size, short cracks did not propagate faster than long cracks. But the reverse was true in all the studies where the crack length was less than grain size, and a faster short crack propagation rate was reported.

For short cracks in this project, growth rates were

faster than predicted by L.E.F.M. in line with the results of this review.

CHAPTER FOUR - REFERENCES

- [1] HUNTER, M.S. & FRICKE, W.M.G. Jr. (1956)  
"Fatigue crack propagation in aluminium alloy"  
proc. ASTM 56 p.1038-1046
- [2] DE LANGE, R.G. (1964)  
"Plastic replica methods applied to a study of  
fatigue crack propagation in steel 35 CD4 & 26  
St Aluminium alloy"  
Trans. A.I.M.E. 230 p.644-648
- [3] PALMGREM, A.Z. (1924)  
"Die Lebensdauer Von Kugellagern"  
Z. Ver dt. Ing. 68 p.339
- [4] MINER, M.A. (1945)  
"Cumulative damage in fatigue"  
J. of Appl. Mech. 12 p.A159-A166
- [5] FROST, N.E. MARSH, K.J. & POOK, L.P. (1974)  
"Metal Fatigue"  
Clarendon Press, Oxford p.309-310
- [6] MANSON, S.S. FRECHE, J.C. & ENSIGN, C.R. (1967)  
"Application of a double linear damage rule to

cumulative fatigue"  
ASTM STP 415 p.384-412

- [7] IBRAHIM, M.F.E. & MILLER, K.J. (1980)  
"Determination of fatigue crack initiation life"  
Fatigue Engng. Mater. Struct. 2 p.351-360
- [8] TAYLOR, D. & KNOTT, J.F. (1981)  
"Fatigue crack propagation behaviour of short cracks;  
the effect of microstructure"  
Fatigue Engng. Mater. Struct. 4 p.147-155
- [9] TAYLOR, D. (1982)  
"Euromech colloquiom on short fatigue cracks"  
Fatigue Engng. Mater. Struct 5 p.305-309
- [10] KITAGAWA, H. & TAKAHASHI, S. (1976)  
"Applicability of fracture mechanics to very small cracks  
or the cracks in the early stage"  
2nd International Conference on the Mechanical Behaviour  
of Materials, Boston, U.S.A.  
American Society for Metals, Metals Park, Ohio p.627-631
- [11] SMITH, R.A. (1977)  
"On the short crack limitations of fracture mechanics"  
Int. J. Fract. 13 p.717-720

- [12] LANKFORD, J. (1980)  
"On the small crack fracture mechanics problem"  
Int. J. Fract. 16 p.R7-R9
- [13] LANKFORD, J. (1977)  
"Initiation and early crack growth of fatigue cracks in  
high strength steels"  
Engng. Fract. Mech. 9 p.617-624
- [14] LANKFORD, J. COOK, T.S. & SHELDON, G.P. (1981)  
"Fatigue microcrack growth in a nickel-base superalloy"  
Int. J. Fract. 17 p.143-155
- [15] LANKFORD, J. (1982)  
"The growth of small fatigue cracks in 7075-T6 aluminium  
alloy"  
Fatigue Engng. Mater. Struct. 5 p.233-248
- [16] LANKFORD, J. (1983)  
"The effect of environment on the growth of small fatigue  
cracks"  
Fatigue Engng. Mater. Struct. 6 p.15-31
- [17] STALEN, F.B. (1959)  
Proceedings of the symposium on fatigue of aircraft  
structures  
Wright Patterson Air Force Base, Ohio, U.S.A. p.644-682

- [18] BROWN, C.W. & HICKS, M.A. (1983)  
"A study of short fatigue crack growth behaviour in titanium alloy IMI 685  
Fatigue Engng. Mater. Struct. 6 p.67-75
- [19] DE LOS RIOS, E.R. TANG, Z. & MILLER, K.J. (1984)  
"Short crack fatigue behaviour in a medium carbon steel"  
Fatigue Engng. Mater. Struct. 7 p.97-108
- [20] ELBER, W. (1970)  
"Fatigue crack closure under cyclic tension"  
Engng. Fract. Mech. 2 p.37-45
- [21] CHANG, R. MORRIS, W.L. & BUCK, O. (1979)  
"Fatigue crack nucleation at intermetallic particles in alloys. - A dislocation pile-up model"  
Scripta Metall. 13 p.191-194
- [22] MORRIS, W.L. JAMES, M.R. & BUCK, O. (1981)  
"Growth rate models for short surface cracks in Al 2219-T851"  
Metal Trans. 12A p.57-64
- [23] ZUREK, A.K. JAMES, M.R. & MORRIS, W.L. (1983)  
"The effect of grain size on fatigue growth of short cracks"

Metal Trans. 14A p.1697-1705

- [24] MORRIS, W.L. JAMES, M.R. & BUCK, O. (1983)  
"A simple model of stress intensity range threshold and crack closure stress"  
Engng. Fract. Mech. 18 p.871-877
- [25] FRANDSEN, J.D. INMAN, R.V. & BUCK, O. (1975)  
"A comparison of acoustic and strain gauge technique for crack closure"  
Int. J. Fract. 11 p.345-348
- [26] JAMES, M.N. (1983)  
"The growth of small surface cracks in structural steels"  
Ph.D. thesis, Jesus College Cambridge, p.39
- [27] MORRIS, W.L. & BUCK, O. (1977)  
"Crack closure measurements for microcracks developed during the fatigue of Al 2219-T851"  
Metal Trans. 8A p.597-601
- [28] SURESH, S. & RITCHIE, R.O. (1984)  
"The propagation of short fatigue cracks"  
Int. Met. Rev. 29 p.445-476
- [29] CHAN, K.S. & LANKFORD, J. (1983)  
"A crack tip model for the growth of small fatigue

cracks"

Scripta. Metall. 17 p.529-532

[30] LANKFORD, J. (1985)

"The influence of microstructure in the growth  
of small fatigue cracks"

Fatigue Engng. Mater. Struct. (in press)

[31] MILLER, K.J. & IBRAHIM, M.F.E. (1981)

"Damage accumulation during initiation and short crack  
growth regimes"

Fatigue Engng. Mater. Struct. 4 p.263-277

## CHAPTER FOUR - FIGURES

- 4.1 Cumulative damage results from Miller & Ibrahim [31]
- 4.2 Critical crack lengths suggested by Taylor & Knott [8]

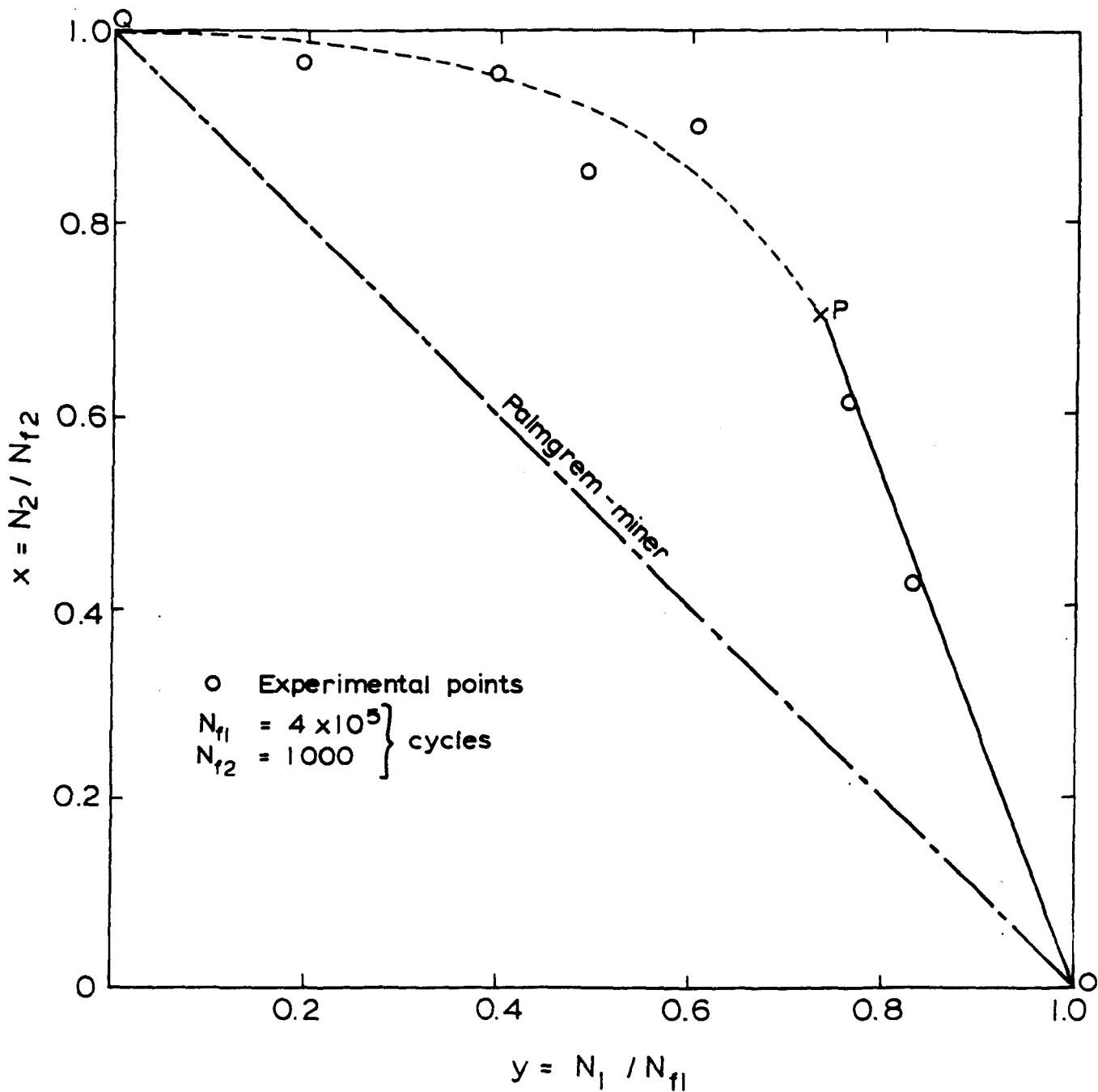


FIGURE 4.1 - Cumulative damage results from Miller & Ibrahim [31]

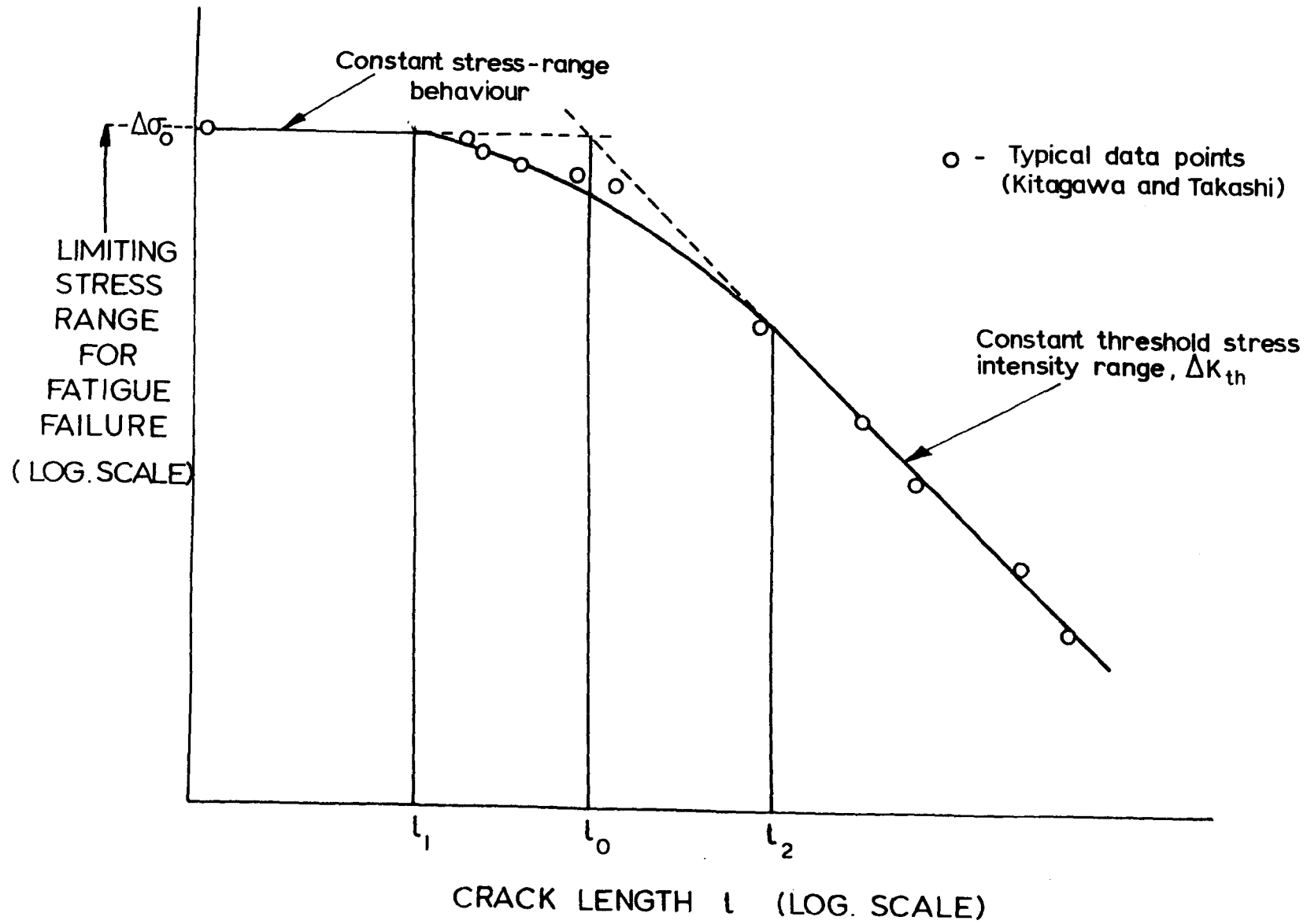


FIGURE 4.2 - Critical crack lengths suggested by Taylor & Knott [8]

CHAPTER FIVE  
ANALYSIS OF CRACK GROWTH RESULTS

5.1 Derivation of Short Crack Growth Equation

In order to formulate a crack growth equation to model the anomalous behaviour of short cracks discussed in Chapter 4, it is necessary to account for microstructural influences. As fracture mechanics analyses of fatigue crack growth assume microstructural independence, a separate and distinct crack growth equation is needed to describe behaviour within the first grain, to account for the decelerating crack growth rate as the grain boundary is approached.

By considering parameters which might be expected to affect the growth of the crack in the first grain, a general expression for crack growth rate in this region can be given by

$$\frac{da}{dN} = f(\Delta\sigma, \Delta\varepsilon, E, k, n, \sigma_y, a, d) \quad (5.1)$$

where  $f$  is an unknown function and  $\sigma_y$  is the cyclic yield stress. For stresses greater than yield  $\Delta\sigma = k \Delta\varepsilon^n$ . Hence equation 5.1 includes sufficient parameters to describe the cyclic deformation behaviour of a material, and the microstructural influences, eg, the grain size, is incorporated as parameter  $d$ . It is assumed for this study on carbon steel that the presence of a grain boundary provides the dominant

microstructural feature that retards fatigue crack extension, as was observed for the second material considered in this chapter, an aluminium alloy.

Dividing the left hand side of equation 5.1 by (a) and collecting all the quantities into dimensionless groups one obtains:

$$\frac{1}{a} \frac{da}{dN} = f\left(\frac{\Delta\sigma}{k}, \frac{\Delta\varepsilon}{k}, \frac{E}{k}, n, \frac{\sigma_y}{k}, \frac{d}{a}\right) \quad (5.2)$$

Replacing d by d-a for convenience and using a series form leads to:

$$\frac{1}{a} \frac{da}{dN} = \sum_i C_i \left(\frac{d-a}{a}\right)^{1-\alpha_i} \quad (5.3)$$

where  $C_i = C_i \left(\frac{\Delta\sigma}{k}, \frac{\Delta\varepsilon}{k}, \frac{E}{k}, n, \frac{\sigma_y}{k}\right)$

or if only the first term is employed:

$$\frac{da}{dN} = Ca^\alpha (d-a)^{1-\alpha} \quad (5.4)$$

This equation embodies both the remaining slip band plastic zone (d-a), and the crack length (a).

In order to be of practical use, one experimentally observed aspect of the growth of short cracks that must be met by equation 5.4 is that  $da/dn$  should decrease with increasing  $(a)$  as the crack approaches the grain boundary.

Differentiating equation 5.4 with respect to  $a$ :-

$$\frac{d}{da} \left( \frac{da}{dN} \right) = \frac{Ca^{\alpha-1} (d-a)}{(d-a)^{\alpha}} \quad (5.5)$$

for  $0 < a < d$ ,  $d/da(da/dN) > 0$  when  $\alpha > 1$  implying a steady and continuous acceleration of the crack as it approaches the grain boundary, so clearly values of  $\alpha$  greater than unity cannot be considered. Note  $d/da (da/dN) = 0$  when  $d = a$ , so the maximum value of  $da$  is given when  $a = d$ . For  $a > d$ ,  $da/dN$  decreases with increasing  $(a)$ , as observed in practice.

Taking nominal values of  $C$  equal to unity and  $d$  of 100, the form of equation 5.4 can be seen, for different values of  $\alpha$ , in figure 5.1. This shows that equation 5.4 is only very sensitive to the value of  $\alpha$  when  $a < d/2$  or 1 0.5. Negative values of  $\alpha$ , give  $da/dN \rightarrow \infty$  as  $a \rightarrow 0$ , so realistic values of  $\alpha$  for equation 5.4 should lie in the range,  $0 \leq \alpha \leq 1$  [1].

## 5.2 Application of Short Crack Growth Equation

### 5.2.1 Short Crack Growth in 7075-T6 Aluminium Alloy

Before all the experimental data was gathered for short crack growth in the carbon steel used in this study, an attempt was made to apply equation 5.4 to some data obtained elsewhere [2]. This has been reported previously in [1], but it is included here also as this work is relevant to this project.

#### 5.2.1.1 Crack Growth within the First Grain

Some crack growth data from reference [2] is shown in Figure 5.2. In this study of 7075-T6 aluminium alloy the average grain width was reported to be about  $18\mu\text{m}$ , being the smallest dimension across the pancake grain structure, so all the data in the figure relates to crack growth of a particular crack within the first grain. For crack length greater than about  $10\mu\text{m}$ , the rate of crack growth was observed to decrease with increasing crack length. The data shows the crack growth rate tending to zero at a value of  $(a)$  of about  $16.5\mu\text{m}$ , so this value was chosen for  $d$  in equation (5.4). It was observed that the crack stopped on reaching the grain boundary. Values of  $C$  and  $\alpha$  were chosen using a best fit analysis, where  $(a)$  was measured in microns and  $da/dN$  in microns per cycle, resulting in the equation:

$$\frac{da}{dN} = 2.22 \times 10^{-4} (16.5 - a)^{0.6} a^{0.4} \quad (5.6)$$

showing a good fit to the data. The curve representing equation (5.6) is also shown in figure 5.2.

#### 5.2.1.2 Long Crack Growth

The data for crack growth in [2] showed that the first grain boundary influenced crack growth far more than subsequent grain boundaries, although cracks did also show signs of slowing down on approaching the grain boundary. To simplify the analysis it was assumed that crack growth should not be affected by microstructural features beyond the first grain boundary. In order to describe the propagation of cracks which had grown out of the first grain, it was necessary to use a different crack growth equation.

An equation of the form:

$$\frac{da}{dN} = C ((\Delta K)^m - (\Delta K_{th})^m) \quad (5.7)$$

was assumed to be able to describe L.E.F.M. behaviour down to threshold [5]. To find values for C and m, results were compiled from various sources [2], [3], [4], [6], which are plotted in figure 5.3. By taking  $\Delta K_{th} = 2.2 \text{ MNm}^{-3/2}$  [4] and  $m = 2$  (to conform with the predictions of dimensional

analysis), a "best-fit" analysis to correlate this data gave the equation:

$$\frac{da}{dN} = 3.48 \times 10^{-4} (\Delta K)^2 - 1.68 \times 10^{-3} \quad (5.8)$$

where  $da/dN$  is in  $\mu\text{m}/\text{cycle}$ . Notice from figure 5.3 that only points  $\Delta K < 6\text{MNm}^{-3/2}$  were taken into consideration when finding a value for C, ie, close to threshold conditions.

By using  $\Delta K = 1.32\Delta\sigma\sqrt{a}$  and  $\Delta\sigma = 414\text{MPa}$  (as used in reference [2]) and substituting for  $\Delta K$  in equation 5.8,  $da/dN$  was expressed as function of (a) (in  $\mu\text{m}$ ) rather than  $\Delta K$ . This is given by the equation:

$$\frac{da}{dN} = 1.04 \times 10^{-4} a - 1.68 \times 10^{-3} \quad (5.9)$$

Note it is assumed that for this material the L.E.F.M. representation of crack growth is valid for a stress level of 414MPa, compared to a yield stress of 515MPa.

### 5.2.1.3 Lifetime Prediction

We now have two equations (5.6) and (5.9) to describe the crack growth rates of short and long cracks respectively. The next problem is to consider the range of crack lengths for which each equation is valid.

Equation 5.6 predicts that crack arrest occurs at a crack length of 16.5 m, which means that the crack cannot continue propagating, unless equation 5.9 is able to contribute to crack growth when the crack length is less than 16.5 m. Thus applying the two crack growth equations, three regions of integration can be defined:-

(i) Short crack zone

This was defined as the region where the crack grows from its initial length (taken as the inclusion radius of 5 m, as cracks were observed to grow from inclusions in [2]), to the crack size corresponding to the threshold stress intensity  $a_{th}$  (found from figure 5.3). Equation 5.6 was integrated between these bounds to describe crack extension in this region.

(ii) The interactive zone

This is the zone where both the "long" and "short" growth mechanisms characteristic of equations 5.9 and 5.6 respectively may operate. during this period the crack extends from its length of  $a_{th}$  to the first grain boundary. A composite crack propagation equation which was a simple addition of equation 5.9 and equation 5.6 was assumed to describe the crack growth rate, namely

$$\frac{da}{dN} = 2.22 \times 10^{-4} (16.5 - a)^{0.6} a^{0.4} + 1.04 \times 10^{-4} a - 1.68 \times 10^{-3} \quad (5.10)$$

which was then integrated throughout the interactive zone.

(iii) Long crack zone

This is the final region of accelerating crack growth from the first grain boundary to failure at  $a_f$ . the value of  $a_f$  was taken to be the width of the specimen [2], however the predicted lifetime was not very sensitive to substantial changes in  $a_f$ . In this area equation 5.9 alone was integrated. Combining the results of these calculations in region (i), (ii) and (iii) a plot of crack length (a) versus number of cycles to failure (N) is shown in figure 5.4. This now illustrates not only the conventional long crack growth behaviour, but also the early and much more rapid growth of the short crack within the first grain in the surface layer of the material.

In addition, this approach predicts that at lower stresses fatigue failure will not occur. If the crack length corresponding to  $\Delta K_{th}$  is greater than  $d$ , the grain

diameter, then cracks that initiate at the surface will grow up to the first grain boundary and arrest according to equation 5.6. This is because the length is too short for the linear elastic mechanism to operate. Behaviour of this type is also illustrated in figure 5.4. Non-propagating cracks of this type were observed by Lankford [2], and indicates that a definite fatigue limit can be observed in this alloy.

## 5.2.2 Short Crack Growth in a Medium Carbon Steel

### 5.2.2.1 Crack Growth in the First Grain

All crack growth data obtained from application of the replication technique were presented in Appendix I. In order to use a short crack equation of the form of equation 5.4 it is necessary to find values of  $d$  for each crack. For cracks where the associated grain boundary could be seen on the replicas a value for  $d$  may be measured, but it may not always be the case that the minimum crack growth rate occurs precisely at that grain boundary. So to find  $d$  firstly the values of  $da_s/dN$  were plotted with linear scale against  $a_{mean}$  for each crack, using the secant method to obtain the average crack growth rate, then a "least squares" fit was performed on those points where  $da_s/dN$  was decreasing for increasing crack length. The dimension  $d$  was then taken to be the value of  $a_s$  where the extrapolated "least squares" equation intersected the

length axis. This method is illustrated by a schematic in figure 5.5. The values of  $(d-a_s)$  in column 6 of Appendix I could then be obtained by subtracting  $a_{\text{mean}}$  from the calculated value for  $d$ .

Because of the insensitivity of the value of  $\alpha$  on crack growth rate when  $a_s > d/2$  (shown in figure 5.1), which is the area containing most data points, and in order to simplify the analysis, a value for  $\alpha$  of zero is first considered. This also gave an equation of the same type suggested by De Los Rios et al [7] in which cracks were measured on specimens subjected to high cycle torsional fatigue using the same batch of carbon steel.

One way to determine whether this value of  $\alpha$  is reasonable, is to assume an equation of the form:

$$\frac{da_s}{dN} = C (d - a_s)^n \quad (5.11)$$

and to see which values of  $n$  give a best fit to experimental data. For two successive pairs of data points of the form  $(d-a_{s,\text{mean}}, da_s/dN)$  equation 5.11, can be written

$$\frac{da_{s,1}}{dN} = C (d - a_{s,1,\text{mean}})^n \quad (5.12)$$

and

$$\frac{da_{s,2}}{dN} = C (d - a_{s,2,mean})^n \quad (5.13)$$

Combining 5.12 and 5.13 gives:

$$n = \frac{\text{Log}_e \left( \frac{da_{s,1}}{dN_1} \right) - \text{Log}_e \left( \frac{da_{s,2}}{dN_2} \right)}{\text{Log}_e (d - a_{s,1,mean}) - \text{Log}_e (d - a_{s,2,mean})} \quad (5.14)$$

which was calculated for each pair of successive points for each crack. Figures 5.6a - 5.6c show plots of  $d - a_{s,mean}$  versus  $da_s/dN$  for each crack observed at three stress levels. The dotted line represents the slope corresponding to a value for  $n$  of unity, in each plot. It can be seen that choosing  $n = 1$  is not unreasonable as the average values of  $n$  for each plot were 1.16, 1.65 and 1.28 for stress levels of 638.5, 815.9 and 998.4 MPa respectively. The dotted line on figures 5.6a - 5.6c represent  $n = 1$ .

It should also be apparent from figures 5.6a - 5.6c, that there is a lot of scatter of points about the dotted lines. Taking  $n = 1$  in equation 5.11 gives:

$$\frac{da_s}{dN} = C (d - a_s) \quad (5.15)$$

so scatter is related to changes in the value of  $C$ . For each data point on figure 5.6a - 5.6c, a value of  $C$  was then

calculated assuming equation 5.15 to hold. Then all the values for C were plotted against the relevant stress range, as shown in figure 5.7. This produces an enormous amount of scatter in the values of C, but this is to be expected due to some cracks being able to propagate much more quickly than others, depending on how favourably orientated an individual grain is for crack growth.

It can be reasonably assumed that fast growing cracks are more likely to be the cause of the final fatigue failure than those cracks which are growing slowly, so any equation expressing C as a function of stress and which is used to estimate fatigue lives should take this fact into consideration.

Using a standard statistical method for calculating a confidence level around a linear regression line [8]; for n pairs of data of the form (x,y) there is a probability  $1 - \beta$  that a future observation on y at the point x will lie between the two values:

$$\hat{a}_0 + \hat{a}_1 x_0 \pm t_{\beta/2, n-2} S_{y/x} \left[ 1 + \frac{1}{n} + \frac{(x_0 - \bar{x})^2}{\sum_{i=1}^n (x_i - \bar{x})^2} \right] \quad (5.16)$$

when  $y = \hat{a}_0 + \hat{a}_1 x$  is the regression line,  $\bar{x}$  is the mean value of x,  $t_{\beta/2, n-2}$  is the t-test statistic assuming a normal distribution, and  $S_{y/x}$  is given by:

$$S_{y/x} = \sum_{i=1}^n \frac{(y_i - \hat{a}_0 - \hat{a}_1 x_i)^2}{n - 2} \quad (5.17)$$

As we are more interested in the fast growing cracks, a one-sided t-test giving a 95% confidence interval is used, (given by using a t-statistic of  $t_{0.05, n-2}$  in expression 5.16 and taking the "+" sign).

This equation is shown in figure 5.7, which produces a slight curve for this data. Taking values for a 95% confidence interval at both the lower stress of 638.5MPa, and the upper stress of 998.4MPa, a straight line between these points is given by the equation:

$$C = 1.64 \times 10^{-34} (\Delta\sigma)^{11.141} \quad (5.18)$$

and substituting for C in equation 5.15 gives:

$$\frac{da_s}{dN} = 1.64 \times 10^{-34} (\Delta\sigma)^{11.141} (d - a_s) \quad (5.19)$$

Note the exponent is quoted to five significant figures simply because truncation to give less figures in order to reflect the accuracy of determination (fig. 5.6) produces a significant deviation in the calculated values for C.

### 5.2.2.2 Long Crack Growth

Crack growth data obtained from replicas where the crack length ( $a_s$ ) was greater than  $d$  are plotted for each of three stress levels in figures 5.8a - 5.8c. For cracks with which a value of  $d$  could not be obtained due to insufficient data, only crack growth data such that  $a_s > 2d_{\text{mean}}$  is plotted where  $d_{\text{mean}}$  is the average of all calculated  $d$  values, in order to be reasonably certain that the crack had propagated beyond the first grain boundary. Crack growth rates obtained from striation counting are also shown in this figure.

An equation of the form:

$$\frac{da_s}{dN} = Ca_s - D \quad (5.20)$$

was assumed to describe the crack growth rate being based on equations 5.7 and 5.9 discussed above for the aluminium alloy.

A regression line was fitted to data points obtained from replicas where the crack length was greater than 400 microns to obtain three values for  $C$ , assuming that  $Ca_s \gg D$  for  $a_s > 400\mu\text{m}$  in equation 5. The best fit lines are also shown in figures 5.8a - 5.8c.

Expressing  $C$  as a function of  $\Delta\varepsilon_t$  determined from equation 3.1 the power law relationship given by:

$$C = C_1 (\Delta\varepsilon_t)^\alpha \quad (5.21)$$

is plotted against the total strain range in figure 5.9, giving values of 4.102 and 2.0604 for  $C_1$  and  $\alpha$  respectively. Combining equation 5.20 and 5.21 gives:

$$\frac{da_s}{dN} = 4.102(\Delta\epsilon_t)^{2.0604} a_s - D \quad (5.22)$$

for  $a_s$  in  $\mu\text{m}$ .

To determine  $D$ , use was made of the threshold data obtained on the notched specimen, figure 3.10. Re-arranging equation (3.10), and assuming  $a_s = 2a$  for a semicircular crack shape, for

$$a_s = \frac{2\Delta K_{th}^2}{\pi Y^2 \Delta\sigma^2} \quad (5.23)$$

and noting that for linear elastic conditions  $\epsilon_t = \frac{\Delta\sigma}{E}$  substitution of equation 5.23 into 5.22 gives:

$$\frac{da_s}{dN} = 5.629 \times 10^{-3} (\Delta\epsilon_t)^{0.0604} - D \quad (5.24)$$

using values of  $\Delta K_{th} = 6.0\text{MPa}\sqrt{\text{m}}$ ,  $Y = 2/\pi$  and  $E = 203\text{ GPa}$ . As equation 5.24 is obtained for threshold conditions for zero crack growth rate, then  $da_s/dN = 0$ , giving:

$$D = 5.269 \times 10^{-3} (\Delta\epsilon_t)^{0.0604} \quad (5.25)$$

Although D varies with change in strain range, the lowest strain level used in the fatigue tests (shown in Table 3.1), gives a value for  $(\Delta\varepsilon_t)^{0.0604}$  of 0.70, and the highest strain level gives  $(\Delta\varepsilon_t)^{0.0604}$  a value of 0.81. So, because D does not vary significantly with strain level, an average value of  $(\Delta\varepsilon_t)^{0.0604}$  was used to calculate D, which was then substituted into equation 5.22, giving:

$$\frac{da_s}{dN} = 4.102 (\Delta\varepsilon_t)^{2.0604} a_s - 4.237 \times 10^{-3} \quad (5.26)$$

which was assumed to describe crack growth for  $a_s > d$  for all strain levels. This equation is shown along with the experimental data in figures 5.8a - 5.8c.

### 5.2.2.3 Lifetime Calculations

Following the same procedure explained in detail in section 5.2.1.3, to perform lifetime predictions three regions of integration are first defined.

In the first region, for short crack growth, equation 5.19 was integrated between  $a_o$  and  $a_{th}$ , where  $a_o$  was equated to the peak to trough surface roughness measurement  $R_t$  of  $0.4\mu\text{m}$ , and  $a_{th}$  was calculated for each strain range by taking the value of  $a_s$  which makes  $da_s/dN$  zero in equation 5.26.

For the second region an equation representing a simple sum of equation 5.19 and 5.26, namely:

$$\frac{da_s}{dN} = 1.64 \times 10^{-34} (\Delta\sigma)^{11.141} (d - a_s) + 4.102 (\Delta\epsilon_t)^{2.0604} a_s - 4.237 \times 10^{-3} \quad (5.27)$$

was integrated between  $a_{th}$  and  $d_{mean}$ , where  $d_{mean}$  was taken to the average value of all the calculated values of  $d$ , which was  $116.37\mu m$ .

For the final region of integration the long crack equation 5.26 alone was integrated between  $d$  and  $a_f$ , where  $a_f$  was taken to be  $4.0mm$ , representing half the diameter of the specimen.

By summing the three areas of crack growth, the lifetime may be calculated.

Results of the integrations for some typical strain levels are shown in table 5.1, along with actual lifetimes. Graphs showing equation 5.19 and 5.26 for the highest and lowest strain levels in table 5.1, are shown in figures 5.10a and 5.10b.

It can be seen from the results in table 5.1, that the calculated lifetimes agree well with actual lifetimes. Even for the lowest stress range less than 2.5% of the calculated lifetime is spent in Region 1, suggesting that the number of cycles spent in initiating a crack (as defined in chapter 1) may be taken as zero.

CHAPTER FIVE - REFERENCES

- [1] HOBSON, P.D. (1982)  
"The formulation of a crack growth equation for short cracks"  
Fatigue Engng. Mater. Struct. 5 p.323-327
- [2] LANKFORD, J. (1982)  
"The growth of small fatigue cracks in 7075-T6 aluminium alloy"  
Fatigue Engng. Mater. Struct. 5 p.233-248
- [3] FLECK, W.G. & ANDERSON, R.B. (1969)  
"A mechanical model of fatigue crack propagation"  
Proceedings of the 2nd International Conference  
on Fracture, Brighton  
Chapman & Hall, London p.790-802
- [4] LINDER, B.M. (1965)  
"Extremely slow crack growth rates in aluminium alloy  
7075-T6"  
M.S. thesis, Lehigh University, U.S.A.
- [5] FROST, N.E. MARSH, K.J. & POOK, L.P. (1974)  
"Metal Fatigue"  
Clarendon Press, Oxford. p.263

- [6] PARIS, P.C. (1963)  
"The fracture mechanics approach to fatigue"  
Proc. 10th Sagamore Army materials research Conference  
Syracuse University Press, U.S.A. p.107
- [7] DE LOS RIOS, E.R. TANG, Z. & MILLER, K.J. (1984)  
"Short crack fatigue behaviour in a medium carbon steel"  
Fatigue Engng. Mater. Struct. 7 p.97-108
- [8] STATISTICS FOR TECHNOLOGY  
Christopher Chatfield  
Chapman & Hall, London p.174-177

## CHAPTER FIVE - TABLES

- 5.1 Fatigue lifetime calculations

## CHAPTER FIVE - FIGURES

- 5.1 Sensitivity of crack growth equation 5.4 to variations in  $\alpha$
- 5.2 Short crack growth rates in 7075-T6 aluminium alloy
- 5.3 Fatigue crack growth rates in 7075-T6 aluminium alloy
- 5.4 Crack growth rates in 7075-T6 aluminium alloy at low stresses showing crack arrest at a grain boundary
- 5.5 Schematic to illustrate the method used to calculate  $d$
- 5.6 a - c Short crack growth results
- 5.7 Coefficient C of short crack growth equation versus stress range
- 5.8 a - c Crack growth results
- 5.9 Coefficient C of long crack growth equation versus total strain range
- 5.10 a) & b) Crack growth rate versus crack length as predicted by the two crack growth equations

TABLE 5.1

FATIGUE LIFETIME CALCULATIONS

Cyclic Ranges		Threshold Crack Lengths		Calculated Lifetimes (Number of cycles)			Calculated Lifetime	Actual Lifetime
Stress	Strain	Short Cracks	Long Cracks	ZONE			Using Equations 5.19 & 5.26	
				1	2	3		
MPa	Plastic	d (μm)	a <sub>th</sub> (μm)	Eqn. 5.19	Eqn. 5.19 + Eqn 5.26	Eqn. 5.26	Number of Cycles	
	Total							
998.4	0.02496	116.37	1.89	0	12	1,586	1,598	1,254
	0.02611							
815.9	0.0086	116.37	7.08	1	97	6,014	6,112	6,214
	0.0138							
700	0.0039	116.37	19.29	22	455	16,907	17,384	12,643
	0.0085							
638.5	0.0024	116.37	35.20	122	1,276	32,308	33,706	35,778
	0.0063							
550	0.0011	116.37	93.41	2,912	4,907	113,248	121,067	73,508
	0.0039							

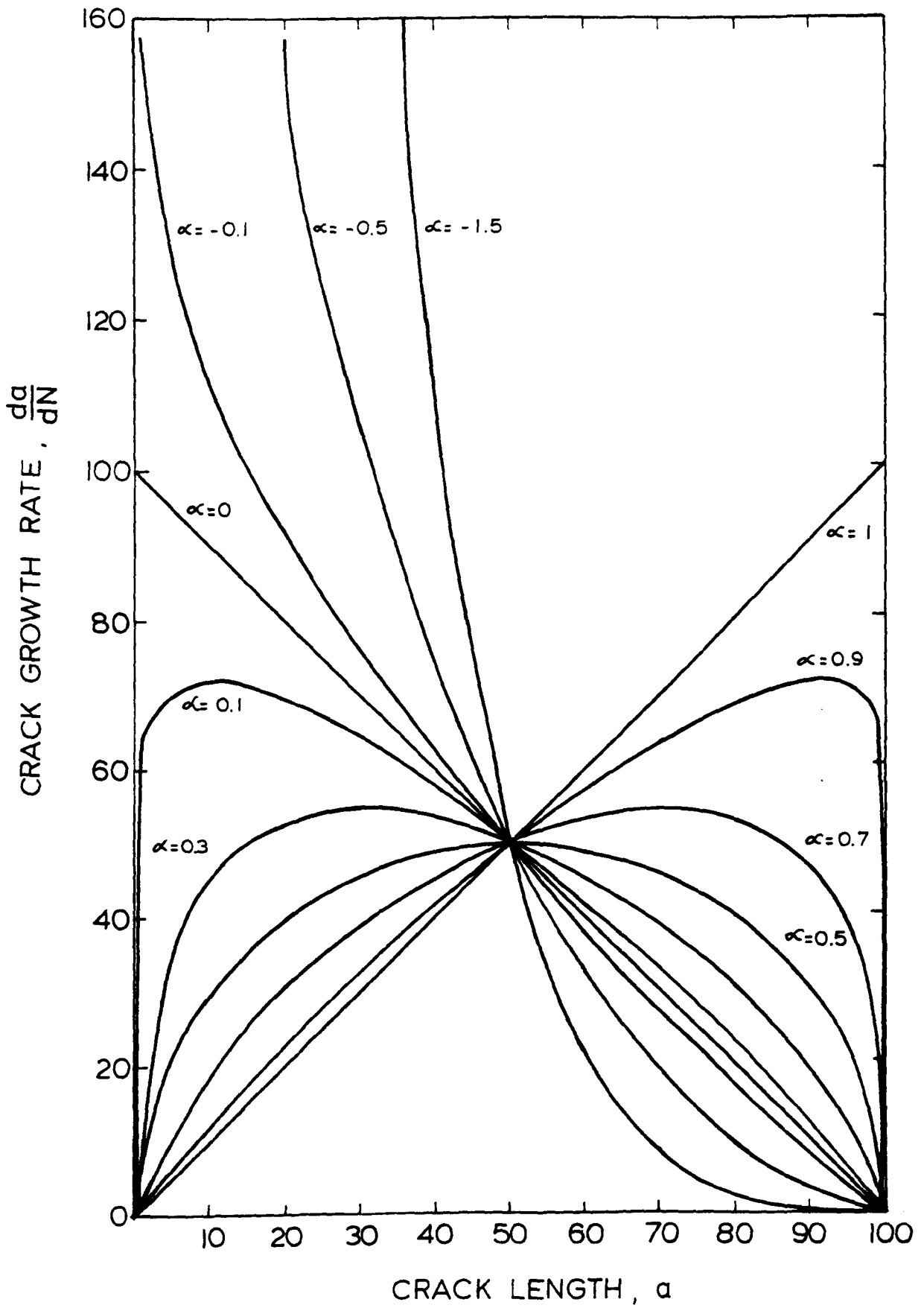
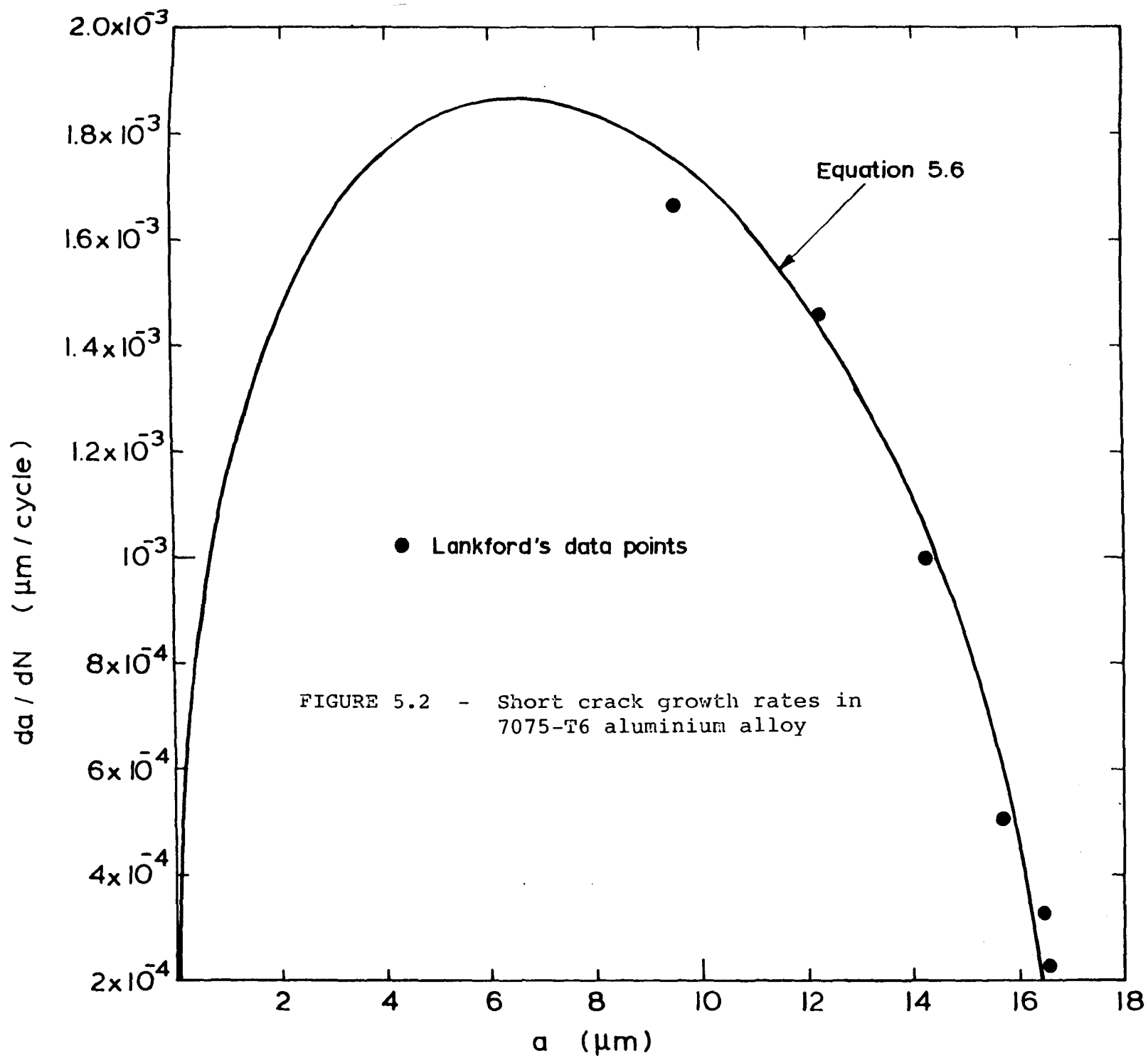


FIGURE 5.1 - Sensitivity of crack growth equation 5.4 to variations in  $\alpha$



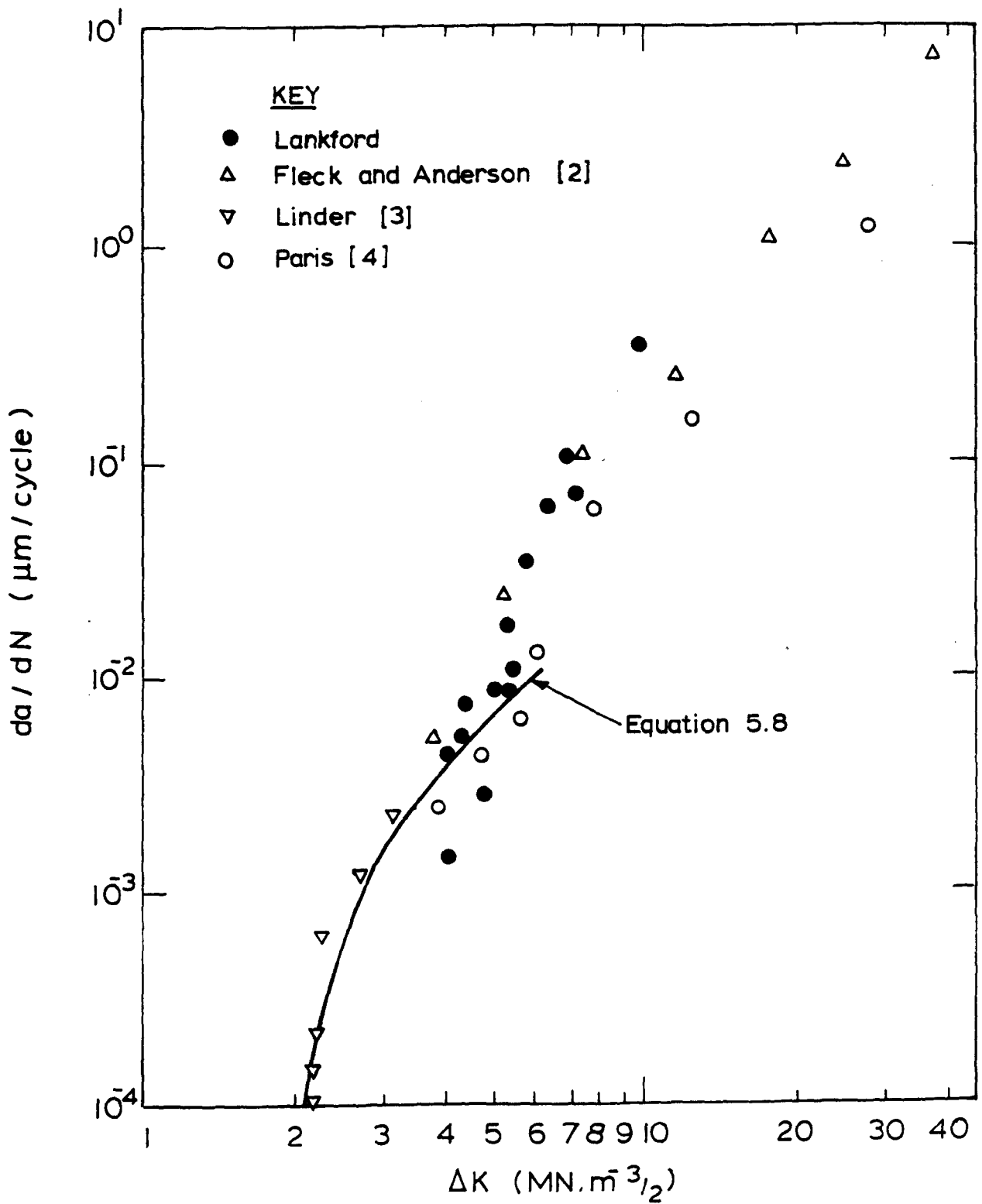


FIGURE 5.3 - Fatigue crack growth rates in 7075-T6 aluminium alloy

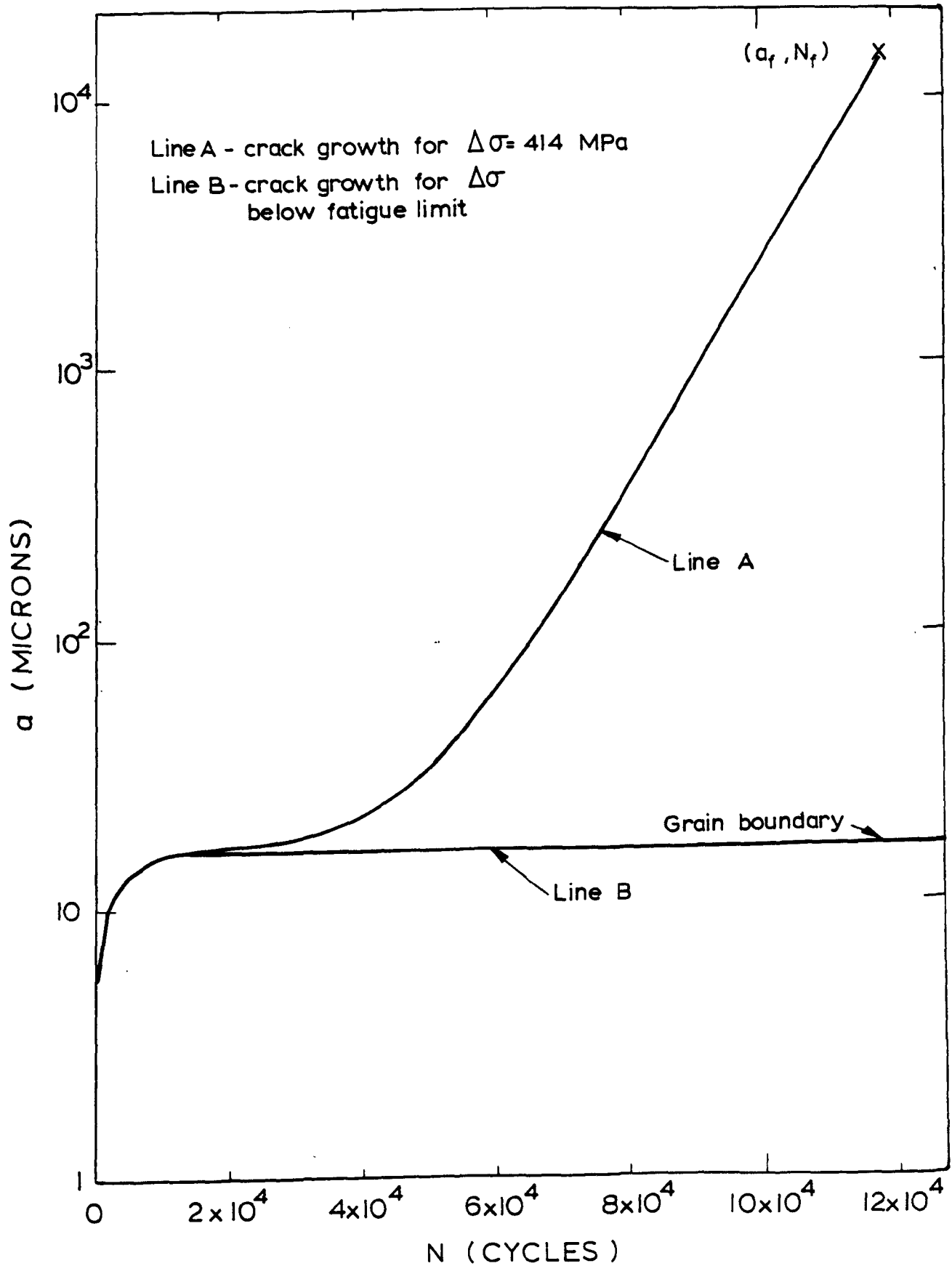


FIGURE 5.4 - Crack growth rates in 7075-T6 aluminium alloy at low stresses showing crack arrest at a grain boundary

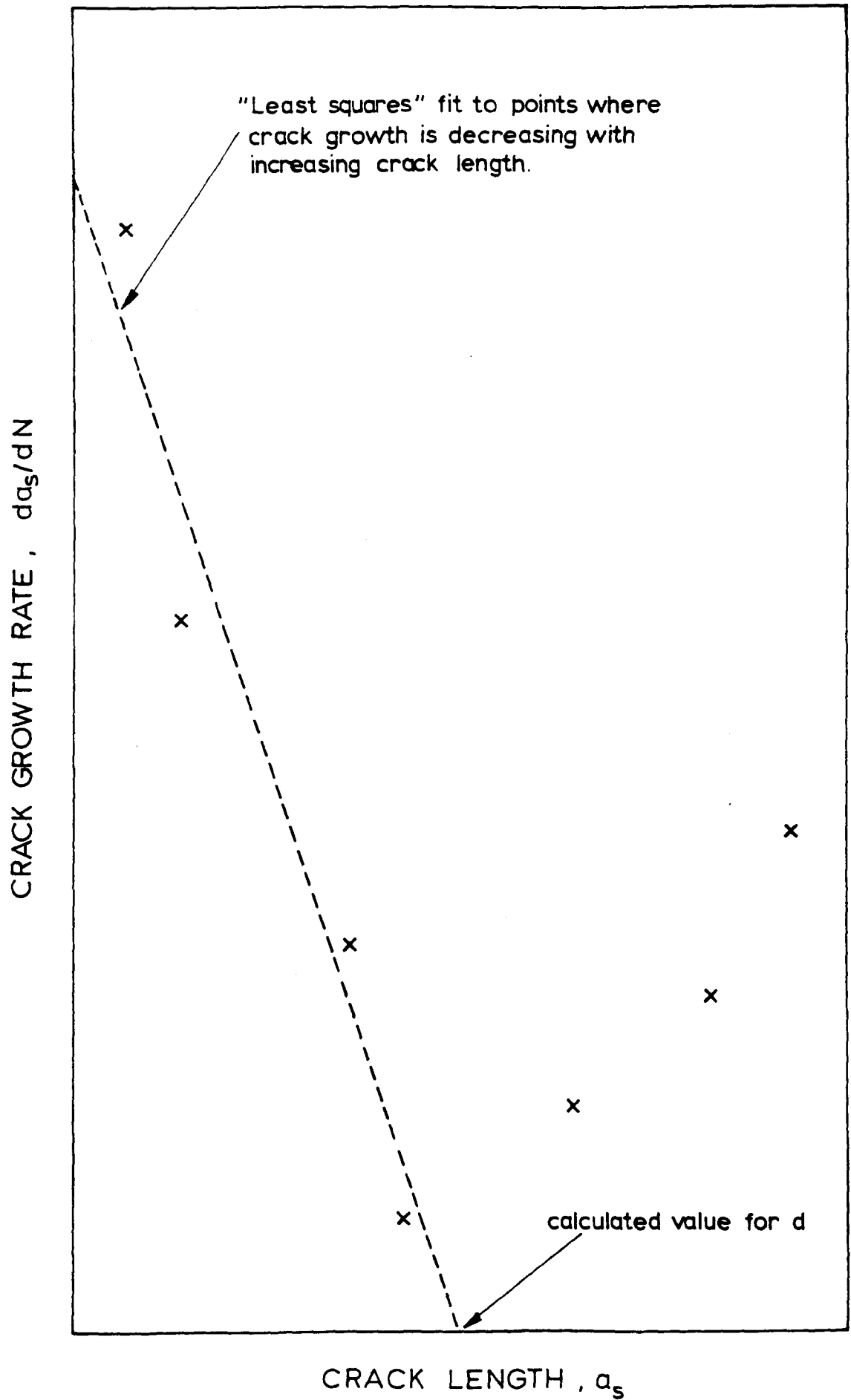


FIGURE 5.5 - Schematic to illustrate the method used to calculate  $\bar{d}$

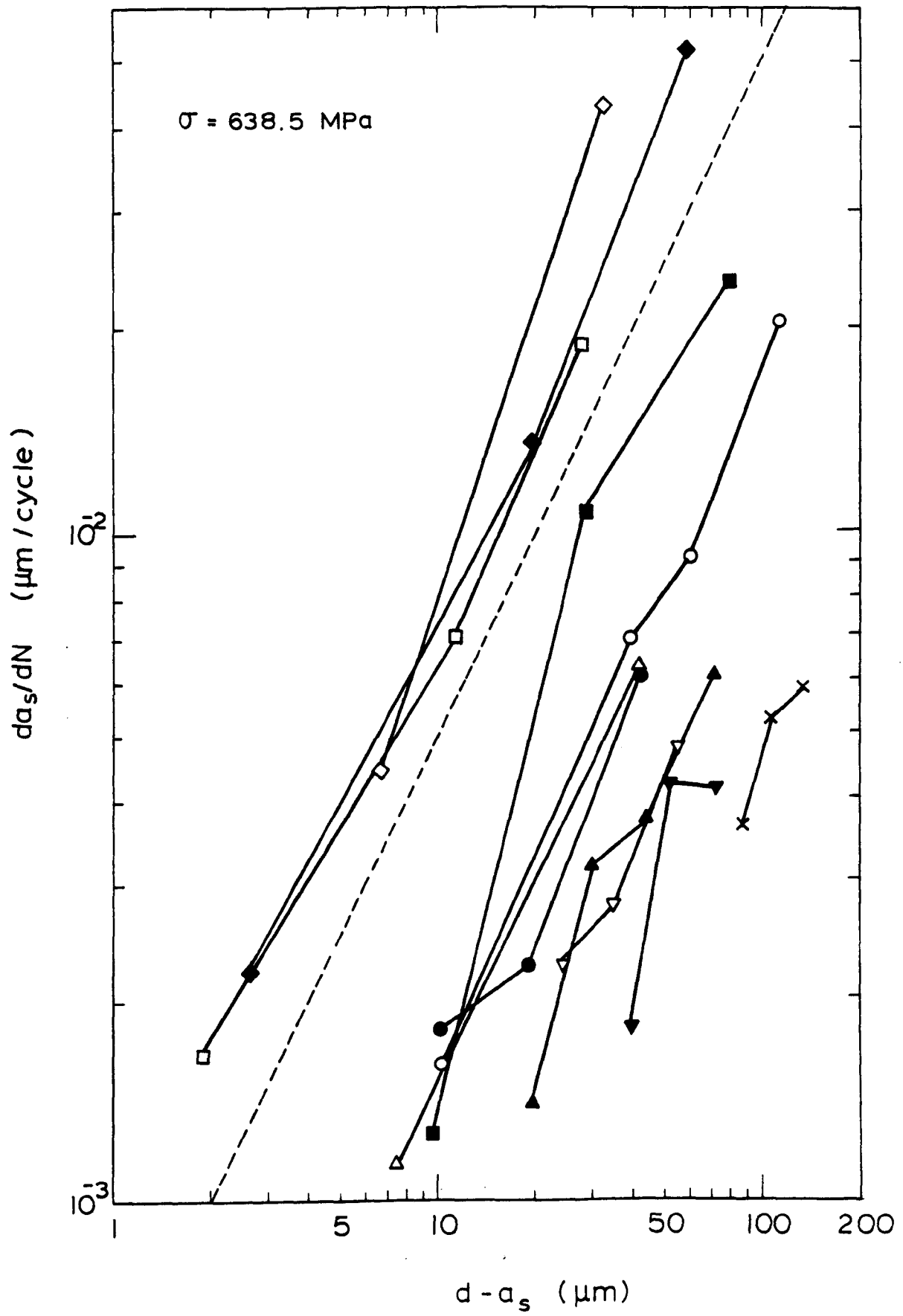


FIGURE 5.6a - Short crack growth results

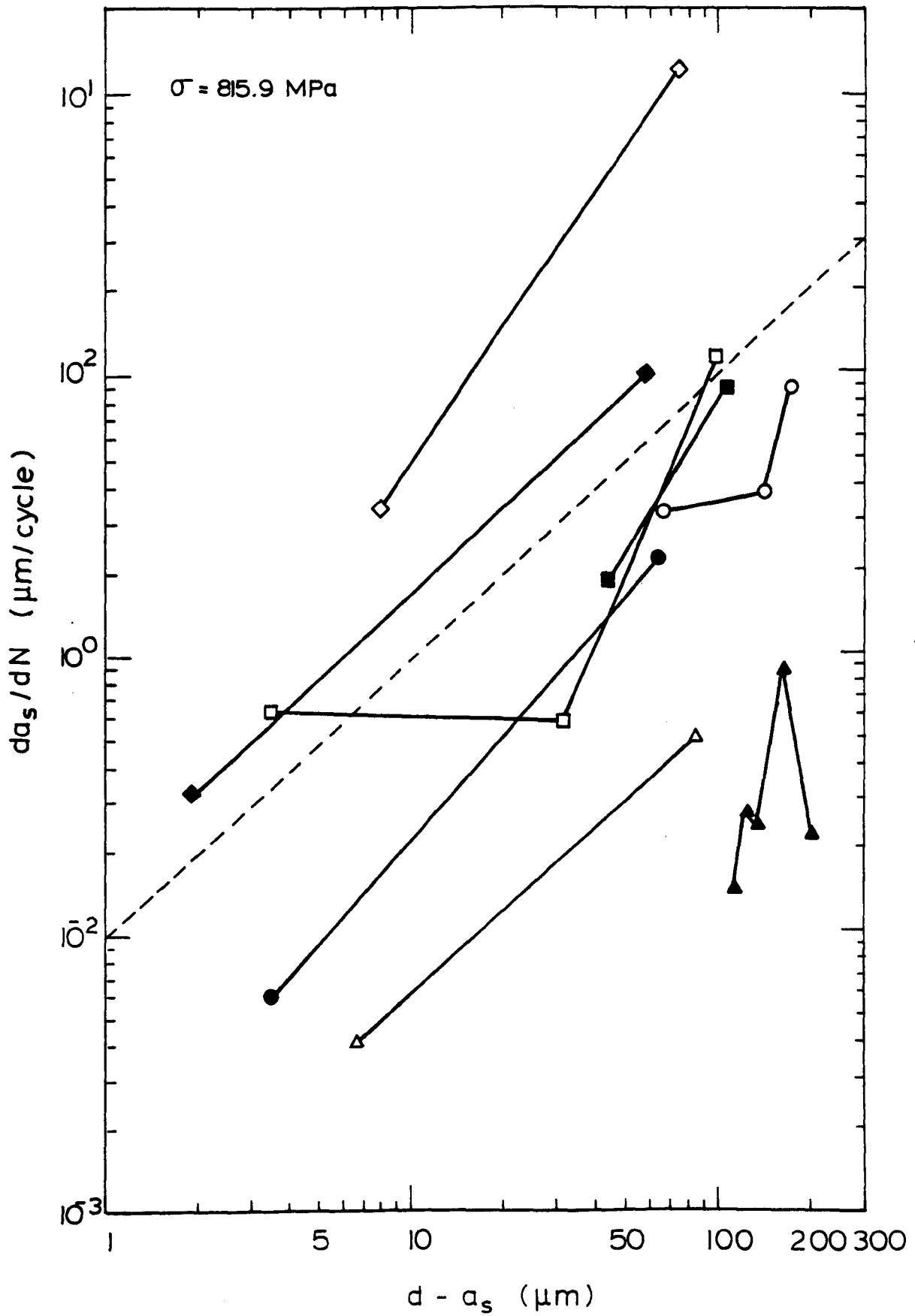


FIGURE 5.6b - Short crack growth results

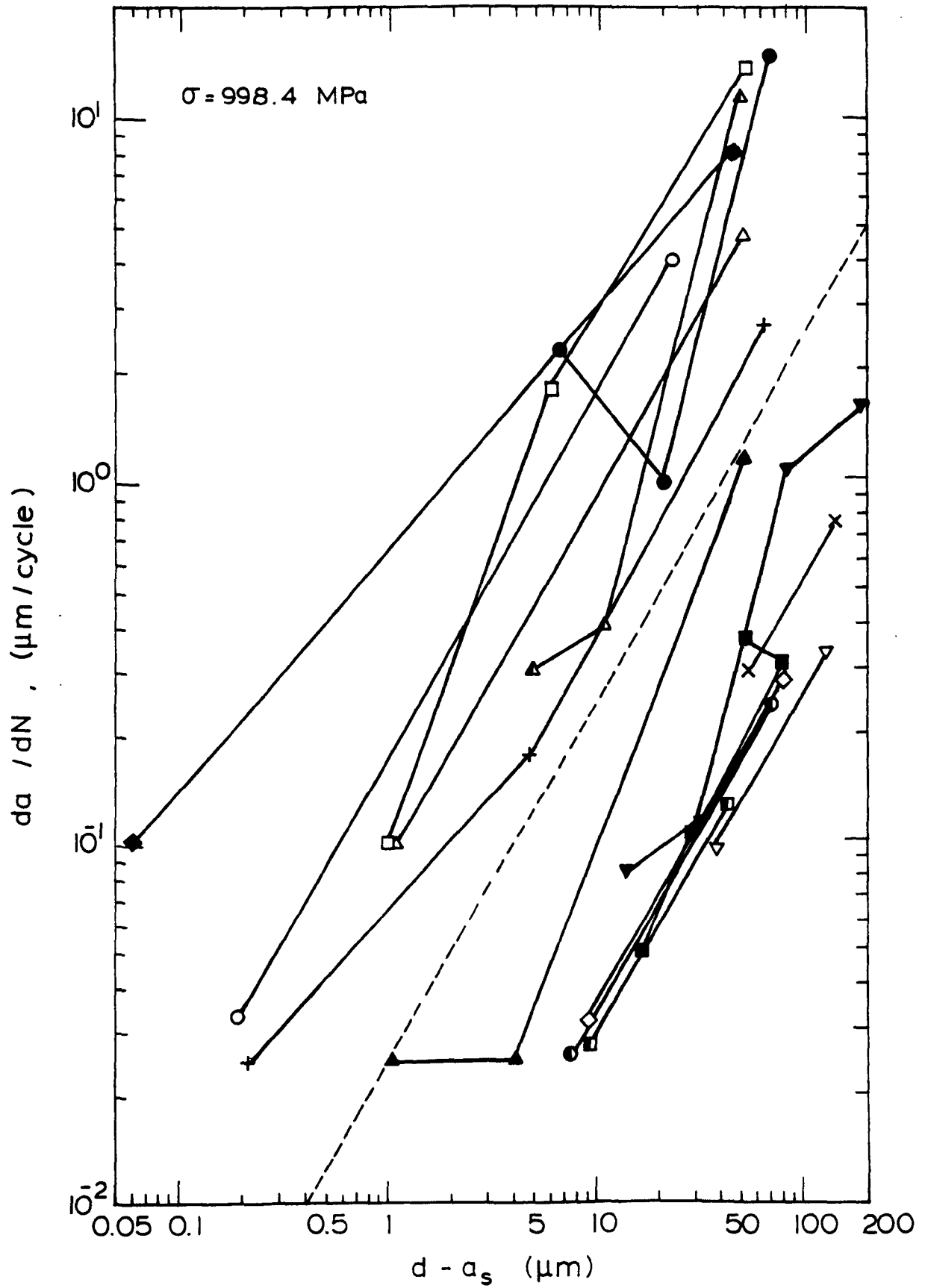


FIGURE 5.6c - Short crack growth results

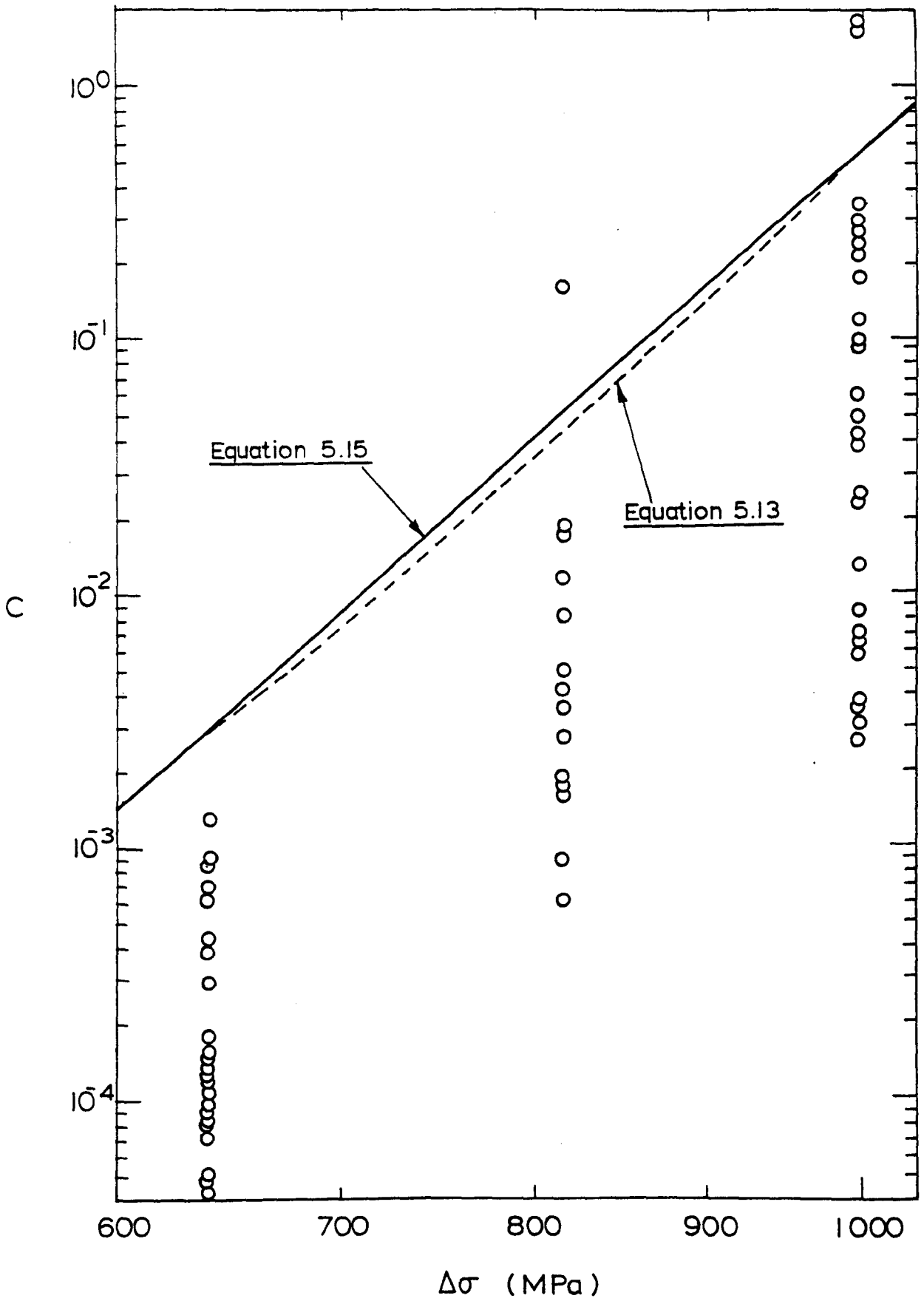


FIGURE 5.7 - Coefficient C of short crack growth equation versus stress range

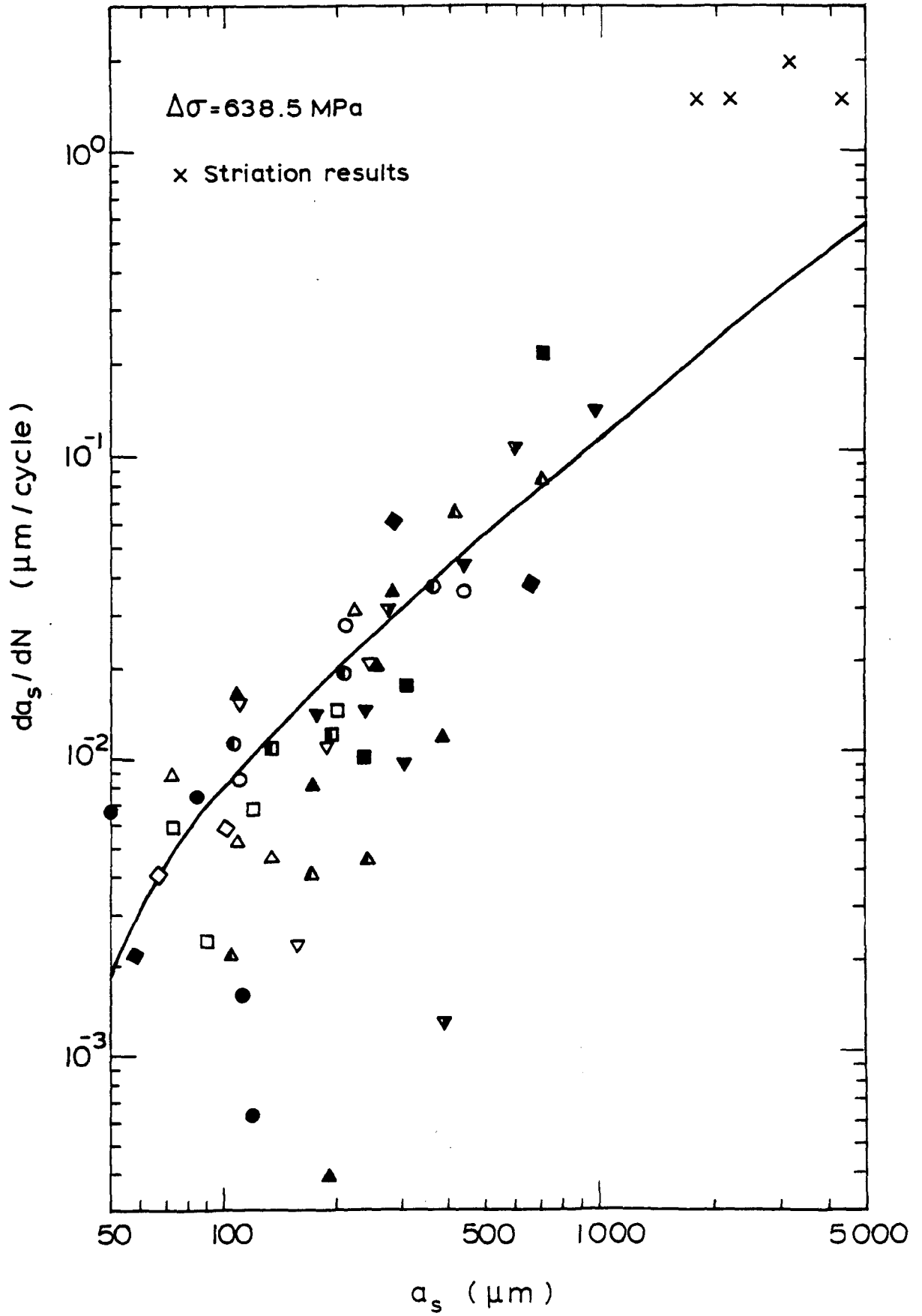
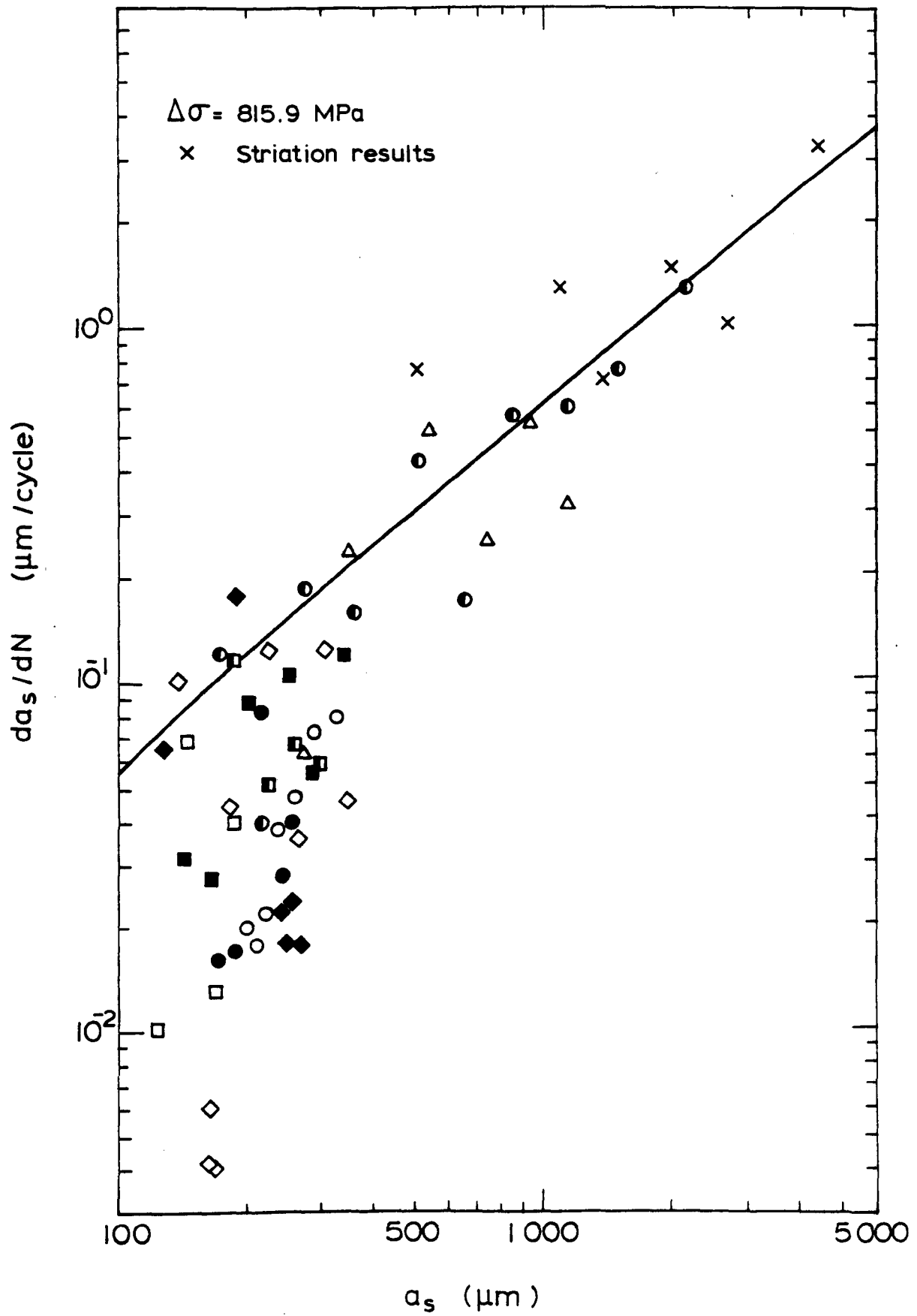


FIGURE 5.8a - Crack growth results



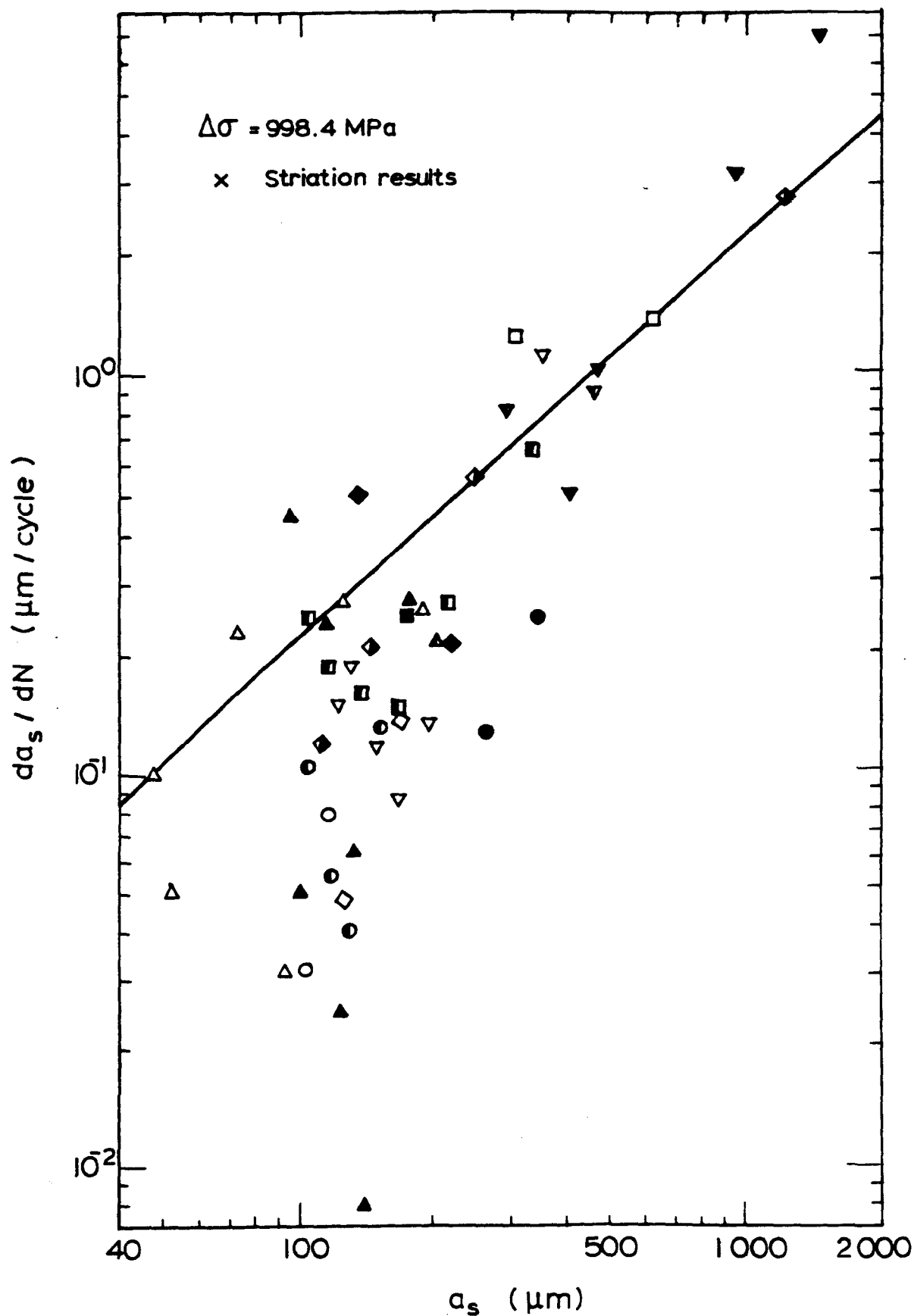


FIGURE 5.8c - Crack growth results

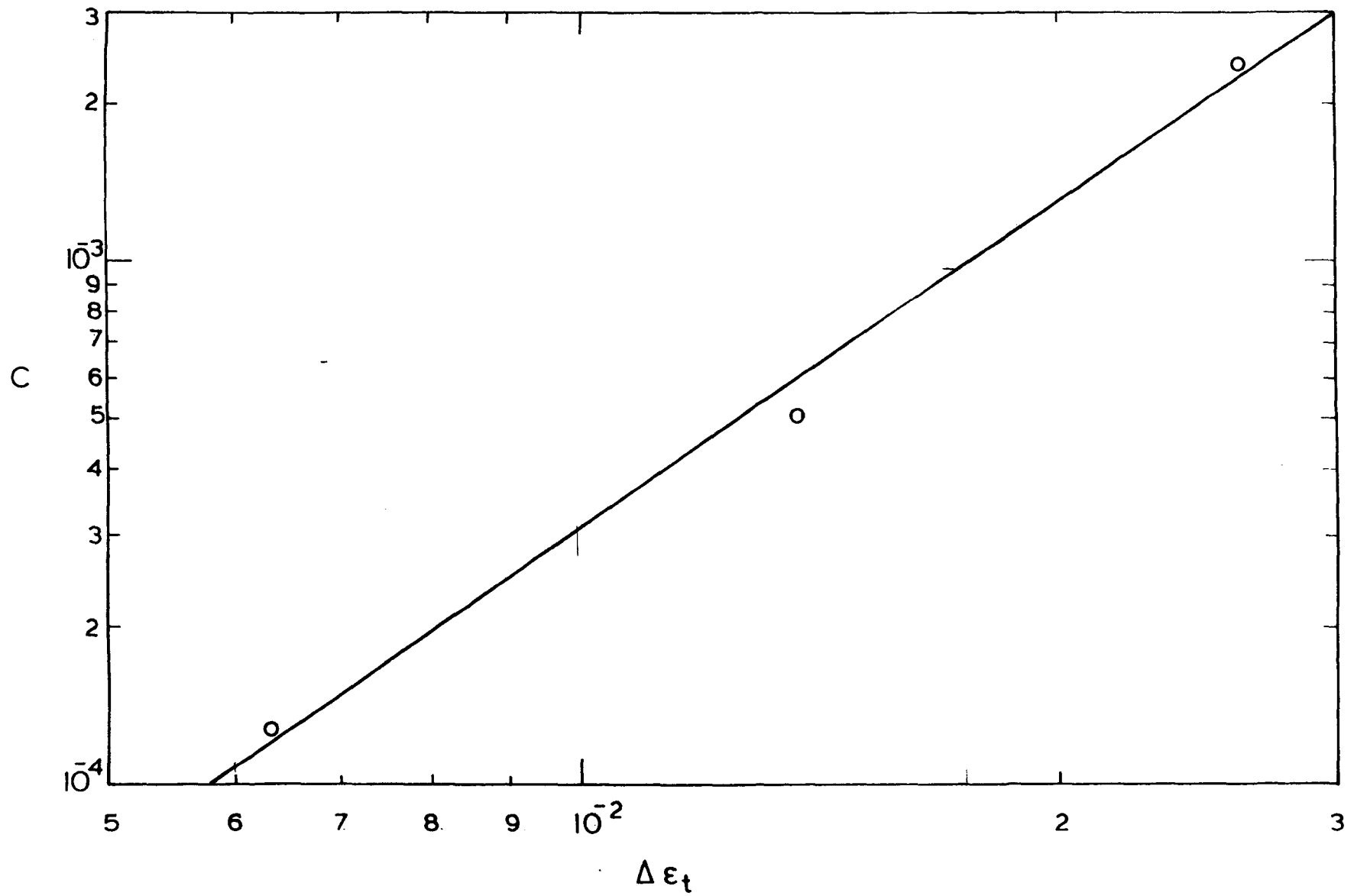


FIGURE 5.9 - Coefficient C of long crack growth equation versus total strain range

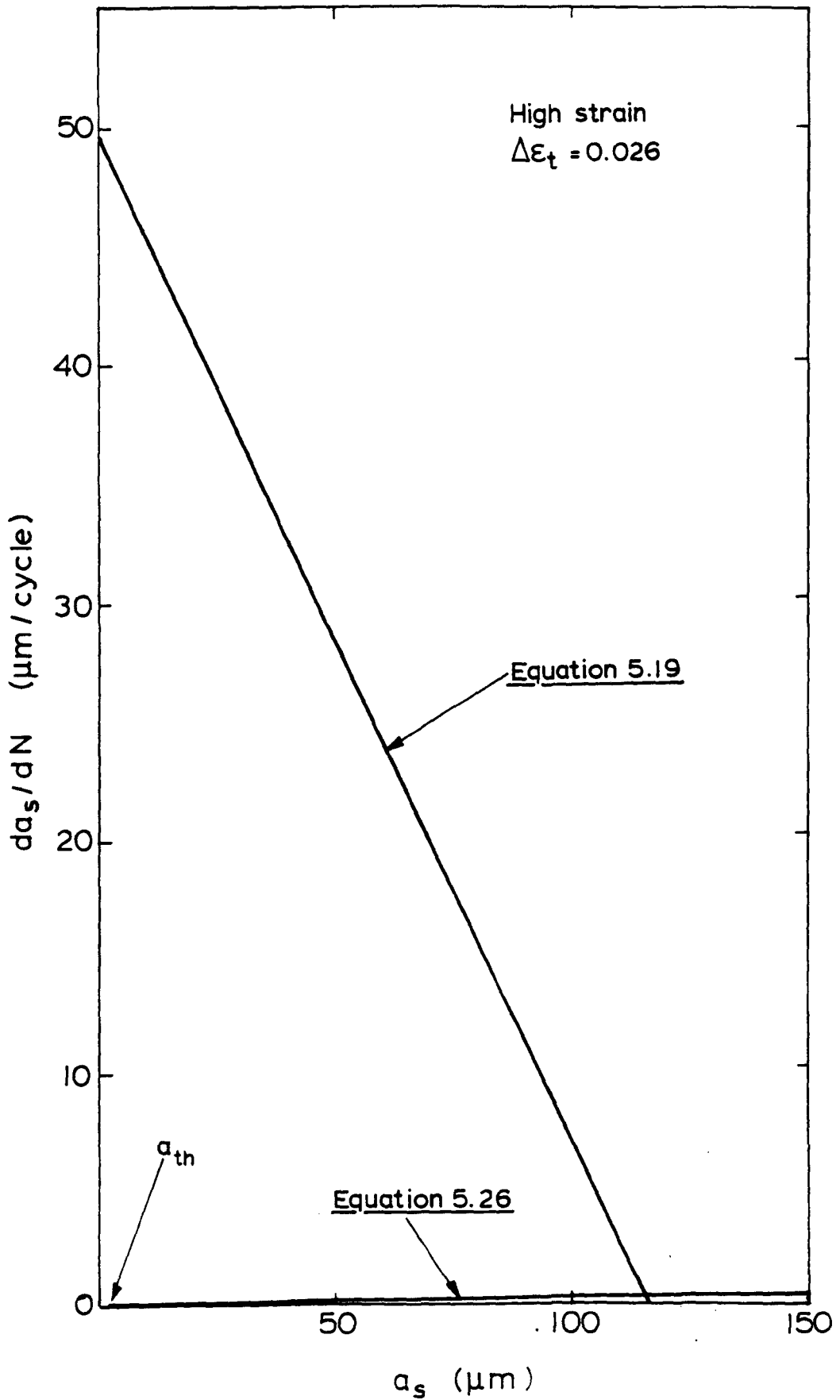


FIGURE 5.10a - Crack growth rate versus crack length as predicted by the two crack growth equations

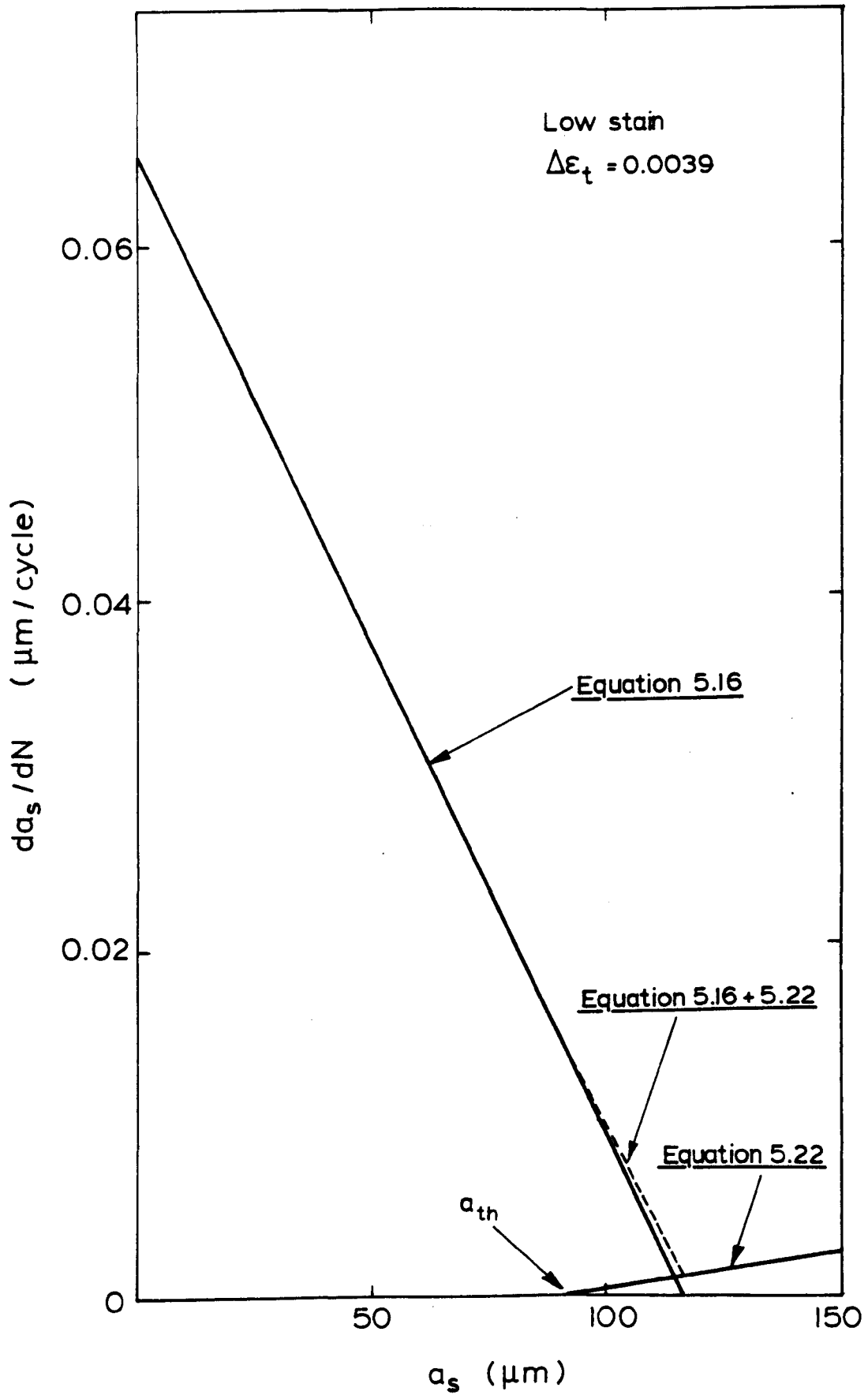


FIGURE 5.10b - Crack growth rate versus crack length as predicted by the two crack growth equations

## CHAPTER SIX

### Discussion

This discussion presents a critical assessment of the various issues raised by the project and comments on their relevance to past and future work. The issues are not presented in any order of priority, but rather reflect traditional methods of examining fatigue deformation and failure.

#### 6.1 Stress-Strain Behaviour

The cyclic stress-strain curve is plotted in figure 3.1(a). However it is interesting to replot the data in order to show how much of the scatter may be accounted for by bar to bar variability. Results from this study are plotted in figure 6.1 along with Ibrahim's data [1] obtained from the same material.

For Ibrahim's data, there is reasonable agreement with the results from bar A, although if anything the results predict a lower strain range for a given stress. Thus, Ibrahim's data lie within the spread of experimental data found in this study. It is important to remember at this point that the results were obtained for both strain and load control. Ibrahim's results were from a single specimen subjected to a multiple step test in load control. Results shown from bar A were all conducted in

strain control. Those shown from bar C are from strain controlled fatigue tests, a load controlled multiple step test and one load controlled fatigue test. Unfortunately, no strain readings were taken for specimens from bar B. It is clear that most of the data from bar C falls on one line regardless of whether the test was conducted in load or strain control.

By plotting plastic strain range versus stress range figure 6.2 is obtained, which is the same as figure 3.2 except that Ibrahim's results are also shown. These tests correspond with those shown in figure 6.1. Reference [1] did not give values for plastic strain, so this was calculated from the total strain range by subtracting the elastic strain  $\Delta\sigma/E$ .

Similar observations to those made for figure 6.1 can be seen. Ibrahim's data gave reasonable agreement with results from bar A, and the data from bar C showed fair agreement between load and strain control. For low stresses the large scatter was probably due to more percentage error incurred in the plastic strain reading than to the very small plastic strain range, or the slightly different yield stresses between bars.

The good agreement between load and strain controlled tests for total strain range plotted against stress gives support to the validity of using equations connecting total strain range with stress range when applying the long crack growth equation 5.26 to obtain lifetime predictions for tests conducted in load control.

Although errors are incurred in amassing all the data into a single stress-strain equation, scatter in these results is far less than the scatter in short crack growth rates. So these errors are not going to be as important as errors in calculating values for C and n in equation 5.11, using crack growth rates.

The stress-strain equation 3.1 is used to calculate strain ranges for tests performed in load control, in which the strain was not measured, before applying equation 5.26 to lifetime calculations. Although equation 3.1 was formulated for all the test data, if this equation was formulated for only results from bar A, there is less than 4% difference in the resulting lifetime calculated from equation 5.26 for any stress level.

Because of this small difference, and also the lack of stress-strain response data for bar B (which was used for all tests at 998.4MPa and 815.9MPa) it was decided to use all the available stress-strain data from both bar A and bar C in formulating equation 3.1.

## 6.2 S-N Curves

The results of figure 3.4 are replotted in figure 6.3, to examine whether the trend noticed for the stress-strain data  <sup>$\Delta\sigma/N_f$</sup>  whereby the cyclic stress-strain properties vary slightly from bar to bar) is repeated in the lifetime data.

Results from Ibrahim [1] are also shown for comparison with data obtained from this study in figure 6.3. For the fatigue tests, specimens were taken from three bars, and using a "least squares" fit a Basquin relationship can be derived for the four sets of data:-

For Ibrahim's data

$$\Delta\sigma N_f^{0.106} = 2080 \quad (6.1)$$

For bar A

$$\Delta\sigma N_f^{0.141} = 2794 \quad (6.2)$$

For bar B

$$\Delta\sigma N_f^{0.128} = 2488 \quad (6.3)$$

For bar C

$$\Delta\sigma N_f^{0.127} = 2255 \quad (6.4)$$

These equations are also plotted in figure 6.3.

It can be seen that for a given stress range the longest fatigue life is predicted by equation 6.1 for Ibrahim's data, for  $N_f > 4000$ . The results from bars A and B are very similar, whereas equation 6.4 derived for results for bar C gives the shortest lifetime. For low cycle fatigue, Ibrahim's data showed a shorter lifetime for a given stress than the predictions of the other equations. However, this arises because the two tests performed by Ibrahim at a stress range greater than 1000MPa gave

a shorter lifetime than to be expected from extrapolation of his other results, which caused the "best fit" line to Ibrahim's data to cross the corresponding "best fit" lines to data from bar B and bar A as observed in figure 6.3.

As in the analysis of the cyclic stress-strain data, it has to be noted that some tests were performed in load control and some in strain control. All Ibrahim's tests (and also data obtained from bar B) were from load controlled tests. All except one test from bar C were performed in strain control, whereas for bar A, four tests were strain controlled and seven tests were load controlled.

Results from bar A showed good agreement between strain and load controlled tests, as was the case for the cyclic stress-strain data obtained from bar C in figure 6.1.

A correspondence should be noticed between figure 6.1 and figure 6.3. For a given stress range, the data for bar C predicts the highest strain range (see figure 6.1), which corresponds to the lowest lifetime curve in figure 6.3. Similarly, the data of Ibrahim predicts a low strain range value for a given stress range which is reflected by the fact that this produces the highest lifetime curve suggesting a unique correlation with strain for all bars. Indeed figure 6.4 shows a better correlation between bar A, Ibrahim's data and bar C if strain range is plotted against lifetime, rather than stress against lifetime.

Also lifetime predictions shown in table 5.1 agree well with lifetimes for bars A and B, from which specimens were made for the crack growth studies using the replication technique. (The two notched specimens from which long crack data was produced were made from bar B).

Summarizing, both figure 6.1, the stress-strain response, and figure 6.3, the S-N curve, show that bar C diverges from the behaviour of other batches of this carbon steel. All subsequent discussions of the growth of short cracks refers to observations on bars A and B alone. Nevertheless, the discrepancy for bar C is not large, being within a factor of 2 on endurance, or about double the scatter observed for repeated tests from bar A.

### 6.3 Crack Growth Considerations

The results of the crack growth studies show two distinct regions of crack growth. For a crack contained within a single grain there was a strong influence of microstructure, predominantly grain boundary effects whereas for cracks which had grown beyond the first grain boundary crack growth was far less influenced by microstructure.

For convenience the discussion is split into these two areas of crack growth.

### 6.3.1 Long Crack Growth

For cracks which had grown beyond the first grain boundary, some did experience subsequent retardation periods, presumably on reaching the next grain boundary. In deriving the long crack growth equation, it was assumed that a continuum exists, ie, crack growth was not influenced by the surrounding microstructure. Now, if this simplification was unacceptable then the fatigue life would have been underestimated in section 5.2.2.3. However, as calculated lifetimes were in good agreement with actual test data, it is probable that this assumption was valid, and it can be stated that if cracks do experience retardation periods after the first grain boundary, such local retardation does not significantly alter the fatigue lifetime.

Although it has been established that the assumption of no microstructural influence gives good lifetime predictions, it is interesting to examine in more detail the crack growth mechanisms in this region by means of scanning electron microscopy. Two procedures were employed, in the first place an examination of the fracture surfaces from several specimens was carried out, and in the second method sectioning was performed on particular cracks.

#### 6.3.1.1 Fractography

Examination of the fracture surface revealed striations from which crack growth data could be inferred; these results were plotted along with the crack growth data obtained from replicas in chapter 5, figures 5.8a-5.8c. It was assumed that the crack was extended by one striation spacing in every cycle.

Figure 6.5a shows a photograph of some striations from specimen 1FB taken at a magnification of x510, and figure 6.5b also illustrates striations from specimen 1AB at a higher magnification of x930.

Observations of fracture surfaces on tests performed at different stress levels provided information of the proportion of transgranular to intergranular growth, which is discussed in the next section.

#### 6.3.1.2 Crack Sectioning

By opening up a particular crack, after a specimen has failed it is possible to examine its growth history in detail.

Figure 6.6 shows a photograph of a crack taken at a magnification of x25 from which three distinct areas of growth may be observed. This is from test IEB performed at a stress level of 815.9MPa. In order to show the early crack growth more clearly, figure 6.7 is an enlargement of the edge region at a

magnification of x200 (readily identified as the initiation site in figure 6.6.

Each sub-division in figure 6.6 represents 100 microns of the scale whereas in figure 6.7 it corresponds to ten microns. Thus the first period of growth (probably contained within the first grain) occupied about 100 microns, probably being shear mode propagation across a ferrite plate on a prior austenite grain boundary, (identified by the dark semi-circular region in figure 6.7). The second stage of crack growth was of a transgranular nature, showing no striations and some features reminiscent of crystallographic growth covering a distance of about 400 microns. This was followed by a third region of crack growth characterised by a striated fracture surface and predominantly transgranular propagation for a distance of about one millimetre. Finally prior to the fracture stage there was a rapid intergranular period of crack growth, with cracks following the weak ferrite paths for a distance of just over one millimetre. The final fracture may also involve linking up of other fatigue cracks across the remaining ligament.

Below figure 6.6 is a drawing based on the photograph showing the extent of each region of crack growth.

From these studies it was noticed that the proportion of transgranular to intergranular crack growth decreased as the stress increased. Also the ratio of transgranular crystallographic to transgranular striation crack growth decreased as the stress range increased.

The crack growth equation describing growth within the first grain (5.4) corresponds to the crack growth, designated stage I in figure 6.6, with the crack growth equation 5.9 for growth beyond the first grain typically stage III growth. Stage IV growth is rapid and ignored, and stage III growth is assumed to be the area corresponding to the "interactive zone" of section 5.2.1.3., where the crack grows from the first grain boundary to the long crack threshold of equation 5.9 with low crack growth rates.

### 6.3.1.3 Long Crack Growth Equation

The long crack growth equation derived in Chapter 5, equation 5.26, has been seen to give reasonable lifetime predictions when used in conjunction with the short crack growth equation 5.19. The value of  $\Delta K_{th}$  of 6.0MPa/m which was used in the derivation of the long crack growth equation is in agreement with that of similar reference [2].

By substituting for  $(a_s)$  in equation 5.26 using the relationship between  $(a_s)$  and  $\Delta K$  in equation 3.10, figure 3.10 can be replotted incorporating the resulting equation for crack propagation across the specimen.

$$\frac{da}{dN} = \frac{1}{2} (1.177 \times 10^{-4} \Delta K^2 - 4.237 \times 10^{-3}) \quad (6.5)$$

also shown in figure 6.8. Note the factor 1/2 is introduced to

convert surface crack length determined from replicas to crack depth.

It can be seen that the equation is an approximate fit to the data, especially when considering that it is an extrapolation from tests conducted at higher strains. This gives more justification to those lifetime predictions of chapter 5, which was determined for low strain tests.

It is possible that an improved correlation of the low strain crack growth measurements and high strain surface replication data could be obtained by use of other elasto-plastic fracture mechanics fatigue crack growth equations, employing for example  $\Delta J$ , C.O.D., plastic zone size or the strain intensity factor [3]. However, such improved criteria would not significantly change the life predictions here, because the fitted crack growth data correspond to the strain levels of interest.

### 6.3.2 Short Crack Growth

In deriving equation 5.19, there was a problem of trying to rationalize a large amount of scatter into a suitable model to describe short crack growth in a usable form. As microstructural variations strongly influence short crack growth, the extensive scatter in the short crack growth plots of figures 5.6a - 5.6c is to be anticipated. Intense strain in ideally orientated slip systems leads to easy glide and fast

crack growth rate in some grains, whereas multiple slip on intersecting slip planes leads to dislocation jogging with greater difficulty of slip and low crack growth rates in other grains.

The need to have ideal orientation of both slip plane and slip direction to get the upper bound  $da/dN$  implies a wide range of  $da/dN$ , and statistically very few grains with such fast growth rates. But these few grains are crucial to determining fatigue life, so a statistical approach has to be employed.

Although an equation 5.4 was used successfully to model some of Lankford's data [4], it would have been difficult to use this equation on all the data obtained in this study. Also Lankford's data was on an Aluminium alloy with a regular and well defined pancake structure which reduced the statistical variations of the microstructure to a low level.

Fortunately, taking a value of  $\alpha$  equal to one, thereby reducing equation 5.4 to its simplest form, gave a reasonable model for the short crack growth results from this study in carbon steel. As short crack growth data was not collected for either different types of loading or other materials, it is not possible to state categorically whether the approach of taking a value of  $\alpha$  equal to one will be applicable in the more general case of other materials and microstructures. However  $\alpha = 1$  would give a satisfactory fit to Lankford's data also.

After choosing  $\alpha$ , there was still the problem of how to choose a value for C. In the analysis of section 5.2.2.1., C was expressed as a function of stress range and a line representing a one-sided 95% confidence interval was calculated.

By assuming that a crack which led to failure was likely to be amongst the fastest growing in the initial stages the 95% line was used to calculate C. If a 99.9% confidence interval is used rather than 95%, equation 5.19 becomes:

$$\frac{da_s}{dN} = 1.94 \times 10^{-33} (\Delta\sigma)^{11.131} \quad (6.6)$$

which reduces the lifetime spent in initiation to about 9% of the values calculated in zone 1 of table 5.1. However this does not significantly alter the total calculated lifetime for the current tests since most of the lifetime is spent in crack growth beyond the first grain boundary. However a slightly greater influence of the short crack equation should be observed in high cycle fatigue and at the fatigue limit. For the confidence interval, a 95% level was chosen as being a reasonable value to model the fastest growing crack as approximately twenty cracks were observed at the highest and lowest stress levels, hence 5% is 1 in 20 and therefore a 95% confidence interval is representative of the fastest growing crack that was measured on the replicas.

For this particular study, because of the small number of cycles spent in initiating the failure crack and growing to the

first grain boundary it can be argued that a simple or first order approach would be to ignore this region altogether. This has the advantage of only having to make crack growth measurements when the crack is longer than  $100\mu\text{m}$ , which should be relatively easy to locate on the replicas. From these crack growth measurements an S-N curve can then be produced by integration of equation 5.26 alone, which will be more than adequate for design purposes as even for the lowest stress value in table 5.1, the number of cycles spent on growth within the first grain did not exceed 6.5% of the total lifetime. However, the lower limit crack length for integration purposes should correspond with  $d$ , if this is greater than the largest flaw size for the material concerned.

### 6.3.3 Grain Size Effect

To use the crack growth equations it is necessary to determine representative value for  $d$ . For this study  $d$  was calculated by extrapolating linearly the short crack growth data on a graph of  $a$  versus  $da/dN$  (where  $da/dN$  was decreasing as  $a$  increased) and then taking  $d$  to be the point of interaction where  $da/dN$  was equal to zero. This was preferred to direct measurement of  $(d)$  for individual cracks by trying to look for grain boundaries on replicas, since this required not only the shadowing of replicas, which was time consuming, but also and more importantly taking a value of  $d$  equal to the grain size implies beforehand that cracks should stop at grain boundaries. However extrapolated values for  $d$

compared well to the ferrite band length, confirming the dominant effect of triple points in the prior austenite structure on fatigue cracking for this material.

Ferrite bands were clearly the sites for nucleating short crack growth, and the characteristic microstructural dimension was the ferrite band length. To use this type of approach employed in this study for other materials, it is necessary to examine the microstructure and to determine which dominant features influence crack growth significantly by undertaking short crack studies. Then it should be possible to produce S-N curves in a similar fashion to those generated in this work, or to obtain a fair prediction from just considering accelerating crack growth beyond the area of significant retardation of crack growth caused by microstructural variations.

#### 6.4 Cumulative Damage Testing

Using cumulative damage results obtained from Miller and Ibrahim [5], it is interesting to see how their data compares with observations made in this study as the work was done on the same material.

Referring to figure 4.1, the equation of line OP can be written as:

$$\frac{1-x}{y} = \left( \frac{\Delta\gamma_{p2}}{\Delta\gamma_{p1}} \right)^\alpha \frac{N_{f2}}{N_{f1}} \quad (6.7)$$

where  $x$ ,  $y$ ,  $N_{f2}$ ,  $N_{f1}$ , are as defined in section 4.2, and  $\Delta\gamma_{p2}$  is the plastic strain range at the high strain level and  $\Delta\gamma_{p1}$ , the plastic strain range at the low strain level.

Now for the high strain level, assuming no initiation period [5], and that the crack propagates to a length  $d$  immediately:

$$\text{Log}_e \frac{a_f}{d} = C (\Delta\gamma_{p2})^\alpha (N_{f2}) \quad (6.8)$$

Combining equation (6.7) and (6.8)

$$y = \frac{C(1-x) \Delta\gamma_{p1}^\alpha N_{f1}}{\text{Log}_e (a_f / d)} \quad (6.9)$$

or differentiating to obtain the slope of OP,

$$\frac{dy}{dx} = \frac{-C \Delta\gamma_{p1}^\alpha N_{f1}}{\text{Log}_e (a_f / d)} \quad (6.10)$$

Values of 4 mm and 116.37 $\mu$ m are taken for  $a_f$  and  $d$  respectively, as used in the integration for the lifetime calculations of section 5.2.2.3., along with a value of 2.0 for  $\alpha$

as used in reference [5]. Using the Coffin-Manson relationship derived in [5], of:

$$\Delta\gamma_p N_f^{0.42} = 0.85 \quad (6.11)$$

substitution for  $\Delta\gamma_p$  into equation 6.10 gives:

$$\frac{dy}{dx} = -0.204 C N_f^{0.16} \quad (6.12)$$

Using the assumption made in reference [5], that there is no initiation at the high strain level, which implies  $dy/dx=1$  when  $N_f = 1000$ , substitution of these values into equation 6.12 gives a value for C of 1.62.

Finally using this value of C in equation 6.12, gives values for  $dy/dx$  at the five initial strain levels on substitution of the corresponding lifetimes of Table 1, reference [5].

These values of  $dy/dx$ , which is the slope of line OP', are plotted in figure 6.8 for the cumulative damage results. Lines OP' and P'Q represent the predictions from my study, which fit well to the data of figure 6.9.

Another application of the theory presented in Chapter 5, is given in Appendix II.

## 6.5 Plastic Replication Technique

The plastic replication technique used in this study provided a cheap and useful way of measuring crack lengths. Disadvantages of the technique which were apparent before using the method are listed at the end of section 2.5.2. problems which came to light when using the technique were:-

- a) Because the replicas were not perfectly flat, they were difficult to observe at magnifications much above x400.
- b) Storage of replicas can become a problem due to bulk, and difficulties arise when trying to remove dust from their surfaces.
- c) Observation is time-consuming but at present unavoidable as no rapid method exists to "home-in" on the cracks. In particular, trying to locate an individual crack on a series of replicas requires a great deal of effort despite the aids described in section 2.5.2. Obtaining crack growth data can take longer than performing the actual fatigue tests, and several crack measurements had to be discarded due to uncertainties over the precise location of the crack tips.
- (d) Problems arose when trying to produce continuous crack growth curves from discrete data points, which were

discussed in section 3.2.

However in the absence of a better technique suitable to the study of short cracks, the plastic replication method offered the only realistic solution, and although labour intensive, it provides a versatile and effective procedure for evincing the mechanics of fatigue crack nucleation.

## CHAPTER SIX - REFERENCES

- [1] IBRAHIM, M.F.E. (1981)  
"Early damage accumulation in metal fatigue"  
Ph.D. thesis, Sheffield University
- [2] POOK, L.P. (1975)  
"Analysis and application of fatigue crack data"  
J. Strain Anal. 10 p.242-250
- [3] KNOTT, J.F. (1973)  
"Fundamentals of fracture mechanics"  
Butterworths, London
- [4] LANKFORD, J. (1982)  
"The growth of small fatigue cracks in 7075-T6 aluminium alloy"  
Fatigue Engng. Mater. Struct. 5 p.233-248
- [5] MILLER, K.J. & IBRAHIM, M.F.E. (1981)  
"Damage accumulation during initiation and short crack growth regimes"  
Fatigue Engng. Mater. Struct. 4 p.263-277

## CHAPTER SIX - FIGURES

- 6.1 Stress range versus total strain range
- 6.2 Stress range versus plastic strain range
- 6.3 Stress range versus cycles to failure
- 6.4 Total strain range versus cycles to failure
- 6.5 Photographs of striations a) specimen 1FB and  
b) specimen 1AB
- 6.6 Photograph of crack, specimen 1EB at x 25
- 6.7 Photograph of crack, specimen 1EB at x 200
- 6.8 Crack growth rate versus stress intensity factor for  
notched specimens
- 6.9 Cumulative damage results of Miller & Ibrahim [5]



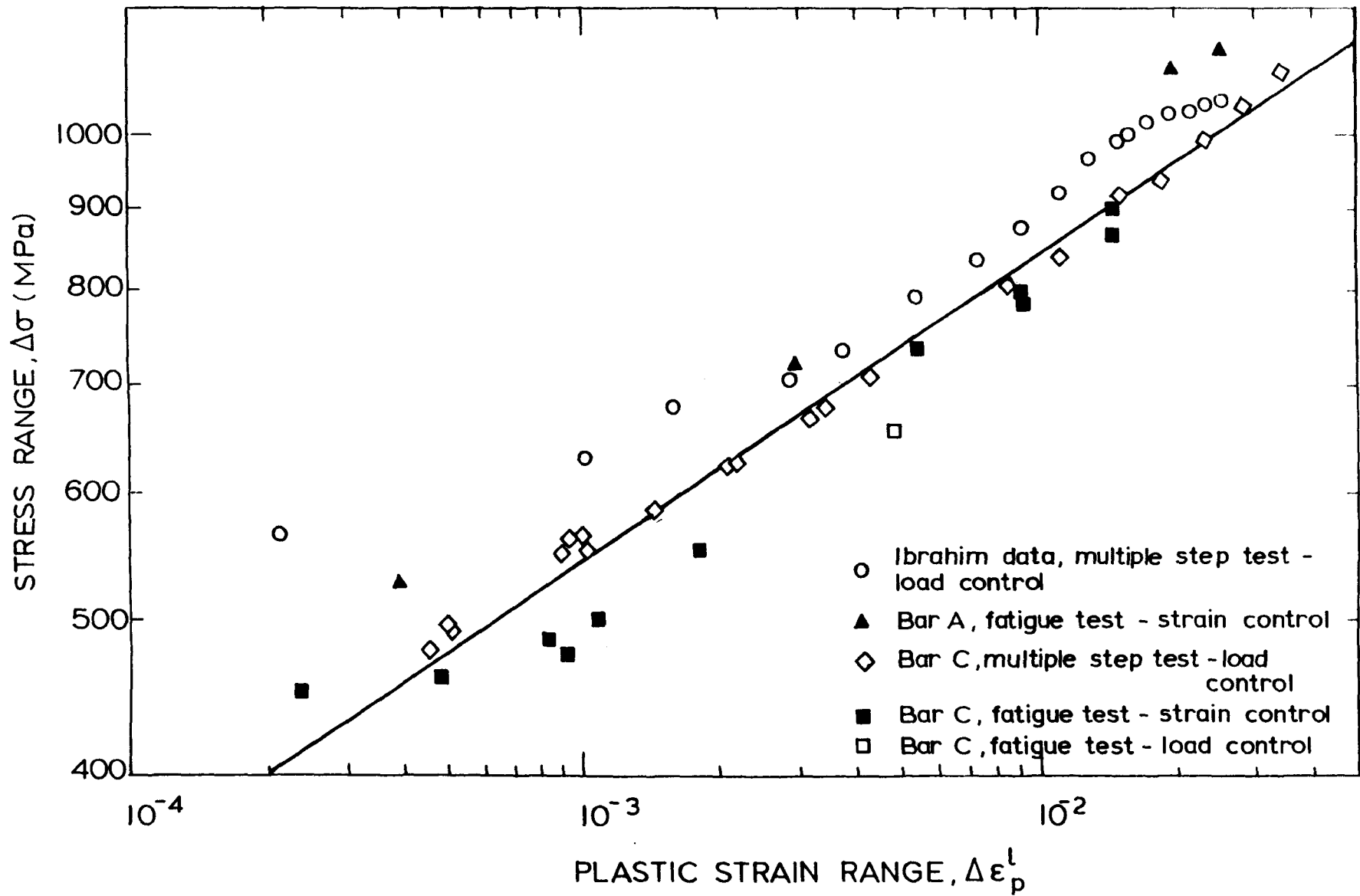


FIGURE 6.2 - Stress range versus plastic strain range

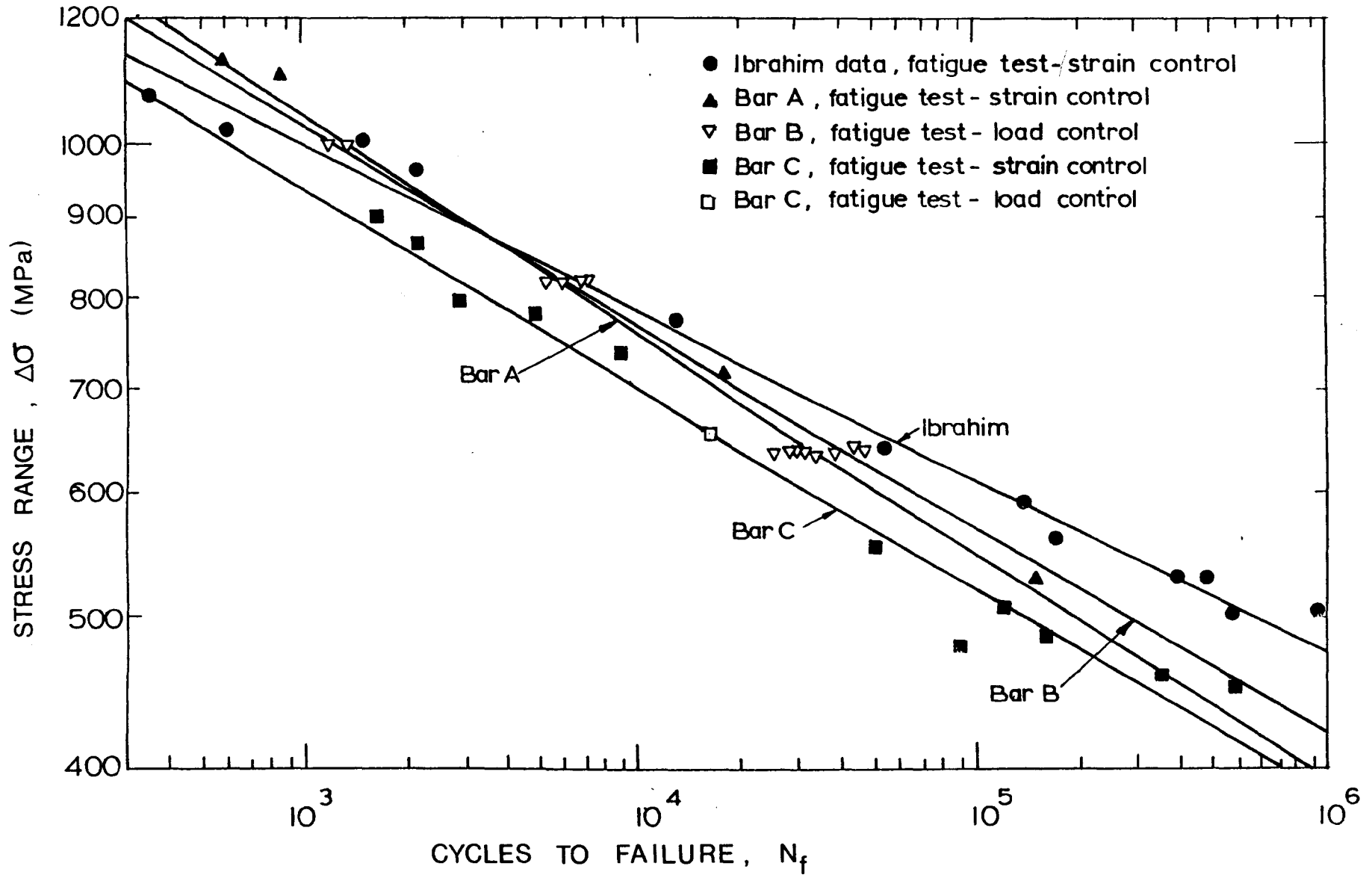


FIGURE 6.3 - Stress range versus cycles to failure

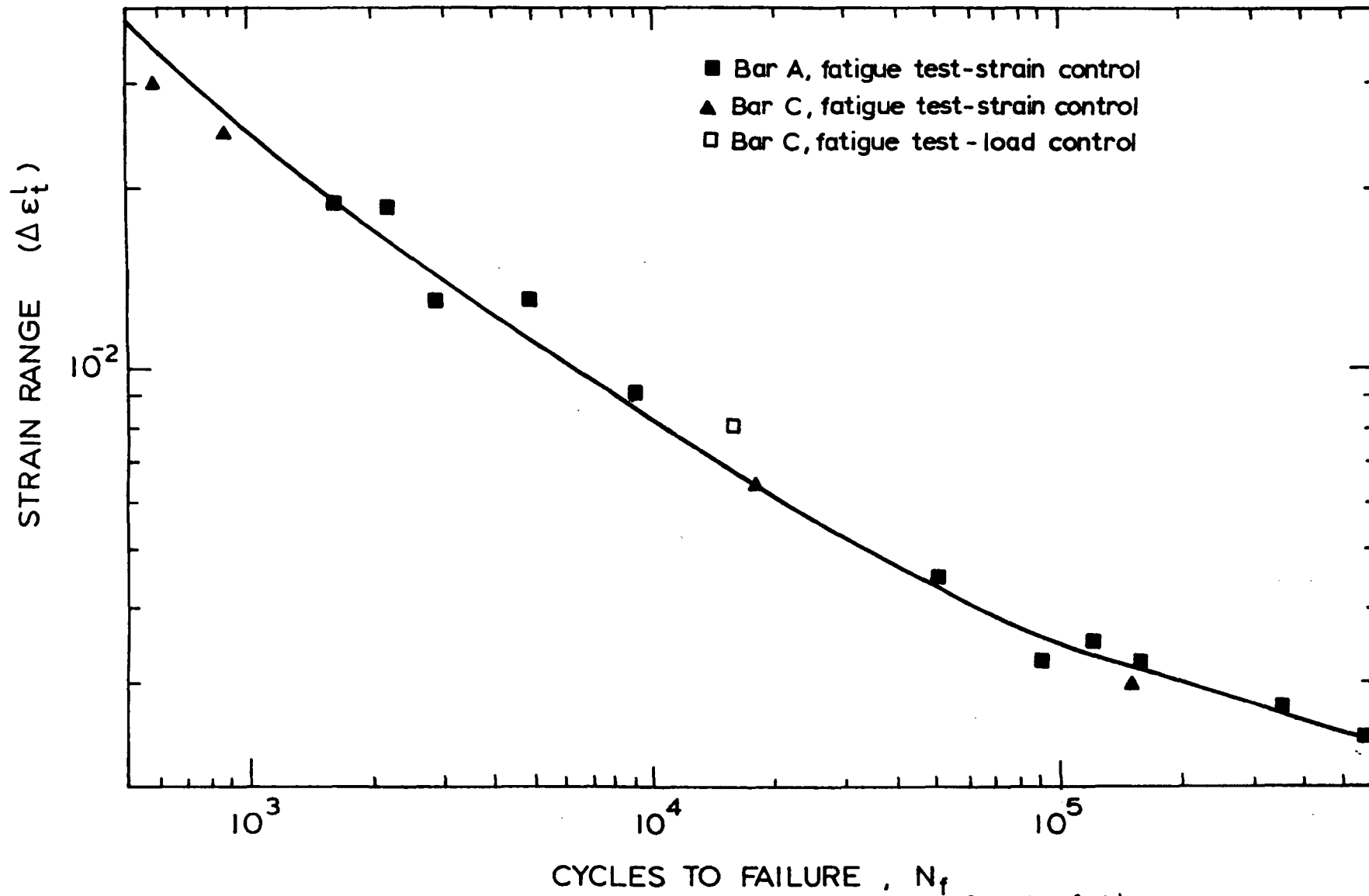
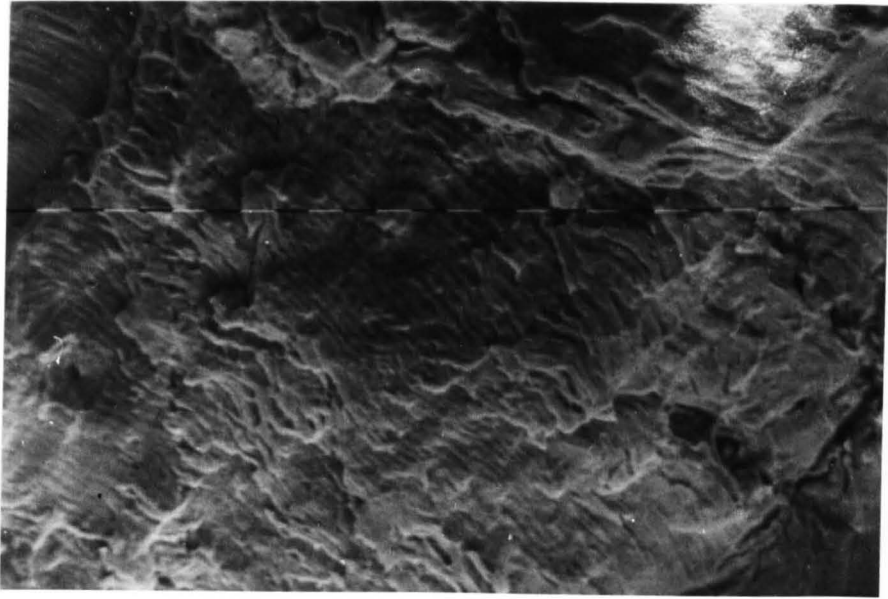
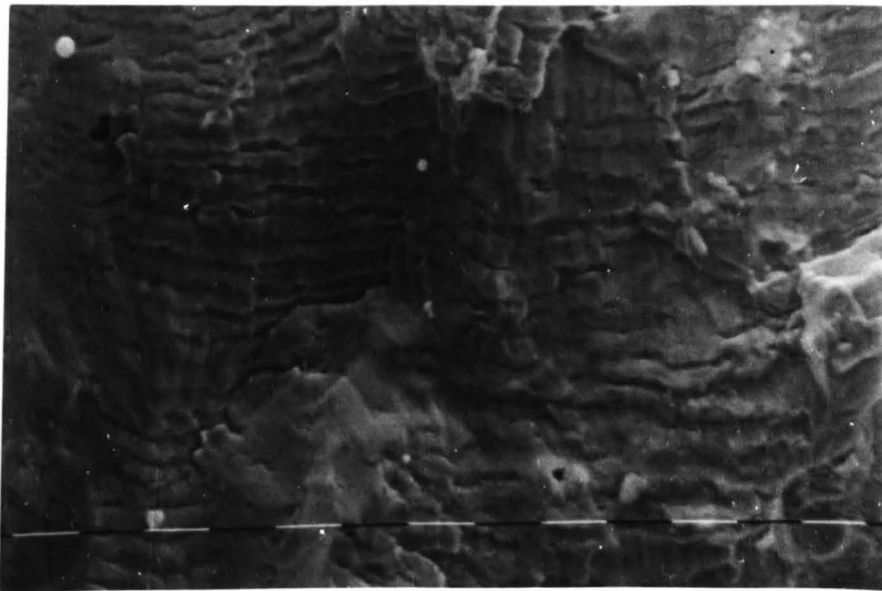


FIGURE 6.4 - Total strain range versus cycles to failure



(a) SPECIMEN 1FB (x 510)



(b) SPECIMEN 1AB (x 930)

FIGURE 6.5 - PHOTOGRAPHS OF STRIATIONS

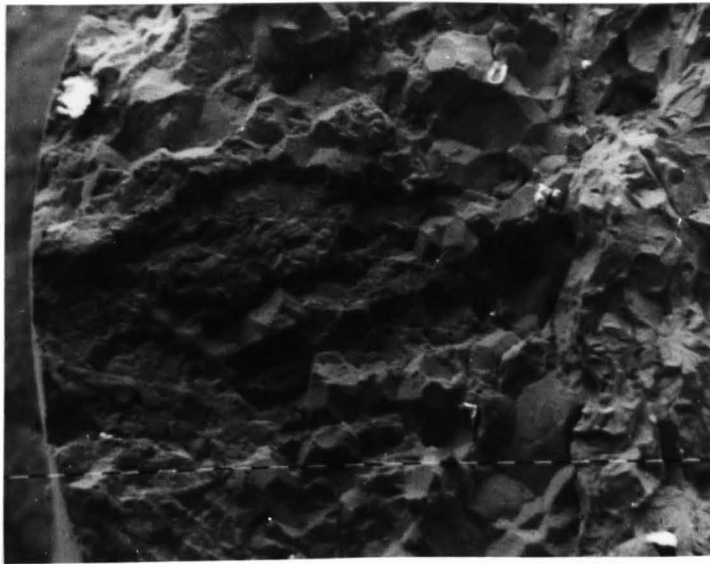
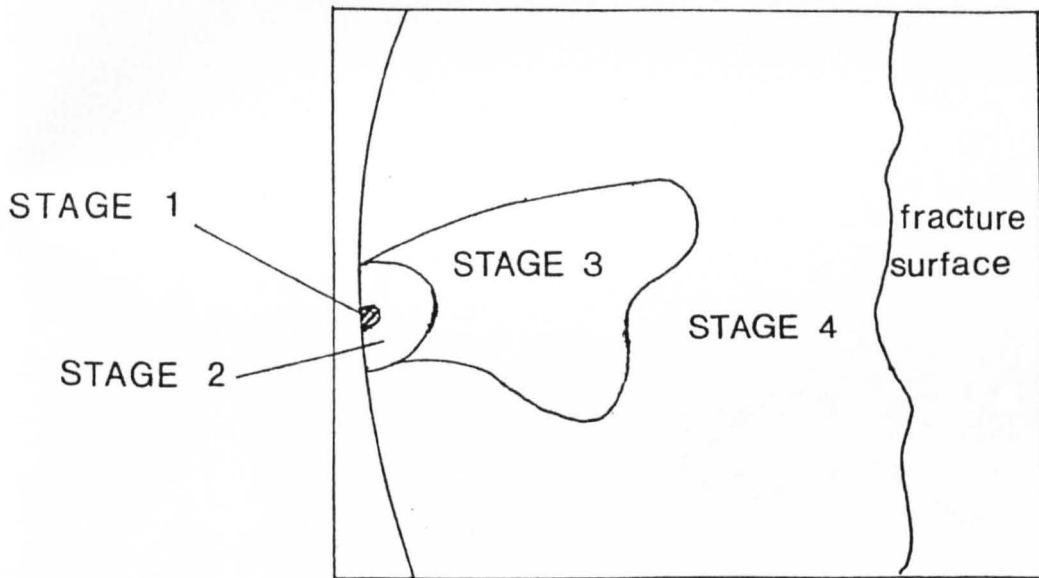


FIGURE 6.6 PHOTOGRAPH OF CRACK SPECIMEN 1EB x 25



SKETCH OF PHOTOGRAPH (FIGURE 6.6)

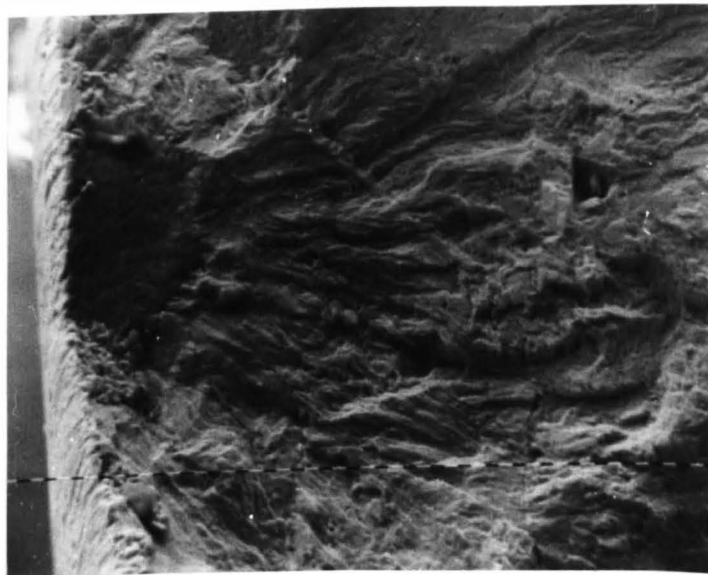


FIGURE 6.7 PHOTOGRAPH OF CRACK SPECIMEN 1EB X 200

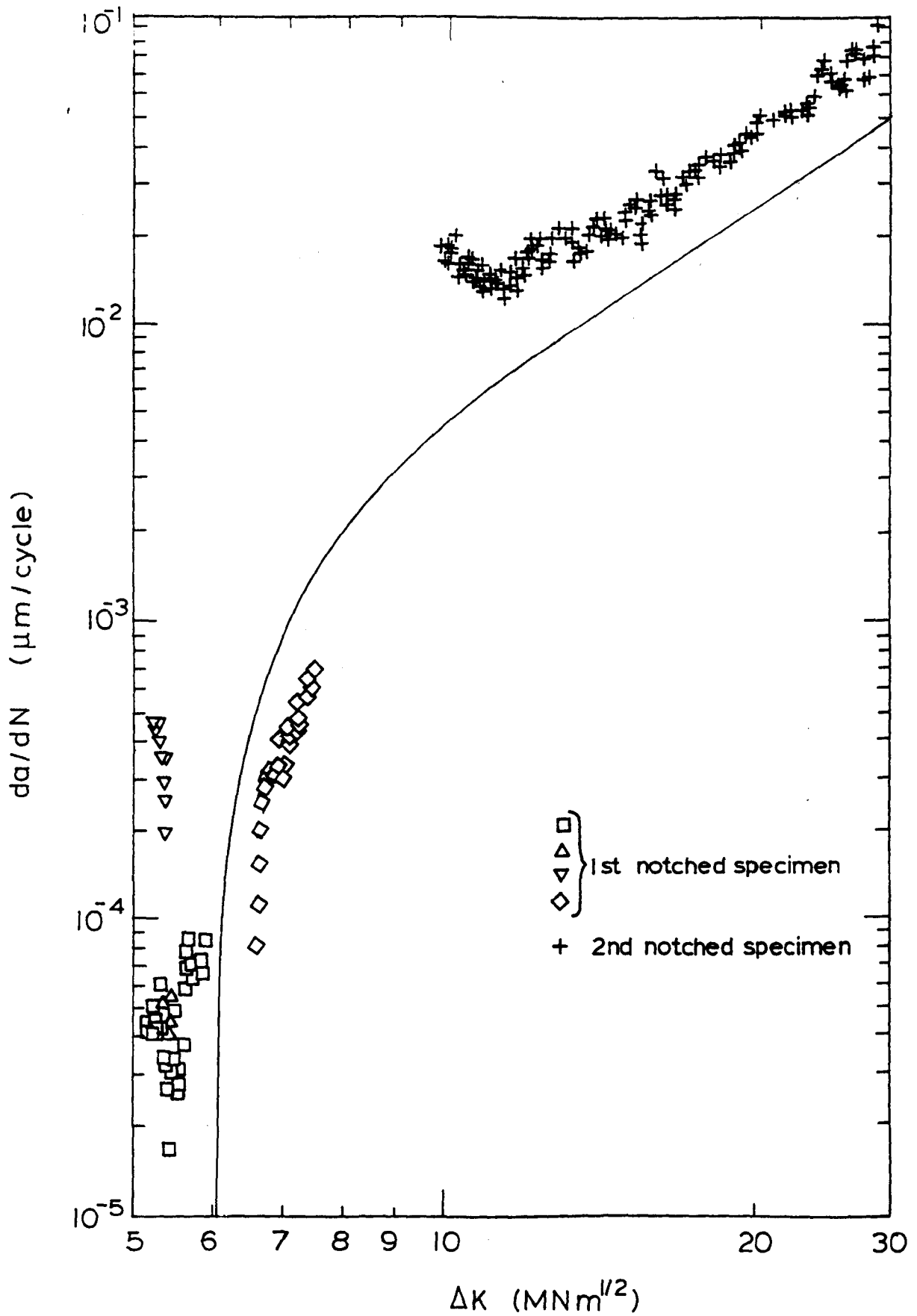


FIGURE 6.8 - Crack growth rate versus stress intensity factor for notched specimens

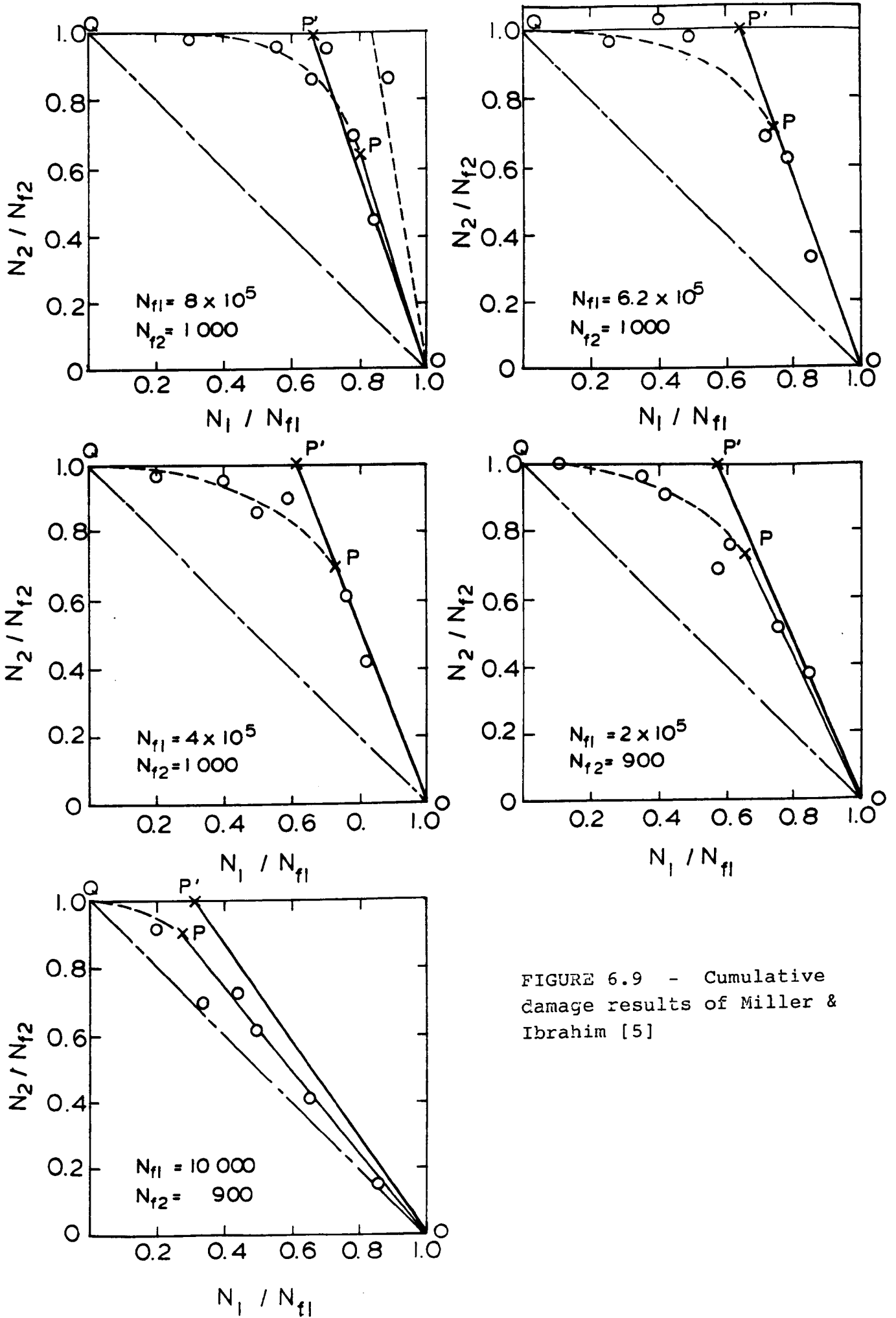


FIGURE 6.9 - Cumulative damage results of Miller & Ibrahim [5]

## CHAPTER SEVEN

### CONCLUSIONS

1. A new theory for short fatigue crack behaviour is presented, which states that crack growth rate is a function of not only crack length ( $a$ ), but also of a characteristic dimension between adjacent microstructural obstacles to propagation ( $d$ ) given by the equation:-

$$\frac{da}{dN} = C_1 (d-a)^{1-\alpha} a^\alpha \quad (7.1)$$

for  $a < d$ , where  $C$  is a function of stress or strain range.

2. The microstructural dimension ( $d$ ) for the medium carbon steel used in this study corresponds to the ferrite band length, contrasted with the grain size for an Aluminium alloy.

3. Accurate fatigue lifetime predictions were made by integrating equation 7.1 together with a second equation to describe long crack growth which was of the form:-

$$\frac{da}{dN} = C_2 a + D \quad (7.2)$$

Here  $C_2$  is a function of applied strain range and  $D$  corresponds to the threshold for long crack growth.

4. A combination of the two equations (7.1) and (7.2) makes it possible to model a complete description of crack growth

from initiation to fracture, including the occurrence of a fatigue limit. Quantitative expressions of the form (7.1) and (7.2) have been obtained for medium carbon steel covering low and high cycle fatigue.

5. From fatigue lifetime predictions, it was found that the percentage of life spent in initiating a crack and its subsequent propagation to the edge of the first ferrite plate was very small. A plastic strain range as low as 0.1% gave an estimated life in this period of less than 7%.
6. After determination of the growth characteristics of both short and long cracks in a given metal or alloy, it is possible to make good fatigue life predictions as has been shown for both the specimen and an engineering component.
7. From observations on etched specimens it could be seen that ferrite plates were preferred sites for crack initiation.
8. Cracks were only observed to grow in ferrite plates which intersected the surface at an angle between  $45^{\circ}$  and the normal to the stress axis, indicating that they were growing in a shear mode.
9. Short cracks contained within a single ferrite band exhibited faster growth rates than those that would be predicted by conventional fracture mechanics.

10. As a crack approached the edge of the ferrite plate in which it had been initiated, the crack growth rate decreased. Crack growth continued along the path of the next ferrite plate which often involved a change in crack growth direction. However below the fatigue limit, the edge of the ferrite plate provided a sufficiently strong barrier to inhibit further growth.
11. After a crack had extended beyond one ferrite plate, it showed a steadily increasing growth rate with subsequent microstructural variations having little effect on the crack growth rate.
12. Several cracks were observed to be growing simultaneously for each test, and only in the last few cycles did one crack become dominant. The final fracture often involved cracks linking up across the remaining ligament.
13. This model can be applied to two-stage cumulative damage studies and predicts the load sequence effects correctly.
14. The plastic replication technique provides a useful method for determining crack length for short cracks of less than grain size. It produces a library of information, and allows for higher magnifications than can be obtained from direct observation on round specimens.

APPENDIX I

CRACK GROWTH RESULTS

Test No.	Lifetime (cycles)	Crack No.	Replication stage (cycles)	Crack Length	d-a ( $\mu\text{m}$ )	Lifetime %	$\Delta a$ ( $\mu\text{m}$ )	$\Delta N$ (cycles)	$\Delta a/\Delta N$ ( $\mu\text{m}/\text{cycle}$ )	$a_{\text{mean}}$ ( $\mu\text{m}$ )
1CB	1186	1	480	157	126.31	40.6	157	480	0.327	78.5
			700	178	37.31	59.0	21	220	0.0955	167.5
			950	232	-	80.1	54	250	0.216	205
		2	81	92	51.05	6.8	92	81	1.14	46
			161	94	4.05	13.6	2	80	0.025	93
			321	98	1.05	22.1	4	160	0.025	96
			482	100	-	40.6	2	161	0.0124	99
			700	107	-	59.0	7	218	0.0321	103.5
			950	127	-	80.1	20	250	0.080	117
		3	482	61	42.76	40.6	61	482	0.127	30.5
			700	67	9.26	59.0	6	218	0.0275	64
			950	117	-	80.1	50	250	0.20	92
		4	81	25	78.95	6.8	25	81	0.309	12.5
			161	54	51.95	13.6	29	80	0.363	39.5
			321	71	28.95	27.1	17	160	0.106	62.5
			482	79	16.45	40.6	8	161	0.0497	75
			700	190	-	59.0	111	218	0.509	134.5
			950	244	-	80.1	54	250	0.216	217
		5	161	141	-	13.6	141	161	0.876	70.5
			321	223	-	27.1	82	160	0.513	182
			482	354	-	40.6	131	161	0.814	288.5
			700	552	-	59.0	198	213	0.908	453
			950	1,346	-	80.1	794	250	3.18	949
		6	482	137	81.18	40.6	137	482	0.284	68.5
700	144		9.18	59.0	7	218	0.0321	140.5		
950	208		-	80.1	64	250	0.256	176		

Crack Growth Results,  $\sigma = 998.4$  MPa

Test No.	Lifetime (cycles)	Crack No.	Replica-tion stage (cycles)	Crack Length	d-a ( $\mu\text{m}$ )	Lifetime %	$\Delta a$ ( $\mu\text{m}$ )	$\Delta N$ (cycles)	$\Delta a/\Delta N$ ( $\mu\text{m}/\text{cycle}$ )	$a_{\text{mean}}$ ( $\mu\text{m}$ )	
1BB	1,192	7	482	114	70.63	40.6	114	482	0.237	57	
			700	114	-	59.0	-	218	-	-	
			950	126	7.63	80.1	12	250	0.0256	120	<i>127.83</i>
			8	482	134	-	40.6	134	482	0.278	67
				700	186	-	59.0	52	218	0.239	160
				950	269	-	80.1	83	250	0.332	227.5
			9	11	45	23.19	0.9	45	11	4.09	22.5
				21	45	-	1.8	0	10	-	45
				41	46	0.19	3.5	1	20	0.0333	45.5
		81		50	-	6.8	4	40	0.1	48	
		161		54	-	13.6	4	80	0.050	52	
		321		91	-	27.1	37	160	0.231	72.5	
		482		96	-	40.6	5	161	0.0311	93.5	
		700		156	-	59.0	60	218	0.275	126	
		950		222	-	80.1	66	250	0.264	189	
		1		11	88	44.56	0.9	88	11	8.0	44
			21	89	0.06	1.8	1	10	0.10	88.5	<i>88.56</i>
			41	91	-	3.4	2	20	0.10	90	
			81	91	-	6.8	0	40	-	91	
			161	96	-	13.5	5	80	0.0417	93.5	
			321	113	-	26.9	17	160	0.106	104.5	
			540	125	-	45.3	12	219	0.0548	119	
			790	135	-	66.3	10	250	0.040	130	
			1040	168	-	87.3	33	250	0.132	151.5	

Crack Growth Results,  $\sigma = 998.4 \text{ MPa}$

Test No.	Lifetime (cycles)	Crack No.	Replication stage (cycles)	Crack Length	d-a ( $\mu\text{m}$ )	Lifetime %	$\Delta a$ ( $\mu\text{m}$ )	$\Delta N$ (cycles)	$\Delta a/\Delta N$ ( $\mu\text{m}/\text{cycle}$ )	$a_{\text{mean}}$ ( $\mu\text{m}$ )
			6	68	47.96	0.5	68	6	11.3	34
			21	74	10.96	1.8	6	15	0.40	71 <i>81, 96</i>
			41	80	4.96	3.4	6	20	0.30	77
		2	161	86	-	13.5	6	120	0.050	83
			321	93	-	26.9	7	160	0.0438	89.5
			540	119	-	45.3	26	219	0.119	106
			790	174	-	66.3	55	250	0.22	146.5
			1040	316	-	87.3	142	250	0.568	245
			21	98	51.09	1.8	98	21	4.67	49
			41	100	1.09	3.4	2	20	0.10	99 <i>100, 99</i>
			81	110	-	6.8	10	40	0.25	105
		3	161	125	-	13.5	15	80	0.188	117.5
			321	151	-	26.9	26	160	0.163	138
			540	184	-	45.3	33	219	0.151	167.5
			790	252	-	66.3	68	250	0.272	218
			1040	416	-	87.3	164	250	0.656	334
			6	88	67.22	0.5	88	6	14.7	44
			11	93	20.72	0.9	5	5	1.00	90.5 <i>110, 95</i>
			21	116	6.72	1.8	23	10	2.300	104.5
			41	118	-	3.4	2	20	0.10	117
		4	81	124	-	6.8	6	40	0.15	121
			161	139	-	13.5	15	80	1.880	131.5
			321	158	-	26.9	19	160	0.119	148.5
			540	177	-	45.3	19	219	0.0868	167.5
			790	211	-	66.3	34	250	0.136	194
			1040	488	-	87.3	277	250	1.11	349.5

Crack Growth Results,  $\sigma = 998.4 \text{ MPa}$

Test No.	Lifetime (cycles)	Crack No.	Replica-tion stage (cycles)	Crack Length	d-a ( $\mu\text{m}$ )	Lifetime %	$\Delta a$ ( $\mu\text{m}$ )	$\Delta N$ (cycles)	$\Delta a/\Delta N$ ( $\mu\text{m}/\text{cycle}$ )	$a_{\text{mean}}$ ( $\mu\text{m}$ )
			41	108	64.21	3.4	108	41	2.63	52
			81	115	4.71	6.8	7	40	0.175	115.5
			161	117	0.21	13.5	2	80	0.025	116 <i>116, 21</i>
		5	321	117	-	26.9	0	160	-	117
			540	135	-	45.3	18	219	0.0475	126
			790	135	-	66.3	0	250	-	135
			1040	204	-	87.3	69	250	0.138	169.5
			6	82	51.33	0.5	82	6	13.7	41
			11	91	6.03	0.9	9	5	1.8	86.5
			21	92	1.03	1.8	1	10	0.10	91.5 <i>92, 53</i>
			41	101	-	3.4	9	20	0.45	96.5
		6	81	103	-	6.8	2	40	0.050	102
			161	122	-	13.5	19	80	0.238	112.5
			321	126	-	26.9	4	160	0.025	124
			540	140	-	45.3	14	219	0.0639	133
			790	142	-	66.3	2	250	0.0080	141
			1040	211	-	87.3	69	250	0.276	176.5
			81	128	189.79	6.8	128	81	1.58	64
			161	213	83.29	13.5	85	80	1.06	170.5
		7	321	231	31.79	26.9	18	160	0.113	222
			540	249	13.79	45.3	18	219	0.0822	240 <i>253, 79</i>
			790	281	-	66.3	32	250	0.128	265
			1040	406	-	87.3	125	250	0.25	343.5

Crack Growth Results,  $\sigma = 998.4 \text{ MPa}$

Test No.	Lifetime (cycles)	Crack No.	Replica- tion stage (cycles)	Crack Length	d-a ( $\mu\text{m}$ )	Lifetime %	$\Delta a$ ( $\mu\text{m}$ )	$\Delta N$ (cycles)	$\Delta a / \Delta N$ ( $\mu\text{m}/\text{cycle}$ )	$a_{\text{mean}}$ ( $\mu\text{m}$ )
				321	221	-	26.9	321	0.688	110.5
		8		540	333	-	45.3	219	0.511	406
				790	591	-	66.3	250	1.03	462
				1040	2343	-	87.3	250	7.01	1467
				161	124	138.31	13.5	161	0.770	62
				321	171	52.81	26.9	160	0.294	147.5
		9		540	444	-	45.3	219	1.25	307.5
				790	795	-	66.3	250	1.40	619.5
				1040	1226	-	87.3	250	1.73	1010.5

Crack Growth Results,  $\sigma = 998.4$  MPa

Test No.	Lifetime (cycles)	Crack No.	Replication stage (cycles)	Crack Length	d-a ( $\mu\text{m}$ )	Lifetime %	$\Delta a$ ( $\mu\text{m}$ )	$\Delta N$ (cycles)	$\Delta a/\Delta N$ ( $\mu\text{m}/\text{cycle}$ )	$a_{\text{mean}}$ ( $\mu\text{m}$ )			
1EB	5,889	1	10	122	75.29	0.2	122	10	12.0	61 <sup>136.2</sup>			
			50	135	7.79	0.9	13	40	0.325	128.5			
			100	138	-	1.7	3	50	0.060	136.5			
			500	143	-	8.5	5	400	0.0125	140.5			
			1000	204	-	17.0	61	500	0.122	173.5			
			1500	224	-	25.5	20	500	0.040	214			
			2000	317	-	34.0	93	500	0.186	270.5			
			2500	397	-	42.5	80	500	0.16	357			
			3000	607	-	50.9	210	500	0.42	502			
			3500	693	-	59.4	86	500	0.172	650			
			4000	978	-	67.9	285	500	0.57	835.5			
			4500	1280	-	76.4	302	500	0.604	1129			
			5072	1720	-	86.1	440	572	0.769	1500			
			5720	2571	-	97.1	851	648	1.31	2145.5			
					2	3000	154	84.60	50.9	154	3000	0.0513	77 <sup>161.6</sup>
						3500	156	6.60	59.4	2	500	0.0040	155
						4000	215	-	67.9	59	500	0.118	185.5
						4500	241	-	76.4	26	500	0.052	228
						5072	280	-	86.1	39	572	0.0682	260.5
5720	318	-				97.1	38	648	0.0586	299			

Crack Growth Results,  $\sigma = 815.9$  MPa

Test No.	Lifetime (cycles)	Crack No.	Replication stage (cycles)	Crack Length	d-a ( $\mu\text{m}$ )	Lifetime %	$\Delta a$ ( $\mu\text{m}$ )	$\Delta N$ (cycles)	$\Delta a/\Delta N$ ( $\mu\text{m}/\text{cycle}$ )	$a_{\text{mean}}$ ( $\mu\text{m}$ )
2DB	7028	1	100	99	57.90	1.4	99	100	0.99	49.5
			500	112	1.90	7.1	13	400	0.0325	105.5
			1000	162	-	14.2	50	500	0.10	137
			1500	165	-	21.3	3	500	0.0060	163.5
			2000	167	-	28.5	2	500	0.0040	166
			2503	167	-	35.6	0	503	-	-
			3000	167	-	42.7	0	497	-	-
			3500	167	-	49.8	0	500	-	-
			4000	169	-	56.9	2	500	0.0040	168
			4500	191	-	64.0	22	500	0.044	180
			5000	254	-	71.1	63	500	0.126	222.5
			5501	272	-	78.3	18	501	0.0359	263
			6000	334	-	85.4	62	499	0.124	303
		6500	357	-	92.5	23	500	0.046	345.5	
		2	1500	33	202.80	21.3	33	1500	0.022	16.5
			2000	77	164.30	28.5	44	500	0.088	55
			2503	89	136.30	35.6	12	503	0.0239	83
			3000	102	123.80	42.7	13	497	0.0262	95.5
			3500	109	113.80	49.8	7	500	0.014	105.5
			4000	142	-	56.9	33	500	0.066	125.5
			4500	231	-	64.0	89	500	0.178	186.5
			5000	242	-	71.1	11	500	0.022	236.5
			5501	251	-	78.3	9	501	0.0180	246.5
			6000	263	-	85.4	12	499	0.0240	257
			6500	272	-	92.5	9	500	0.0180	267.5

Crack Growth Results,  $\sigma = 815.9$  MPa

Test No.	Lifetime (cycles)	Crack No.	Replication stage (cycles)	Crack Length	d-a ( $\mu\text{m}$ )	Lifetime %	a ( $\mu\text{m}$ )	$\Delta N$ (cycles)	$\Delta a/\Delta N$ ( $\mu\text{m}/\text{cycle}$ )	a <sub>mean</sub> ( $\mu\text{m}$ )
1AB	5,246	1	50	44	171.87	1.0	44	50	0.88	22
			100	63	140.37	1.9	19	50	0.38	53.5
			500	194	65.37	9.5	131	400	0.328	128.5
			1000	194	-	19.1	0	500	-	194
			1500	196	-	28.6	2	500	0.002	195
			2000	206	-	38.1	10	500	0.02	201
			2500	215	-	47.7	9	500	0.018	210.5
			3000	226	-	57.2	11	500	0.022	220.5
			3500	245	-	66.7	19	500	0.038	235.5
			4002	269	-	76.3	24	502	0.0478	257
			4500	305	-	85.8	36	498	0.0723	287
		5000	345	-	95.3	40	500	0.08	325	
		2	100	113	98.95	1.9	113	100	1.13	56.5
			500	136	30.95	9.5	23	400	0.0575	124.5
			1000	168	3.45	19.1	32	500	0.064	152
			1500	168	-	28.6	0	500	-	168
			2000	169	-	38.1	1	500	0.001	168.5
			2500	177	-	47.7	8	500	0.016	173
			3000	177	-	57.2	0	500	-	177
			3500	194	-	66.7	17	500	0.017	185.5
			4002	236	-	76.3	42	502	0.0837	215
			4500	250	-	85.8	14	498	0.0281	243
5000	252		-	95.3	2	500	0.040	251		

Crack Growth Results,  $\sigma = 815.9$  MPa

Test No.	Lifetime (cycles)	Crack No.	Replication stage (cycles)	Crack Length	d-a ( $\mu\text{m}$ )	Lifetime %	a ( $\mu\text{m}$ )	$\Delta N$ (cycles)	$\Delta a/\Delta N$ ( $\mu\text{m}/\text{cycle}$ )	$a_{\text{mean}}$ ( $\mu\text{m}$ )
3			500	113	62.95	9.5	113	500	0.226	56.5
			1500	119	3.45	28.6	6	1000	0.006	116
			2000	121	-	38.1	2	500	0.004	120
			2500	126	-	47.7	5	500	0.010	123.5
			3000	161	-	57.2	35	500	0.070	143.5
			3500	161	-	66.7	0	500	-	161
			4002	174	-	76.3	13	502	0.013	167.5
			4500	194	-	85.8	20	498	0.0402	184
	4			50	44	105.93	1.0	44	50	0.88
			500	126	42.93	9.5	82	450	0.182	85
			1000	134	-	19.1	8	500	0.016	130
			1500	135	-	28.6	1	500	0.002	134.5
			2000	151	-	38.1	16	500	0.032	143
			2500	151	-	47.7	0	500	-	151
			3000	179	-	57.2	28	500	0.028	165
			3500	224	-	66.7	45	500	0.090	201.5
			4002	277	-	76.3	53	502	0.106	250.5
			4500	305	-	85.8	28	498	0.0562	291
			5000	366	-	95.3	61	500	0.122	335.5
5				2000	254	-	38.1	254	2000	0.127
			2500	286	-	47.7	32	500	0.064	270
			3000	404	-	57.2	118	500	0.236	345
			3500	664	-	66.7	260	500	0.52	534
			4002	790	-	76.3	126	502	0.251	727
			4500	1059	-	85.8	269	498	0.540	924.5
			5000	1219	-	95.3	160	500	0.320	1139

Crack Growth Results,  $\sigma = 815.9 \text{ MPa}$

Test No.	Lifetime (cycles)	Crack No.	Replication stage (cycles)	Crack Length	d-a ( $\mu\text{m}$ )	Lifetime %	$\Delta a$ ( $\mu\text{m}$ )	$\Delta N$ (cycles)	$\Delta a/\Delta N$ ( $\mu\text{m}/\text{cycle}$ )	$a_{\text{mean}}$ ( $\mu\text{m}$ )
2GA	29324	1	1000	52	59.07	3.3	52	1,000	0.052	26
			3000	79	19.57	10.2	27	2,000	0.0135	65.5
			6166	86	2.57	21.0	7	3,166	0.00221	82.5
			10140	88	-	34.6	2	3,974	0.000503	87
			15047	130	-	51.3	42	4,907	0.00856	109
			20873	294	-	71.2	164	5,826	0.0281	212
			28640	572	-	97.7	278	7,767	0.0358	433
1AA	34301	1	1000	19	27.85	2.9	19	1,000	0.019	9.5
			3000	33	11.35	8.8	14	2,000	0.007	26
			6016	38	1.85	17.5	5	3,016	0.00166	35.5
			10000	63	-	29.2	25	3,984	0.00628	50.5
			15713	106	-	45.8	43	5,713	0.00753	84.5
			22000	116	-	64.1	10	6,287	0.00159	111
			30010	121	-	87.5	5	8,010	0.000624	118.5
		2	1000	44	33.09	2.9	44	1,000	0.044	22
			3000	53	6.59	8.8	9	2,000	0.0045	48.5
			6016	59	-	17.5	6	3,016	0.00199	56
			10000	83	-	29.2	24	3,984	0.00602	71
			15713	97	-	45.8	14	5,713	0.00245	90
			22000	140	-	64.1	43	6,287	0.00684	118.5
			30010	256	-	87.5	116	8,010	0.0145	198
1EA	30767	1	6000	35	133.61	19.5	35	6,000	0.00583	17.5
			10000	56	105.61	32.5	21	4,000	0.00525	45.5
			15000	74	86.11	48.8	18	5,000	0.0036	65
			21000	142	-	68.3	68	6,000	0.0113	108
			28000	275	-	91.0	133	7,000	0.019	208.5

Crack Growth Results,  $\sigma = 638.5$  MPa

Test No.	Lifetime (cycles)	Crack No.	Replica-tion stage (cycles)	Crack Length	d-a ( $\mu\text{m}$ )	Lifetime %	$\Delta a$ ( $\mu\text{m}$ )	$\Delta N$ (cycles)	$\Delta a/\Delta N$ ( $\mu\text{m}/\text{cycle}$ )	$a_{\text{mean}}$ ( $\mu\text{m}$ )
			3000	70	79.04	9.8	70	3000	0.0233	35
			6000	102	28.04	19.5	32	3000	0.0107	86
		2	10000	107	9.54	32.5	5	4000	0.00125	104.5
			15000	162	-	48.8	55	5000	0.011	134.5
			21000	229	-	68.3	67	6000	0.0112	195.5
			28000	488	-	91.0	259	7000	0.037	358.5
			10000	28	-	32.5	28	10000	0.0028	14
		3	15000	53	-	48.8	25	5000	0.005	40.5
			21000	82	-	68.3	29	6000	0.00483	67.5
			28000	127	-	91.0	45	7000	0.00643	104.5
			6000	37	42.12	19.5	37	6000	0.00617	18.5
			10000	46	19.12	32.5	9	4000	0.00225	41.5
		4	15000	55	10.12	48.8	9	5000	0.00180	50.0
			21000	80	-	68.2	25	6000	0.00417	67.5
			28000	121	-	91.0	41	7000	0.00586	100.5
			6000	25	72.66	19.5	25	6000	0.00417	12.5
			10000	42	51.66	32.5	17	4000	0.00425	33.5
		5	15000	51	38.66	48.8	9	5000	0.0018	46.5
			21000	64	-	68.2	13	6000	0.00217	57.5
			28000	488	-	91.0	424	7000	0.0606	276
			10009	55	-	25.4	55	10009	0.0055	27.5
			14446	76	-	36.7	21	4437	0.00473	65.5
			19500	115	-	49.5	39	5054	0.00762	95.5
2EB	39391	1	24500	207	-	62.2	92	5000	0.0185	161
			29622	261	-	75.2	54	5122	0.0102	234
			34500	347	-	87.6	86	4878	0.0177	304
			37743	1049	-	95.8	702	3243	0.216	698

Crack Growth Results,  $\sigma = 638.5$  MPa

Test No.	Lifetime (cycles)	Crack No.	Replication stage (cycles)	Crack Length	d-a ( $\mu\text{m}$ )	Lifetime %	$\Delta a$ ( $\mu\text{m}$ )	$\Delta N$ (cycles)	$\Delta a/\Delta N$ ( $\mu\text{m}/\text{cycle}$ )	$a_{\text{mean}}$ ( $\mu\text{m}$ )
2			6000	29	54.36	15.2	29	6000	0.00483	14.5
			10009	40	34.36	25.4	11	4009	0.00274	34.5
			14446	50	23.86	36.7	10	4437	0.00225	45
			19500	94	-	49.5	44	5054	0.00871	72
			24500	120	-	62.2	26	5000	0.00520	107
			29622	144	-	75.2	24	5122	0.00469	132
			34500	296	-	87.6	152	4878	0.0312	220
3			19500	61	-	49.5	61	19500	0.00313	30.5
			24500	129	-	62.2	68	5000	0.0136	95
			29622	195	-	75.2	66	5122	0.0129	162
			34500	297	-	86.7	102	4878	0.0209	246
4			6000	37	70.56	15.2	37	6000	0.00617	18.5
			10009	52	44.56	25.4	15	4009	0.00374	44.5
			14446	66	30.06	36.7	14	4437	0.00316	59
			19500	73	19.56	49.5	7	5054	0.00139	69.5
			24500	150	-	62.2	77	5000	0.0154	111.5
			29622	162	-	75.2	12	5122	0.00234	156
			34500	217	-	87.6	55	4878	0.0113	189.5
			37743	283	-	95.8	66	3243	0.0204	250
5			19500	69	-	49.5	69	19500	0.00354	34.5
			24500	85	-	62.2	16	5000	0.00320	77
			29622	109	-	75.2	24	5122	0.00469	97
			34500	114	-	87.6	5	4878	0.00103	111.5
			37743	143	-	95.8	29	3243	0.00894	128.5

Crack Growth Results,  $\sigma = 638.5$  MPa

Test No.	Lifetime (cycles)	Crack No.	Replication stage (cycles)	Crack Length	d-a ( $\mu\text{m}$ )	Lifetime %	$\Delta a$ ( $\mu\text{m}$ )	$\Delta N$ (cycles)	$\Delta a/\Delta N$ ( $\mu\text{m}/\text{cycle}$ )	$a_{\text{mean}}$ ( $\mu\text{m}$ )
6			6000	122	114.30	15.2	122	6000	0.0203	61
			10009	150	39.30	25.4	28	4009	0.00698	136
			14446	203	-	36.7	53	4437	0.0142	176.5
			19500	276	-	49.5	73	5054	0.0144	239.5
			24500	324	-	62.2	48	5000	0.0096	300
			29622	545	-	75.2	221	5122	0.0431	434.5
			34500	731	-	87.6	186	4878	0.0381	638
			37743	1,184	-	95.8	453	3243	0.140	957.5
	7			19000	56	-	49.5	56	19500	0.00287
			24500	75	-	62.2	19	5000	0.0038	65.5
			29622	122	-	75.2	47	5122	0.00918	98.5
			34500	146	-	87.6	24	4878	0.00492	134
8			10009	92	59.78	25.4	92	10009	0.00919	46
			14446	99	10.28	36.7	7	4437	0.00158	95.5
			19500	110	-	49.5	11	5054	0.00218	104.5
			24500	230	-	62.2	20	5000	0.00400	170
			29622	253	-	75.2	23	5122	0.00449	241.5
			34500	566	-	87.6	313	4878	0.0642	409.5
			37743	837	-	95.8	271	3243	0.0836	701.5
9			6000	21	-	15.2	21	6000	0.00350	10.5
			10009	48	-	25.4	27	4009	0.00673	34.5
			14446	73	-	36.7	25	4437	0.00563	60.5
			19500	102	-	49.5	29	5054	0.00574	87.5
			24500	148	-	62.2	46	5000	0.00920	125
			29622	239	-	75.2	91	5122	0.0178	193.5

Crack Growth Results,  $\sigma = 638.5$  MPa

Test No.	Lifetime (cycles)	Crack No.	Replication stage (cycles)	Crack Length	d-a ( $\mu\text{m}$ )	Lifetime %	$\Delta a$ ( $\mu\text{m}$ )	$\Delta N$ (cycles)	$\Delta a/\Delta N$ ( $\mu\text{m}/\text{cycle}$ )	$a_{\text{mean}}$ ( $\mu\text{m}$ )
10			19500	145	-	49.5	145	19500	0.00744	72.5
			24500	199	-	62.2	54	5000	0.0108	172
			29622	358	-	75.2	159	5122	0.0310	278.5
			34500	419	-	87.6	61	4878	0.0125	388.5
			37743	763	-	95.8	344	3243	0.106	591
11			10009	64	41.91	25.4	64	10009	0.00639	32
			14446	69	7.41	36.7	5	4437	0.00113	66.5
			19500	151	-	49.5	82	5054	0.0162	110
			24500	192	-	62.2	41	5000	0.00820	171
			29622	194	-	75.2	2	5122	0.00039	193
			34500	368	-	87.6	174	4878	0.0357	281
12			37743	405	-	95.8	37	3243	0.0114	386
			29622	147	-	75.2	147	29622	0.00496	73.5
			34500	162	-	87.6	15	4878	0.00308	154.5
13			37743	199	-	95.8	37	3243	0.0114	180.5
			14446	53	-	36.7	53	14446	0.00367	26.5
			19500	89	-	49.5	36	5054	0.00712	71
			24500	117	-	62.2	28	5000	0.00560	103
			29622	143	-	75.2	26	5122	0.00508	130
			34500	193	-	87.6	50	4878	0.0103	168
14			37743	220	-	95.8	27	3243	0.00833	206.5
			14446	45	-	36.7	45	14446	0.00312	22.5
			19500	84	-	49.5	39	5054	0.00772	64.5
			24500	121	-	62.2	37	5000	0.00740	102.5
			29622	143	-	75.2	22	5122	0.00644	132
			34500	175	-	87.6	32	4878	0.00656	159
		37743	185	-	95.8	10	3243	0.00308	180	

Crack Growth Results,  $\sigma = 638.5$  MPa

APPENDIX II

SHORT CRACK GROWTH IN AN ENGINEERING COMPONENT

## APPENDIX II

### Short Crack Growth in an Engineering Component

Reported below is work done which was not part of the actual Ph.D. project, but did give some interesting results concerning short crack growth in a component.

#### Introduction

Some steering third arms of trucks were found to be cracked after a substantial period of service. During service the steering arms are subject to cyclic stress, the magnitude of which depends to a large extent on the roughness of the road surfaces encountered. Figure 1 gives a distribution of the cyclic stresses experienced by a steering arm that was fixed to a truck subjected to more than 1000km of travel on a typical road surface.

To enable lifetime predictions to be made and to investigate the crack growth a series of fatigue tests were performed.

#### Fatigue Testing Program

All the fatigue tests were performed on the test machine described in section 2 of this thesis. To test the steering arms a special "test-rig" had to be constructed. The facility is shown in figure 2. Two steering arms were used in each test

with one end of each arm supported from its ball-joint at position A, whilst the other end of each arm is connected to a steel joint at position B. Both steel halves of the B grips were then clamped together.

The steering arms were known to develop cracks at position C, and so potential drop (p.d.) leads were attached to the arm in this position in order to monitor crack growth. A constant current was passed through the specimen and test assembly, and voltage readings recorded periodically using a data-logger. As well as p.d. leads being attached at position C, another set of p.d. leads (distant to the area of cracking), checked that the current input did not vary during the test.

To calibrate the voltage readings against crack length, a 2-D analogue representation of the test-rig was made out of aluminium foil. Furthermore, some steering arms were broken open in Liquid Nitrogen after testing to compare actual crack depths to those predicted by the aluminium foil model.

The fatigue tests were performed in load control, each test running to failure. Failure was defined as the point when the testing machine was unable to apply the required load due to extensive cracking. At this stage the crack was growing so fast that the cycles to failure, as defined by complete separation of one of the arms, would have occurred in only a few more applied cycles.

### Calibration of Potential Drop Readings

The results of the Analogue model calibration are shown, together with measured crack depths from actual specimens in figure 3. It was found that the equation (shown as a curve in figure 3),

$$\frac{(V_c - V_o)L}{V_a D} = 3.14 \frac{a^{1.5}}{D} \quad (1)$$

was a good fit to the analogue data, where  $V_c$  is the voltage across the crack,  $V_o$  is the initial voltage,  $V_a$  is the reference voltage for the p.d. leads at a position remote to the area of cracking,  $L$  is the lead spacing,  $D$  is the diameter of the steering arm in the plane of cracking, and  $a$  is the crack depth.

A separate calibration of the voltage ( $V_a$ ) against p.d. lead spacing ( $L$ ) at the reference point showed that  $V_a$  and  $L$  are related by the equation:

$$L = 2.77 V_a \quad (2)$$

Using equation (2) along with a value for  $D$  of 4.55cm, equation (1) reduces to:

$$(V_c - V_o) = 0.5317 a^{1.5} \quad (3)$$

and crack depths calculated from this equation are compared with actual crack depths in Table 1.

### Fatigue Test Results

Altogether twenty eight specimens (ie, 14 pairs) were tested. The main results are shown in Table 2. Failure as previously defined (machine trip-out caused by increasing compliance of cracked steering arms) is shown in column 8 of Table 2. By using potential drop readings a crack of 1 cm can also be used to define failure; this is listed in column 9. Two types of specimens were tested, both types were made of 42 Cr Mo 4 steel but some had been Nitro-Carbonised; these are described as "Nitrite" in Table 2. A plot of lifetime versus stress amplitude is shown in figure 4.

By converting voltage readings to crack lengths, figure 5 can be obtained which shows the crack length as a function of lifetime for six of the arms tested. It can be seen that for the highest stress level used in testing a crack of length 0.2mm was present after a few cycles, and even at the lowest stress level 60% of the lifetime was spent in propagating a crack from 0.2mm to its length at failure. This work correlates with the findings of the main project in that the period of life spent in initiating the crack and the crack subsequently propagating to a size of the order of grain dimensions is small even for low stresses near the fatigue limit.

TABLE 1

Specimen Number	$V_c$ (volts)	$V_o$ (volts)	Actual Crack Depth (cm)	Calculated Crack Depth (cm)
9T	1.55	0.70	1.2	1.37
9B	3.36	0.76	2.9	2.88
10T	2.08	0.80	1.9	1.80
10B	3.18	0.67	2.7	2.81
3T	3.96	0.75	3.1	3.32
3B	1.86	0.70	2.1	1.68
5B	4.66	0.90	3.3	3.68
13T	4.48	0.80	3.4	3.63
13B	1.36	0.80	1.2	1.04

TABLE 2

Test	(kN) load amp	(MPa) stress amp	(Ksi) stress amp	elastic strain amp	plastic strain amp	(cpm) freq. amp	$N_f$ cycles	(1cm crack) $N_f$	Top Arm	Bottom Arm	R = $\frac{\sigma_{min}}{\sigma_{max}}$
1	5.8	361.4	51.60	-	-	120	215,389	-	Plain cracked	Plain fail	0.15
2	6.27	404.1	57.68	-	-	60	181,555	-	Plain cracked	Plain fail	0.074
3	9.25	597.0	85.23	0.00261	0.00045	40	217,064	137,900	Plain fail	Plain cracked	-1
4	14.0	903.6	129.00	0.00327	0.00243	20	51,241	25,900	Nitrite cracked	Plain fail	-1
5	11.6	748.7	106.88	0.00299	0.00128	20	97,579	48,700	Nitrite no crack	Plain fail	-1
6	10.43	672.9	96.06	0.00282	0.00086	25	130,077	64,200	Nitrite no crack	Plain fail	-1
7	12.8	826.1	117.94	0.00313	0.00178	20	85,730	58,000	Plain fail	Nitrite cracked	-1
8	8.7	561.5	80.16	0.00249	0.00356	40	264,977	140,000	Plain fail	Nitrite no crack	-1
9	15.5	1,000.4	142.82	0.00342	0.00327	15	40,690	23,900	Plain cracked	plain fail	-1
10	17.15	1,106.9	158.02	0.00356	0.00436	15	24,944	8,000	Plain cracked	Plain fail	-1
11	18.8	1,213.4	173.22	0.00368	0.00549	10	19,788	11,800	Plain cracked	Plain fail	-1
12	21.05	1,358.6	193.96	0.00382	0.00716	6	12,275	-	Plain fail	Plain cracked	-1
13	7.2	464.7	66.34	0.00213	0.00012	35	570,187	408,000	Plain fail	Plain cracked	-1
14	32.5	2,097.6	299.46	0.00440	0.01897	2.5	2,202	710	Plain fail	Plain cracked	-1

**TEXT  
BOUND INTO THE  
SPINE**

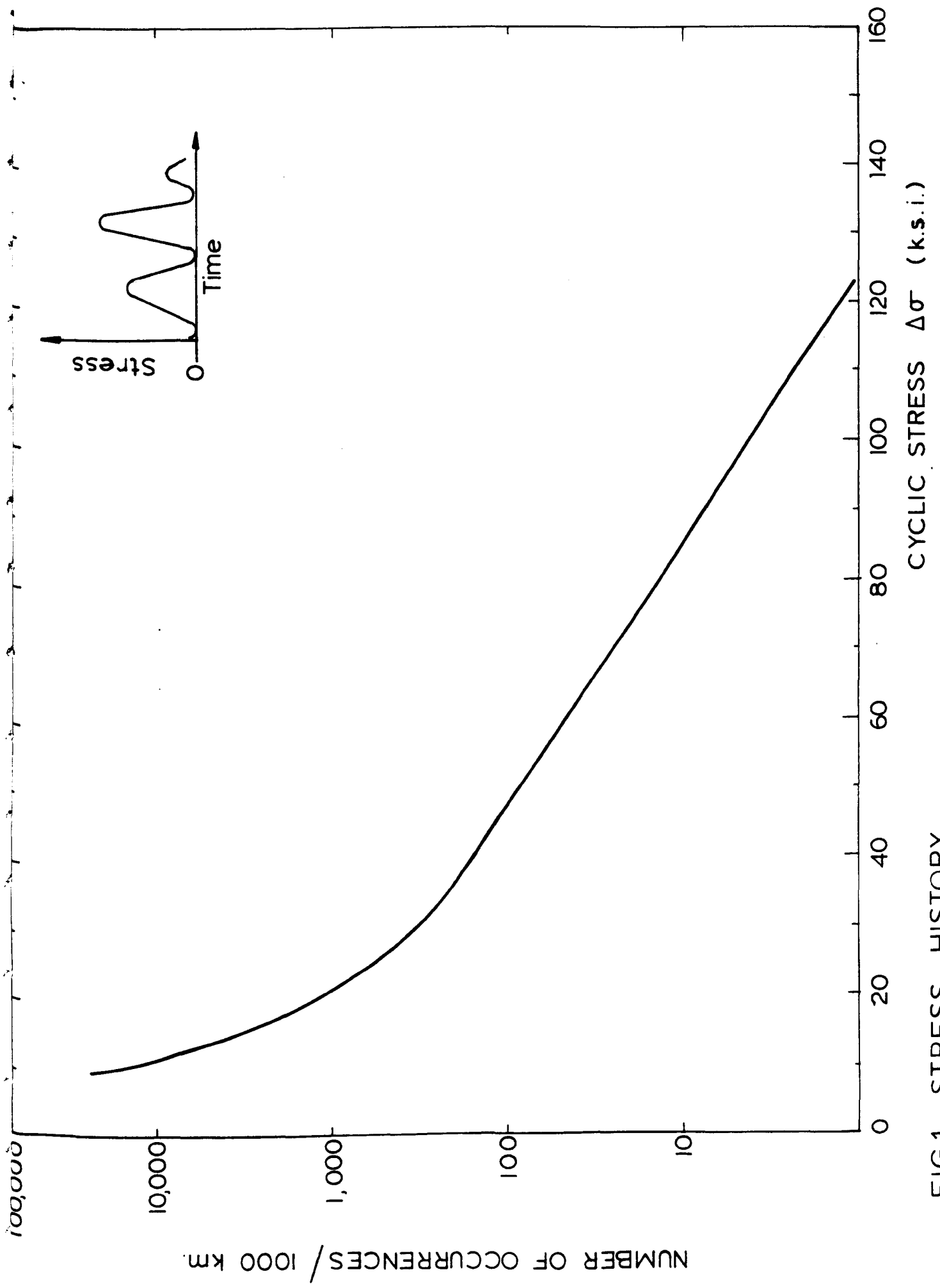


FIG.1. STRESS HISTORY.

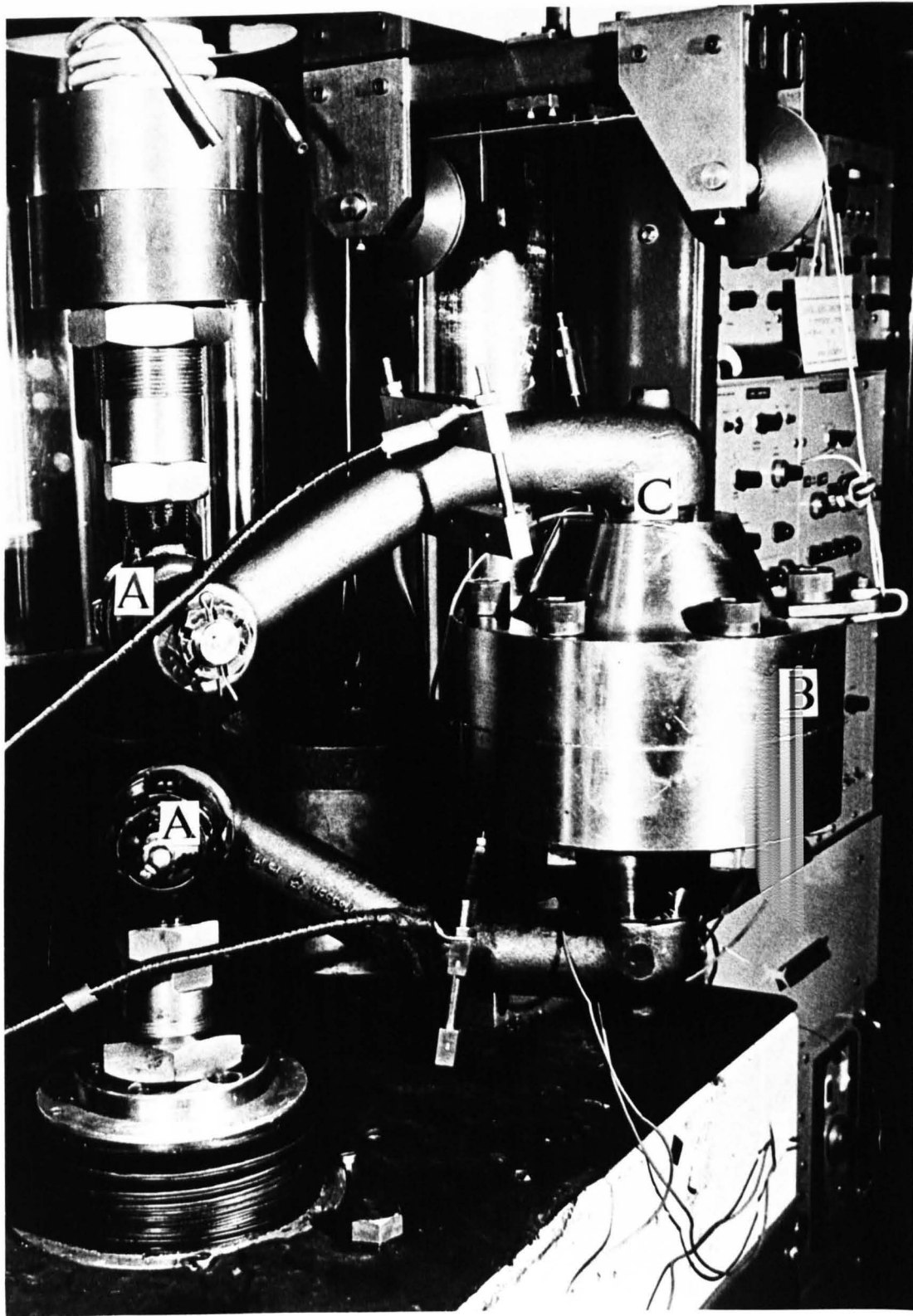


FIGURE 2 - STEERING ARM TEST-RIG

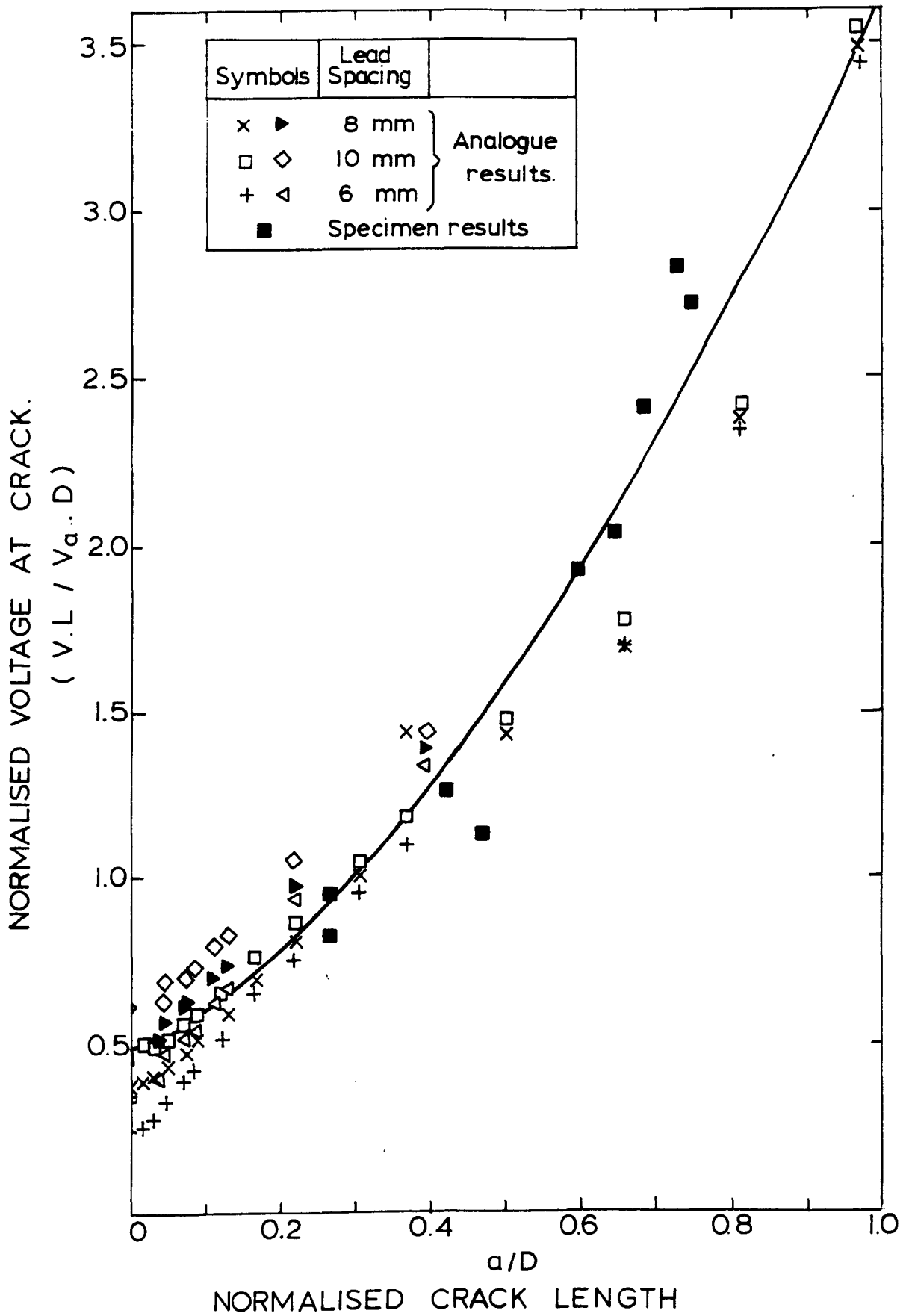


FIG. 3 POTENTIAL DROP CALIBRATION CURVE

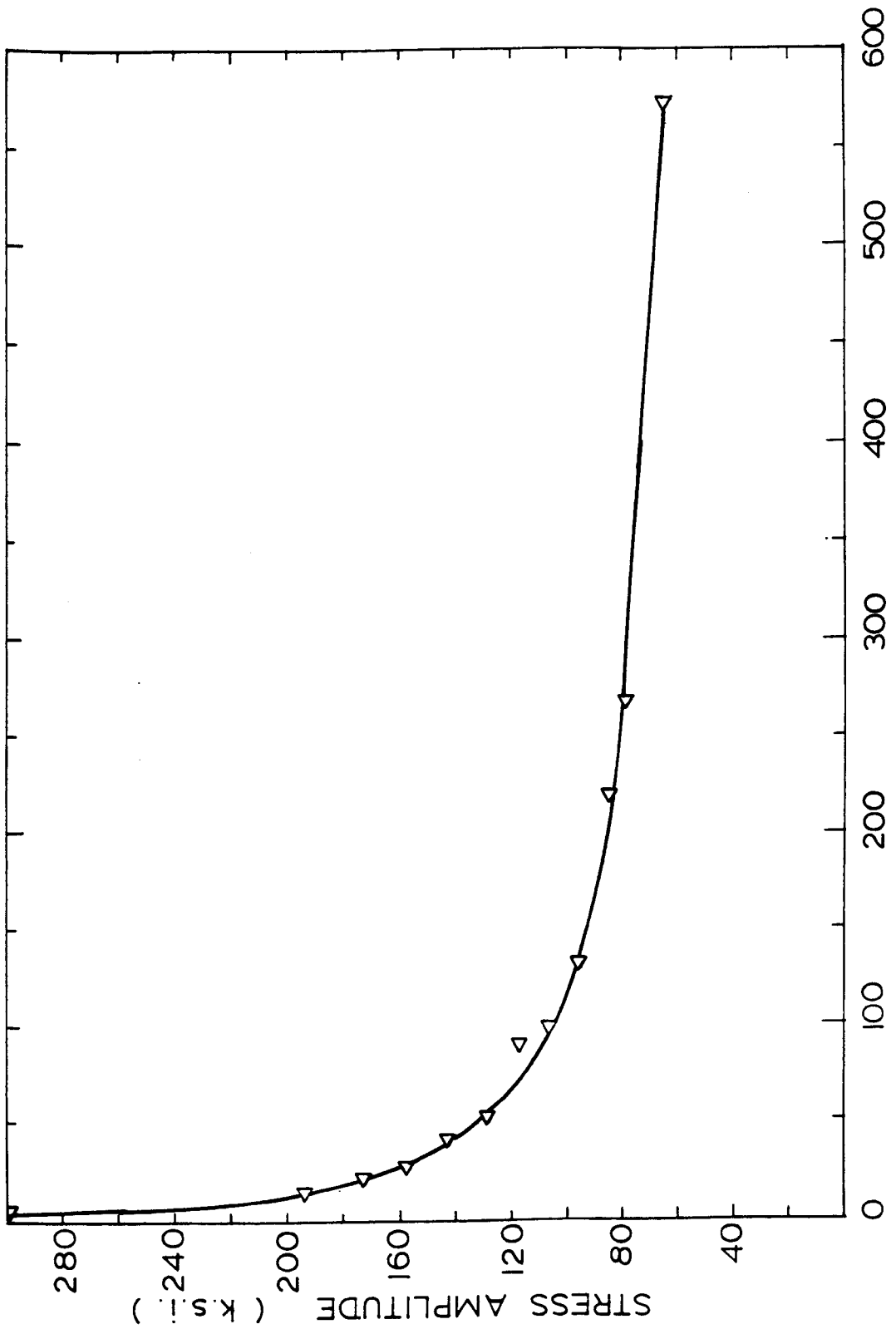


FIG. 4. STRESS AMPLITUDE vs. CYCLES TO FAILURE.

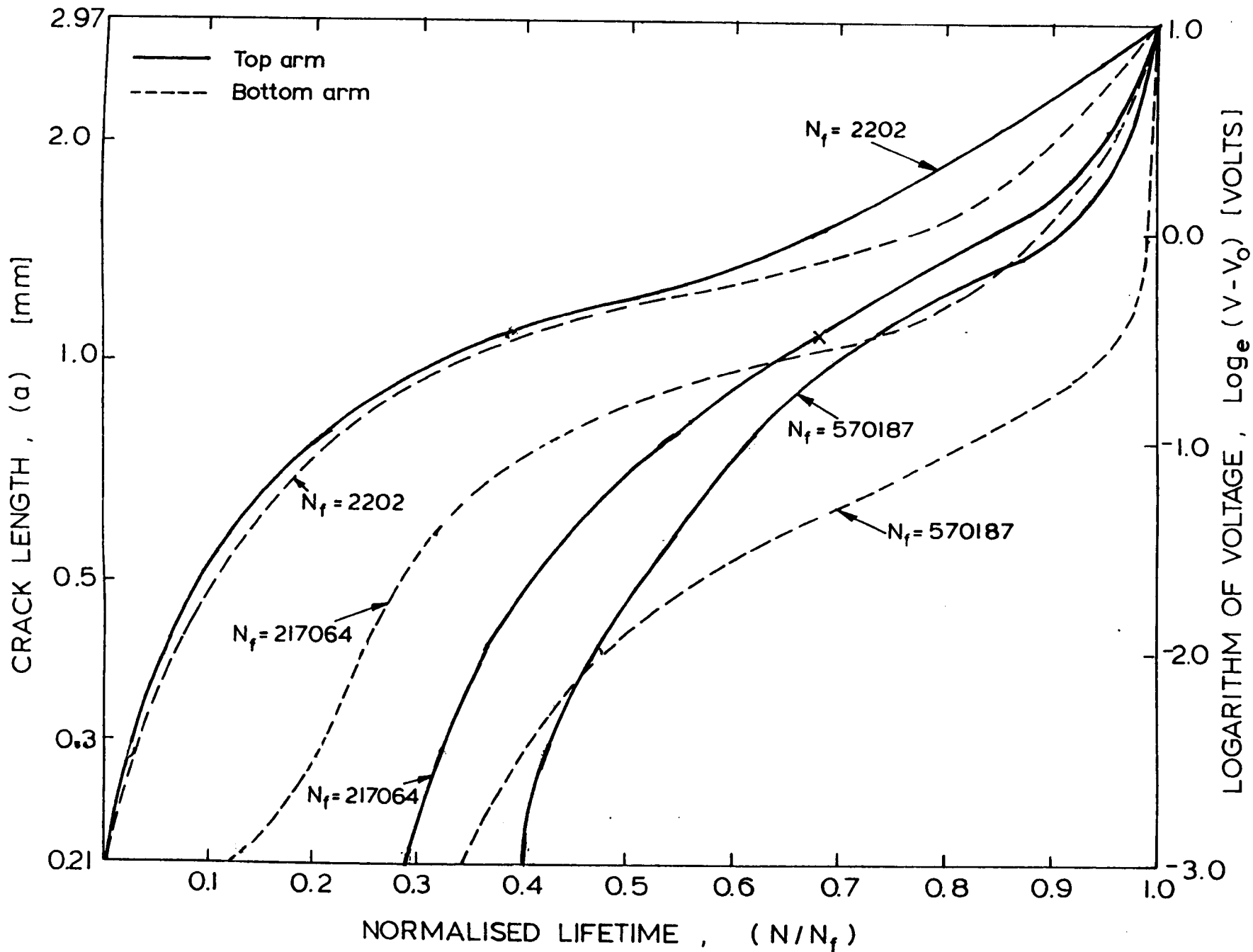


FIGURE 5 CRACK LENGTH VERSUS ELAPSED LIFETIME